The Effect of an Axial Catalyst Distribution on the Performance of a Diesel Oxidation Catalyst and Inverse Hysteresis Phenomena during CO and C_3H_6 Oxidation

.

by

Ali Abdolhamid Abedi

A thesis
presented to the University of Waterloo
in fulfillment of the
thesis requirement for the degree of
Doctor of Philosophy
in
Chemical Engineering

Waterloo, Ontario, Canada, 2012

AUTHOR'S DECLARATION

I hereby declare that I am the sole author of this thesis. This is a true copy of the thesis, including any required final revisions, as accepted by my examiners.

I understand that my thesis may be made electronically available to the public.

Abstract

The Diesel Oxidation Catalyst (DOC) is a key component in the exhaust after-treatment system of diesel engines. In this study two aspects of a DOC were investigated: catalyst distribution and reactant species interactions. In the first part, the effect of an axial Pt distribution along a DOC was investigated by comparing a standard sample, with a homogeneous Pt distribution along the length, with a zoned sample, where the Pt was non-homogeneously distributed along the length. Temperature-programmed oxidation (TPO) and spatially-resolved gas-phase concentration measurement experiments were used to compare the CO, C_3H_6 and NO oxidation performance of the standard and zoned catalysts. Both catalyst types had the same total amount of Pt but different distributions. The zoned catalyst, with more Pt located in the upstream portion, showed better performance than the standard catalyst, especially at high total flow rate and when a mixture of the reactants were used. The superior performance of the zoned sample is due to a larger, localized exotherm in the upstream region, where more Pt is located, and a decrease in the self-poisoning effect downstream, where reaction light-off occurs. In addition, catalyst durability against thermal degradation was tested by exposing the whole catalyst (homogeneous aging) and part of the catalyst (heterogeneous aging) to high temperatures. In general, the zoned catalyst showed better performance than the standard catalyst after thermal aging, especially after heterogeneous aging. The reason for the superior performance of the zoned catalyst, especially after heterogeneous aging, is that the back of the catalyst, which is exposed to higher temperature, contains less Pt than the front; therefore, most of the Pt particles in the zoned catalyst were not affected by thermal aging. However, after homogeneous aging, the

performance of the standard catalyst was better than the zoned catalyst at higher flow rate and temperature most likely due to the different sintering rates in the zoned sample compared to the standard one.

In the second part of this research, the interactions between CO, C_3H_6, H_2, and NO were tested over a commercial Pt/Al_2O_3 monolith sample by studying these reactions during ignition and extinction (warm-up and cool-down). Results showed that CO, C_3H_6, and NO inhibit their own oxidation and each other's oxidation due to the self-poisoning effect and competitive adsorption over active sites. In the case of a CO + C_3H_6 mixture, interesting CO and C_3H_6 oxidation trends were observed during the extinction phase. As the C_3H_6 concentration increased in the mixture, the catalytic activity of CO oxidation during the extinction phase decreased until it was actually poorer than that during the ignition phase. In situ diffuse reflectance infrared Fourier transform spectroscopy (DRIFTS) showed different C_3H_6 oxidation intermediates during the extinction phase on the catalyst surface, thus blocking active sites and lowering catalyst activity.

Acknowledgements

All the praises are due to the ALLAH, the One, the Creator, All Mighty, the Most Beneficent and Most Merciful.

First and foremost, I would like to express my deep appreciation and thanks to my academic supervisor Dr. William S. Epling for his valuable guidance, support, and kindness. He has taught me, both intentionally and unintentionally, patience, enthusiasm, dedication, and hard work. Thank you Bill for your amazing supervision and all your contributions of time, ideas, and funding during my PhD studies. I simply could not wish for a better or friendlier supervisor.

I would like to thank other members of my thesis committee: Dr. Eric Croiset, Dr. Joao Soares, Dr. Elizabeth Weckman, and Dr. Gregory S. Patience.

I am thankful to all my friends in for their support and encouragements. They have been like a family to me in Waterloo. I am also grateful to my colleagues in the catalysis research group: Meshari, Darren, Karishma, April, John, Peter, Crystle, Harry, Izabella, Suad, Ashraf, and Zuhair. Special thanks to the Co-op students who worked with me: Drew, Rohit, Roger, and Melanie.

Deep affection is due especially to my parents for their continuous support, encouragement, prayers, and having trust in me. I owe my success to my mother, who shared with me all good and bad moments during my study. She is the one who carried the heaviest burden and to that I am very grateful. I would like to thank my brothers, Abdullah and Mohammed, and my sisters, Mariam and Fatima, for their support and encouragements throughout my study.

Lastly, I would like to gratefully acknowledge Canadian Automotive Research and Development Program, Auto21, for their financial support and giving me the chance to present my work in their annual conference, where I met the leaders of automotive industry in Canada. I was also

honored to receive the International Doctoral Student Award (IDSA) during my PhD studies. Special thanks to Umicore and University of Alberta for providing catalyst samples.

Dedication

To my mother,

Zainab H. Akber

Table of Contents

List of Figures

List of Tables

Chapter 1: Introduction

One goal of this research is to optimize the performance of a diesel oxidation catalyst (DOC) in terms of cold start emissions reduction and its resistance to thermal degradation, by re-distributing the active metal along the catalyst length. Optimizing the distribution of the active metal will result in a catalyst with higher efficiency and lower cost than the typical uniformly distributed catalyst used today by the automotive industries. In addition, the interaction between different reactant species was studied over a commercial Pt/Al_2O_3 catalyst, as a part of an Auto21 project and due to interesting findings observed during the course of the research. In the first chapter a brief description of a DOC, its function and effect on our health and environment, and the regulations and standards used to control diesel emissions are presented. In the second chapter a literature review on DOC background, reaction, preparation, degradation, and optimization is presented, to better understand the different aspects related to the goals of this study. Methodologies and experimental procedures used to test and characterize the DOC are discussed in Chapter Three. In Chapters Four and Five, the performance of the uniformly and non-uniformly distributed catalysts, before and after thermal degradation, are shown respectively. The interactions between CO, C_3H_6, and NO over a commercial Pt/Al_2O_3 catalyst are discussed in Chapter Six. An unexpected trend in CO oxidation behavior was observed. In Chapter Seven, this trend is described and the reasons for it demonstrated. Finally the conclusions and recommendations of this study are discussed in Chapter Eight.

1.1 Automobiles and Pollution

Air quality in most urban areas is heavily affected by emissions from passenger vehicles and heavy-duty trucks. In the United States, cars, trucks, and off-road vehicles are estimated to be responsible for about 50% of nationwide nitrogen oxides emissions, about 40-50% of hydrocarbon emissions, and 80-90% of CO emissions in urban areas [1]. Diesel trucks and buses are widely used for public transportation due to their superior fuel efficiency and durability. Diesel fuel is a mixture of

hydrocarbons that ideally should produce CO_2 and H_2O during combustion. In reality, however, diesel engine emissions are a mixture of several components including CO, hydrocarbons (HC), nitrogen oxides (NO_X), and particulate matter (PM). These listed products are the major emission concerns in terms of human health and environmental impact. Heavy duty diesel engines are the major source of pollutants in urban areas. For example, diesel engines are a major source of NO_X in California with on-road vehicles contributing 18% and off-road diesels contributing 19% of the total emitted NO_X [2]. The U.S. Environmental Protection Agency (US-EPA) has reported that heavy-duty trucks and buses produce about one-third of NO_X emissions and one-quarter of particulate emissions from all highway cars and trucks, even though they comprise only 2% of the total number of vehicles on the roadways [3]. Table (1-1) shows typical emissions of a diesel engine without a catalytic emissions control system, measured during a transient test cycle [4]. To control diesel engine exhaust emissions, scientists and engineers have developed many technologies. The health and environmental effects of diesel emissions, the standards and regulations, and diesel technologies developed to reduce the effect of diesel exhaust emissions are presented in the following section.

Table 1-1 : Typical emissions of diesel engine.

Emissions species	Emissions, g/KW-h
Carbon monoxide	1.77
Gaseous hydrocarbons	0.44
Oxides of nitrogen	6.31
Extractable particulate	0.037

1.1.1 Health Impacts of Diesel Emissions

Even though there is no consensus on the effect of diesel emissions on humans, several organizations, such as the World Health Organization (WHO) and the International Agency for Research on Cancer (IARC), have studied the health effects of diesel engine exhaust on human health

and found that diesel exhaust gas is a potential carcinogen for humans [5]. According to WHO, many epidemiological studies on people who are exposed to diesel emissions, such as truck drivers and railroad workers, showed that these people have a tendency to have a 20-40% higher incidence of lung cancer [6]. Table (1-2) lists the biological impact of some diesel emissions components [7]:

Table 1-2 : Biological impacts of diesel emission components.

Component	Impact
Carbon monoxide	highly toxic to humans; blocks oxygen uptake
Nitrogen oxides	respiratory tract irritation, major ozone precursor
Sulfur dioxide	respiratory tract irritation and contributes to acid rain
Particulate matter	respiratory tract irritation and carcinogenic

In general, emissions of CO and HC from diesel engines are lower than those from gasoline engines; however, CO, HC, and NO_X emissions from diesel engines are higher than those from gasoline engines equipped with a three-way catalyst (TWC). When released into the atmosphere, NO undergoes a series of reactions to form other substances of much higher toxicity as well as ground level ozone. Most air pollution studies focus on the health and environmental effects of NO_2 which is a product of NO and has higher toxicity than NO.

Diesel particulate matter (PM) emission is a major health concern. Some of the PM is small in size (0.10 μm is the mean size), and therefore can penetrate deep into human lungs [8]. According to a study by the American Cancer Society, PM exposure damages the respiratory system and causes a wide variety of medical problems such as asthma and possible asthma onset, heart attacks and premature death [9]. Several health organizations hold PM responsible for various diseases and consider PM as the most dangerous component in diesel engine emissions.

1.1.2 Environmental Impacts of Diesel Emissions

In addition to the health effects of diesel engine emissions, environmental agencies have reported that diesel emissions contribute to various environmental problems such as air quality issues, photochemical smog, acid rain, and global warming. Table (1-3) lists the environmental impact of some diesel exhaust components [10]

Table 1-3 : Environmental impacts of diesel exhaust components.

Component	Impact
Carbon dioxide	most common greenhouse gas
Nitrogen oxides	photochemical smog, acid rain, and destruction of stratospheric ozone
Particulate matter	reduces atmospheric visibility, and contributes to global warming

CO_2 is one of the most abundant greenhouse gases and contributes to climate warming. Diesel vehicles release lower CO_2 emissions than their gasoline counterparts [11]. Similarly, black carbon soot from diesel emissions can contribute to global warming due to its ability to absorb light and heat [12].

1.2 Standards and Regulations

Governments have authorized regulatory agencies to control and limit known harmful emissions. These agencies are responsible for legislation of laws and standards for diesel engine exhaust emissions, and force engine manufacturers to comply with these standards, which specify the required emission limits. Regulated diesel emissions include the following: PM, NO_X, HCs, and CO [1]. In recent years these standards have become increasingly strict in order to reduce emissions and improve air quality. Table (1-4) lists emission requirements for heavy-duty diesel engines in the US and Canada from 2000 to 2010 [13-15].

Table 1-4 : Emissions requirements for heavy-duty diesel vehicles, g/KW-hr.

United States				
Year	CO	HC	NO_X	PM
2004	20.8	0.67	3.35	0.13
2007	20.8	0.187	1.6	0.013
2010	20.8	0.187	0.26	0.013
Canada				
Year	CO	HC	NO_X	PM
2000	20.8	1.75	5.4	0.13
2005	19.3	$HC + NO_X = 1.0$		0.13
2010	19.3	0.187	0.26	0.013

With advanced after-treatment technologies and engine design, modern diesel engines not only meet the strict emission limits and standards, but also outperform in responsiveness and fuel economy [1].

1.3 Diesel Technologies

Controlling diesel emissions by engine design is not enough to meet the regulations. Catalytic after-treatment devices are required. However, more research is needed to integrate these after-treatment systems to meet the new standards and improve the economics. The most promising after-treatment technologies to control diesel emissions include: (1) DOCs, (2) selective catalytic reduction (SCR) catalysts, (3) NO_X storage and reduction (NSR) catalysts, and (4) PM filters. DOCs provide very effective control of CO and HC emissions, with conversions higher than 90% at exhaust gas temperatures above 300 °C [1]. NSR and SCR are promising technologies to reduce NO_X emissions from diesel engines.

A typical NSR catalyst consists of an oxidizing component (Pt), a NO_X storage component (Ba), and a reducing component (Rh). The NSR system operates by switching between fuel lean and rich phases. In the lean phase, which lasts for a few minutes, NO_X is trapped on the catalyst by bonding to the storage component. When the adsorption capacity becomes saturated, NO_X is reduced to N_2 and released during the rich phase or regeneration, which lasts a few seconds. Figure (1-1) describes the mechanism of the NSR reaction. Several studies have shown that NO_2 enhances the performance of the NSR catalyst by improving NO_X storage, as NO_2 is faster and easier to trap than NO [16, 17]. Therefore, in the exhaust aftertreatment system, it is advantageous to place a DOC upstream of NSR catalysts in order to increase the amount of NO_2.

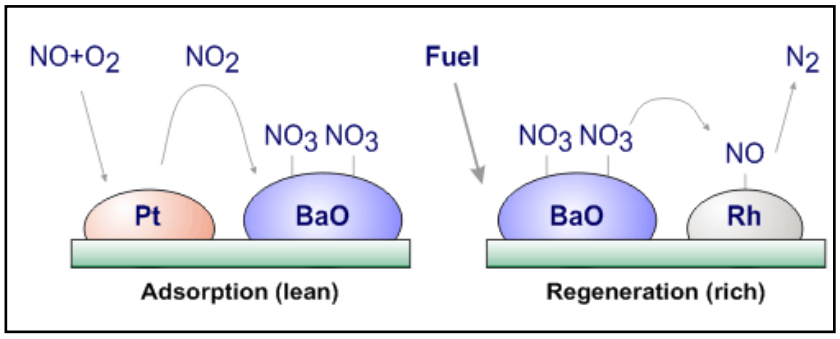

Figure 1-1 : NSR operating cycle (source: www.dieselnet.com).

SCR utilizes ammonia as a reducing agent to reduce NO_X in diesel engine exhaust. The main reaction in the SCR system is:

$$4NO + 4NH_3 + O_2 \rightarrow 4N_2 + 6H_2O \qquad (1)$$

SCR is widely used in industrial application because of its high conversion, which can exceed 90%. SCR has proven successful in stationary diesel engines; however, there is ongoing research for its use in mobile applications [18, 19]. Installing a DOC before the SCR catalyst can further enhance the total conversion of NO_X via SCR by increasing the amount of NO_2 and driving a second reaction, which is faster and occurs at lower temperature than reaction (1):

$$NO + NO_2 + 2NH_3 \rightarrow 2N_2 + 3H_2O \qquad (2)$$

Diesel particulate matter, or soot, is removed from diesel exhaust gas by diesel particulate filters (DPFs), a wall-flow monolith that traps solid particles from the exhaust. When the filter is overloaded with particulate, it is regenerated by exposing it to high temperature to oxidize the accumulated soot. Today's DPFs are capable of removing more than 90% of soot with acceptable mechanical and thermal durability [1]. Further, NO_2 produced in a DOC is beneficial for DPFs, because NO_2 oxidizes soot at lower temperature than O_2. For example, O_2 oxidizes soot at 500-600 °C, whereas NO_2 does at 350 °C. For this reason, DOCs are installed upstream of DPFs to lower soot oxidation temperatures [20, 21].

1.4 Catalyst Optimization

In their aim to optimize the performance and reduce the cost of DOCs, catalyst manufacturers have studied a variety of catalyst aspects including precious metal/support/promoter types, geometry and structure of the honeycomb support, and different preparation conditions. All of these factors have been utilized in optimizing standard catalysts that have a uniform distribution of catalyst material along the catalyst length. However, some studies have shown improvement in catalyst performance by using non-uniformly distributed catalysts. In these catalysts the active metal is not homogeneously deposited along the catalyst length, instead a distribution of active sites is made along the catalyst length. Most published work in non-uniform catalyst distribution is based on mathematical modeling, in which few have considered catalyst deactivation in the optimization model. For example, Tronci et al [22] have considered thermal degradation in their model, and they found that the performance of the uniformly distributed catalyst was more severely affected by thermal aging than a two zoned catalyst, with more Pt loading in the front zone. Therefore more investigations are required before commercializing the non-uniform catalyst converter for diesel engines.

1.5 Objectives

The ultimate goal of this research is to improve the performance of a DOC by redistributing the active sites on the catalyst surface in order to efficiently utilize the amount of precious metal. CO, C_3H_6 and NO oxidation over a DOC will be investigated by studying the competition and inhibition effects of these components of these reactions. The effect of thermal deactivation will also be characterized. This research is divided into two sections in which special tools and techniques will be used. In the first section the performance of uniformly and non-uniformly distributed catalysts are tested before and after thermal degradation by the following sequence:

(1) Making samples with a homogeneous distribution along the axial direction.

(2) Testing and characterizing fresh and aged homogeneous distribution samples.

(3) Making samples with gradients in distribution along the axial direction.

(4) Testing and characterizing the fresh and aged non-homogeneous samples.

Testing the homogenous and non-homogeneous samples will include measuring the distribution of gas compositions, overall conversion, and temperature along the axial direction of a DOC, and measuring how the distribution changes as a function of thermal aging. In the second section of this work, the interactions between CO, C_3H_6, and NO are examined over Pt/Al_2O_3 with the focus on the hysteresis behavior of CO oxidation in a CO and C_3H_6 mixture.

1.6 Contributions

This research work provided valuable information about the DOC that is used in lean burn engines. With the data obtained, and the gradients in activity measured, we can design a new catalyst having axial gradients in active metal that could improve light-off characteristics and minimize degradation. This led to optimizing the DOC to meet mandated emission regulations and reduce the cost of the DOC.

A primary result of this work is a more efficient catalyst by zone-coating the sample with the same overall amount of precious metal. Furthermore, the gradients can be used to slow thermal degradation, also potentially resulting in the need to use less active metal since the catalysts are usually designed for “end-of-useful-life”. In other words, the amount of Pt/Pd/Rh added is sufficient for the catalyst to meet regulation requirements after being used for more than 100,000 miles. If less thermal degradation occurs, less overall metal is required. In addition, understanding the influence of each reactant component on its own, and with other species, oxidation will provide a clear picture of the nature of the reactions on the DOC catalyst. These data can be utilized in the future to build more accurate models for DOC reactions.

Chapter 2: Literature Review

A review of the DOC functions, diesel exhaust species interactions on the catalyst, catalyst aging, catalyst preparation, the influence of active metal distribution on performance, and the hysteresis behavior of CO are presented in this chapter.

2.1 Diesel Oxidation Catalyst (DOC)

2.1.1 DOC Background

A diesel oxidation catalyst is a catalytic device that oxidizes the following components: CO, HCs, NO, and the organic fraction of diesel particulates. Since the 1970s, the DOC has been commercially used in a number of light and heavy duty engine applications. It was first used in construction, tunneling, and material handling to reduce the CO and odor from diesel-powered equipment [13]. In the early 1990s, with the success of the gasoline engine catalytic converter and the strict standards for diesel engine emissions, diesel engine manufacturers considered catalysts for controlling engine emissions [23]. DOCs used in the after-treatment system of diesel engines are normally a flow through cordierite honeycomb shaped configuration coated with Pt or Pt/Pd on an Al_2O_3 support, with CeO_2 and zeolite components sometimes added [24-26]. Today, DOCs are capable of removing more than 90% of CO and HCs and can reduce diesel particulate matter (PM) up to 30% [1].

2.1.2 DOC Reactions

The DOC is designed to oxidize different species in diesel exhaust. Two main reactions are CO and HC oxidation:

$$CO + 0.5\ O_2 \rightarrow CO_2 \quad (3)$$

$$C_nH_{2m} + (n + m/2)\ O_2 \rightarrow nCO_2 + mH_2O \quad (4)$$

The oxidation of NO to NO_2 is another reaction that occurs on a DOC.

$$NO + 1/2O_2 \rightarrow NO_2 \quad (5)$$

Because NO_2 is more toxic than NO, previously scientists classified NO oxidation as an undesired reaction that creates air quality concerns [27]. However, NO oxidation can be beneficial for downstream DPFs, NSR, and SCR catalysts. The optimal ratio of NO_2/NO is 1:1 in SCR catalysis [28, 29], with typical engine out NO_2 values at about 10%. The disadvantage of the presence of NO_2 in the feed of SCR is the formation of N_2O, which is a greenhouse gas and contributes to the depletion of the ozone layer. N_2O is formed at low temperature as a result of the side reaction between NO_2 and NH_3 on the SCR catalyst [28, 30, 31]. In addition, studies have shown NO_X storage efficiencies are significantly improved with NO_2 relative to NO [16, 17, 32], thus an upstream DOC is typically a part of this system also. NO oxidation over a DOC is enhanced with increasing O_2 concentration but suppressed with increasing H_2O concentration [29]. For DPFs, NO_2 formed in the upstream DOC is utilized to oxidize the trapped soot. Since NO_2 is a stronger oxidizer than O_2, the DPF system is more easily (lower temperature and higher rates) regenerated with NO_2 [33].

2.2 Species Interactions in DOC

The performance of a DOC can be evaluated by the light-off temperature, total conversion of reactants, and durability. There are several parameters that influence the overall performance, such as catalyst volume, washcoat type, composition, distribution, loading of precious metal, and preparation methods. Even though it has been used for many years, the mechanism that governs the operation of a DOC and the interactions between different species on the surface of the catalyst remain controversial. A better understanding of the mechanism and resultant rate expressions would be advantageous in helping to model DOCs.

Diesel exhaust gas is primarily composed of CO_2, H_2O, O_2, and N_2. All these gases are environmentally friendly products, except CO_2 which is a greenhouse gas. Traces of other pollutants such as CO, unburned HCs, NO_X, and PM are also emitted. Studies have shown that the activity of

the DOC is greatly influenced by the concentrations of various exhaust gas species [21, 34, 35]. The presence of some species that can strongly adsorb onto active sites may retard the reaction of a more reactive species and delay the light-off temperature until the desorption temperature of the inhibiting adsorbate is reached. The effects of the main reactants on the DOC are evaluated in the following sections.

In 1973, Voltz and his group studied the effects of O_2, CO, C_3H_6 and NO on the rates of CO and C_3H_6 oxidation over a Pt/Al_2O_3 pellet catalyst [35]. CO and C_3H_6 oxidation rates increased with increasing O_2 concentration and decreased with increasing CO and C_3H_6 concentrations. These results agree with other previous work that studied CO and C_3H_6 oxidation [36, 37]. The inhibition effect of CO both on its own oxidation, a phenomenon known as self-poisoning, and on C_3H_6 oxidation is related to strong chemisorption of CO on Pt sites on the catalyst. Similarly, the inhibition effect of C_3H_6 is also related to chemisorption of C_3H_6 on active sites [35]. The chemisorption of both CO and C_3H_6 is sufficient at lower temperature to cause significant inhibition, but at temperatures above 400 °C, CO and C_3H_6 chemisorption is insignificant and thus inhibition effects are reduced or eliminated. As the temperature increases, CO chemisorption decreases, and consequently the effect of CO self-inhibition decreases [35, 38, 39]. Further, NO has an inhibiting effect on CO and C_3H_6 oxidation: this inhibition effect of NO increases with increasing NO concentration. At low temperature, there is no inhibition effect for NO on CO and C_3H_6 oxidation, but at temperatures above 200 °C, NO is chemisorbed onto active sites, once CO and C_3H_6 adsorption decreases leaving some sites free, thus inhibiting CO and C_3H_6 oxidation. Separate studies have also shown that CO and HCs inhibit NO oxidation by delaying the light-off temperature and decreasing the conversion of NO [21, 40]. This negative effect has been attributed to the competition of CO, HC, and NO for the active sites. In addition, NO_2, the product of NO oxidation, is a stronger oxidant than O_2 and therefore NO_2 is consumed preferentially in C_3H_6 and CO oxidation thus resulting in an apparent inhibition of NO

oxidation [21, 41]. Other hydrocarbons such as m-xylene and dodecane had the same effect as C_3H_6 on NO oxidation. Because of its high sticking coefficient on Pt and this strong oxidizing ability, NO_2 can also inhibit NO oxidation by covering the surface of the catalyst with oxygen, preventing NO and other species from reaching the surface [42, 43].

Unlike other compounds, H_2 promotes oxidation reactions on a DOC. In a study of the effect of H_2 on the combustion of methane on a Pt catalyst in a lean methane/air mixture, increasing H_2 decreased the light-off temperature of the methane [44]. Even though exhaust from light-duty and heavy-duty diesel trucks contains very little or no H_2 (CO/H_2 ~40 to 70) as compared to that of a gasoline car exhaust (CO/H_2 ~3), even small amounts of H_2 can promote oxidation reactions over a DOC [45]. Literature evidence shows that when a mixture of H_2, CO, and O_2 passes over a Pt catalyst, CO hinders the H_2 light-off temperature, but H_2 promotes CO light-off [46-48]. CO starts oxidizing first until it reaches ~50% conversion, then H_2 is rapidly converted [49-53]. Studies found that adding a small amount of H_2 showed the greatest effect on CO oxidation, however the rate of the enhancement effect decreased as the H_2 concentration increased [46, 48]. Several explanations were proposed for the H_2 enhancement effect. Sun et al [54], explained the H_2 enhancement effect by the associated increase in temperature due to the exothermic H_2 oxidation reaction. Another explanation was the interaction on the surface between H_2 and other adsorbed species [46, 48]. Mhadeshwar suggested a mechanism that utilizes a parallel path for CO oxidation with a hydroxyl (OH) species that would decrease the CO light-off temperature [55]. Salomons and coworkers have linked the enhancement effect of H_2 on CO oxidation to H_2 adsorption and CO desorption [46]. In their kinetic model of the CO/H_2 oxidation mechanism, the activation energy of CO desorption decreased as function of H_2 adsorption [46].

The most acceptable reaction mechanism of CO oxidation on Pt is the Langmuir-Hinshelwood (L-H) dual-site mechanism, where the rate determining step (RDS) is the surface

reaction between adsorbed CO and O_2 on two different sites [47, 56-58]. Similarly, the L-H mechanism was also proposed for hydrocarbon oxidation reactions, and the surface reaction between adsorbed O_2 and HCs is the RDS [35, 59, 60]. The mechanism of CO and C_3H_6 oxidation are shown in equations (6-9).

$$R\ (g) + AS \leftrightarrow R\text{-}AS \quad (6)$$

$$O_2\ (g) + 2AS \leftrightarrow 2(O\text{-}AS) \quad (7)$$

$$R\text{-}AS + O\text{-}AS \rightarrow CO_2\text{-}AS + AS \quad (8)$$

$$CO_2\text{-}AS \leftrightarrow CO_2\ (g) + AS \quad (9)$$

R: reactant (CO or C_3H_6)

AS: Active Site

Several studies in the literature have shown that CO oxidation is inhibited by CO at low temperatures, due to strong CO chemisorption on active sites, while at high temperature the reaction is mass transfer limited [35, 38, 39]. In a mixture of reactants, CO, C_3H_6, and NO inhibit the oxidation of each other due to competitive adsorption over the active site. The rate equations of CO and C_3H_6 oxidation including the resistance term, that accounts for CO, C_3H_6, and NO inhibition, were reported by Voltz as shown in equations (10-12) [35, 61].

$$r_{CO \text{ or } C_3H_6} = \frac{-k_{r1} \text{or } k_{r2}\ (CO \text{ or } C_3H_6)(O_2)}{[1+k_{a1}(CO)+k_{a2}(C_3H_6)]^2 * [1+k_{a3}(CO)(C_3H_6)]^2 * [1+k_{a4}(NO)]^{0.7}} \quad (10)$$

$$k_{rj} = k_{rj}^{\circ} \exp[-\frac{E_{rj}}{R} /(T+460)] \quad (j=1 \text{ for CO and } 2 \text{ for } C_3H_6) \quad (11)$$

$$k_{ai} = k_{ai}^{\circ} \exp[-\frac{E_{ai}}{R} /(T+460)] \quad (i=1, 2, 3, 4) \quad (12)$$

(CO) = mole % of CO

(O_2) = mol % of O_2

(C_3H_6) = ppm of C_3H_6

(NO) = ppm of NO

kr_i = intrinsic rate constant based on catalyst volume [sec^{-1} O_2^{-1}]

ka_1 = adsorption rate constant for CO $[CO]^{-1}$

ka_2 = adsorption rate constant for C_3H_6 $[C_3H_6]^{-1}$

ka_3 = adsorption rate constant for combination of CO and C_3H_6 $[(CO)\ (C_3H_6)]^{-2}$

ka_4 = adsorption rate constant for NO $[NO]^{-1}$

$k°_{rj}$ = frequency factor for k_{rj}

$k°_{ai}$ = frequency factor for k_{ai}

E_{rj} = activation energy for k_{rj} [btu / lb mol]

E_{ai} = activation energy for k_{ai} [btu / lb mol]

R = ideal gas constant, 1.987 [btu / lb mol °R]

T = catalyst temperature [°F]

Further, it was observed that the CO oxidation reaction rate oscillates depending on the reaction conditions and chemical state of the surface [62-65]. Different reasons were proposed to describe CO oxidation oscillation including temperature inertia and CO concentration; however, Pt oxidation and reduction, proposed by Sale et al. [66], is the most reasonable explanation. With an excess amount of O_2, Pt is oxidized to form Pt oxide (PtO), which is less reactive toward CO oxidation, thus lowering the CO oxidation rate. However, as the CO oxidation rate increases, the PtO reduces back, by CO, to metallic Pt, which is more active than PtO. This oscillation in reaction rate was also observed during C_3H_6 oxidation [61]. Yao, who studied the kinetics of CO and C_3H_6 oxidation under excess O_2 over different precious metals and supports, found that the reaction rate, which was reported in the form of a power law, exhibits negative orders with respect to CO and C_3H_6 and positive order with respect to O_2 [67]. Similarly, for CO oxidation over a $Pt/\gamma\text{-}Al_2O_3$ catalyst, the

CO oxidation rate was found to be proportional to the O_2 and inversely proportional to CO partial pressures and at low temperature, below the light-off temperature, the Pt surface is covered with CO [68].

2.3 Aging Effects

Catalyst deactivation (aging) influences research, development, design, and operation of many commercial processes. In diesel engines, the deactivation of the catalyst causes a gradual decrease in performance, resulting in increased emissions from the vehicle. Catalyst deactivation can be classified as chemical, mechanical, and thermal. All the deactivation methods are applicable to diesel exhaust catalysts, but this thesis research is focused on thermal deactivation.

2.3.1 Thermal Degradation

Thermal degradation is caused by exposure to high exhaust gas temperature or heat generated via exothermic reactions, and is a major source of emissions catalyst deactivation. Even though the diesel engine exhaust temperature is lower than that in gasoline engines, the DOC can still be exposed to high temperatures, imposed for example during regeneration of diesel particulate filters [69]. At high temperature, active phase crystallite growth, collapse of the carrier pore structure and reactions between the active phase and carrier or promoters can occur. If the reaction is structure sensitive, catalyst activity can either increase or decrease with increasing metal crystallite size during sintering [70].

High temperature exposure can result in particle sintering, which typically decreases catalyst activity. Sintering refers to the loss of active surface area via structural modification of the catalyst, which is usually a thermally activated process and is physical by nature [71]. Under high temperature conditions, atoms and molecules migrate to form larger particles on the surface of the catalyst. Sintering has been shown responsible for the loss in performance of an aged DOC [71, 72].

Sintering can be divided into two types: active site sintering and carrier sintering. In active site sintering, the surface area of the typically small particles decreases as the particles aggregate to form larger ones. Support sintering can alter the pore structure and therefore size, typically making pores smaller and more resistant to diffusion. In terms of structure change, an example is when γ-Al_2O_3 is transformed into δ-Al_2O_3, and the surface area of the support decreases from 150 to less than 50 m^2/g [73]. Furthermore, at high temperature, the catalytic species can react with the support forming components that are less active.

The presence of certain additives such as BaO, CeO_2, and La_2O_3 are known to reduce support sintering by forming thermally stable spinel phases with alumina. These stabilizers fix the catalytic components to the surface decreasing their mobility and hence crystal growth [70]. Additives on the carrier can affect thermal properties of the catalyst by changing sites or forming new phases. For example, alkali metals accelerate sintering [70]. Sintering is easier to prevent than cure, because it is kinetically slow and typically irreversible.

2.4 Catalyst Design

In this section, monolithic catalyst composition and preparation methods for DOCs are presented. The composition of the DOC and the preparation methods play an important role in the properties and performance of the final product.

2.4.1 Monolithic Catalyst Compositions

Monolithic catalysts are used extensively in environmental applications due to their low pressure drop associated with high flow rates, and thermal and mechanical stability. A frontal view is shown below in Figure 2-1).

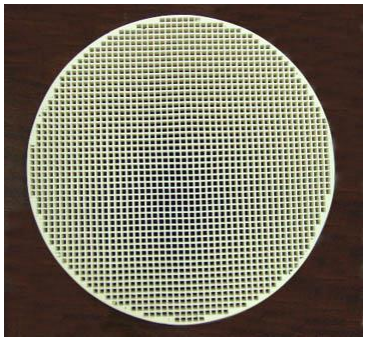

Figure 2-1: Honeycomb monolithic catalyst converter [74].

The monolithic catalyst substrates are usually made of ceramic. Because of the small specific surface area of ceramic substrates, the honeycomb wall is coated with a high surface area material in which the catalytic component is deposited. The majority of commercial ceramic honeycomb catalysts are made of cordierite. Cordierite is most widely used due to its mechanical stability, low thermal expansion coefficient, and the macroporous structure that facilitates the attachment of a powder layer [75].

2.4.1.1 Supports

Catalyst carriers (washcoat) are coated onto the channel wall of the monolith substrate to increase the surface area in order to assist in the dispersion and stability of the active catalytic phase. Most carriers (and all those for vehicle applications) are porous, high surface area metal oxides having high pore volume, capacity, and stability, as well as dispersed catalytic phases during reaction [76]. Zeolites, silica, and alumina are the most common commercial carriers.

High surface area, appropriate pore structure, thermal stability over a wide temperature range, and ability to be used in industry to form pellets or to coat a honeycomb monolith are the most important qualities of the washcoat material [76, 77]. γ–Al_2O_3 combines all these properties and is widely used in DOCs. However, other carriers are sometimes used. For example, in both CO and H_2 oxidation, ceria-supported Pt catalysts are more active than alumina-supported Pt catalysts [78].

2.4.1.2 Active Components

The active phase is the key to the catalysis, and it is usually the most expensive part of catalytic converters. The active phase contains the active sites where the reactions take place. Pt-, Pd-, and Rh-based catalysts are the most common active phases used in automotive pollution control [47, 79, 80]. Rh is very active in NO_X reduction, but its oxidation activity toward CO and HC is less than that of Pt and Pd [81, 82]. Pt catalysts have high oxidation capability for CO and HC, but at the same time are active in SO_2 oxidation at low temperature, which is not desired. SO_2 formation can be lowered by using non precious metal catalysts, although these are typically less active for other reactions compared to Pt [83]. Even though Pd has high thermal stability, it has not been used alone in diesel applications because at low temperature conditions, it is severely poisoned by fuel sulfur [80]. The advantages and disadvantages of Pt and Pd are shown in Table (2-1) [80]. Today, with the reduction of sulfur content in diesel fuel, Pd has become more viable as a DOC component. A Pt/Pd blended catalyst is exceptionally active, more thermally durable, and has a satisfactory tolerance toward sulfur poisoning compared to conventional Pt catalysts in diesel applications [80].

Table 2-1 : Comparison between Pt and Pd in DOC catalyst.

Metal	Advantages	Disadvantages
Pt	• Low temperature activity • NO_2 generation • Lower risk of S poisoning	• More expensive • CO poisoning
Pd	• High CO light-off activity • Low price	• Higher risk of poisoning • Low NO_2 generation

2.4.2 Catalyst Preparation

The catalytic properties of heterogeneous catalysts are strongly affected by every step of the preparation process. The choice of preparation methods depends on the base materials used and the desired physical and chemical properties of the catalyst, with several preparation methods available for a given base material [84]. However, catalyst design is often considered an art. Catalyst manufacturers do not reveal many critical preparation details as they are considered trade secrets to protect the proprietary nature of their product [73]. However, there are well known general procedures for catalyst preparation in the laboratory. Monolith-supported catalysts are prepared in the laboratory through three main steps: impregnation, drying, and calcination.

2.4.2.1 Impregnation

Impregnation is the simplest and most typical commercial procedure for dispersing a catalyst species within a carrier. Often the active metal is dissolved in an aqueous solution and brought into contact with a porous oxide catalyst support. The active metal adsorbs from the aqueous solution onto the support [85].

Based on the total amount of aqueous solution used, impregnation is divided into “wet” and “dry”, also known as incipient wetness. In incipient wetness or capillary impregnation methods, the precursor salt is dissolved in an amount of water equal to the water pore volume of the carrier, whereas in wet impregnation the precursor salt is dissolved in an excess amount of water. Then the aqueous solution containing the precursor is added to the carrier until it is saturated. The carrier adsorbs the catalytic element by capillary force distributing it over the porous surface area. In some cases, after impregnation, additives such as BaO or CeO_2 are added in order to stabilize the active metals and avoid significant movement or agglomeration of the dispersed catalytic species [70]. Dry impregnation is difficult for a large structure, because it is hard to supply the monolith with exactly the amount equal to its pore volume as the liquid needs to travel a long distance to reach all pores

[86]. Therefore, it is difficult to obtain a homogeneous distribution using dry impregnation. On the other hand, in wet impregnation the metal precursor concentration in the liquid is determined based on pore volume of the monolith so that the liquid to be taken by the monolith will produce the desired metal loading. To achieve an even distribution of the metal, it is recommended that the contact time of the monolith in the solution should be short to prevent any excess of metal adsorbing onto the support [86].

There are many studies in the literature on catalyst preparation with attempts to understand the physical and chemical aspects of the impregnation process. The experimental work of Maatman showed that Pt can be uniformly distributed on an alumina carrier by adding salts or acid to the chloroplatinic acid impregnating solution [87]. Heise and Schwarz experimentally and theoretically studied different aspects of impregnation including the effect of pH, ionic strength, and concentration on Pt metal distribution on an alumina support [88-90]. For example, Pt adsorbed and the penetration depth could be controlled by adjusting the pH and ionic strength. Spieker and Regalbuto studied the uptake of Pt on an alumina support as a function of initial Pt concentration, and found that an excess amount of Pt in the impregnating solution leads to Pt self-inhibition based on the ionic strength of the solution [85]. Ruckenstein and Karpe have shown that the total uptake of the metal by the support decreases when the ionic strength of the impregnating solution increases [91]. In addition, Pt uptake increases as the pH moves away from the point of zero charge (PZC), the pH at which the net surface charge is zero [91]. Regalbuto found that Pt uptake increases as the pH is moved away from the PZC, and slowed at extreme pH due to the ionic strength of the impregnating solution [92].

2.4.2.2 Drying

The next step in monolithic catalyst preparation is drying the catalyst, typically at about 110 °C, to get rid of excess water and other volatile species. The rate of drying can influence the deposition of the active materials in the pores [76]. Studies on supported catalysts such as Ni/alumina

have shown that at a low drying rate most of the catalytic species are deposited in the deep end of the pores; whereas, at a high drying rate, they are deposited in the entrance of pores [93, 94]. Drying rate can also affect distribution of the active metal along the monolith. In an oven dried monolith, Figure (2-2), the distribution was much lower in the middle parts of the monolith (as indicated by the lightly gray color in the middle) than that at the ends due to humidity gradients that formed between the inside and the outside on the channels. In room temperature drying, the humidity gradient was lower than that of the oven, but only a small zone, in the middle, was not covered by the active metal because this zone was not completely dried before calcination. It is therefore very crucial to control the temperature and humidity during the drying process.

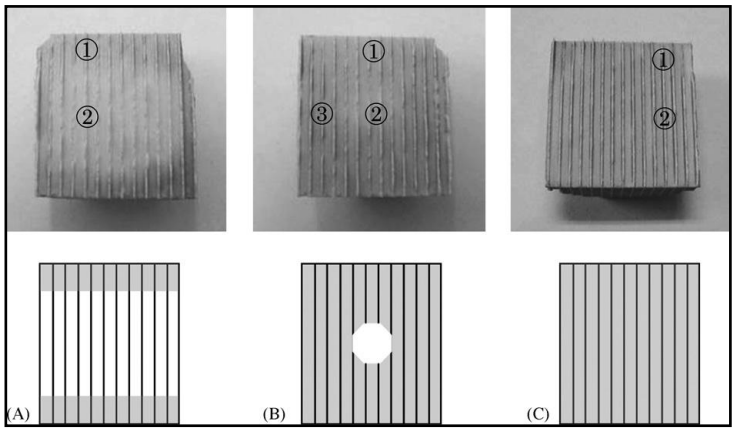

Figure 2-2 : Axial section of Ni impregnated monoliths obtained by (A) oven drying, (B) room temperature drying and (C) microwave drying followed by calcination at 550 °C [93].

2.4.2.3 Calcination

The final stage in monolithic catalyst preparation is calcination. Catalysts are calcined at high temperature to decompose precursor salts and other preparation components. Calcination is typically in air at a temperature higher than that used in the catalytic reactions, thereby also stabilizing the catalyst activity. Calcination at high temperatures, above 500 °C, can crack the monolith by pressure build up in micropores via the rapid heat up of trapped H_2O. Furthermore, at high calcination

temperatures, exothermic reactions due to decomposing salts can accelerate sintering [73]. Therefore care must be taken when calcining the catalysts.

2.4.3 Optimization of Active Metal Distribution

Catalyst manufacturers have studied various design factors to improve the performance of the catalyst, especially in terms of improving cold start performance and reducing degradation effects. Advances in catalyst coating technologies have enabled both washcoat and precious metals to be distributed non-homogeneously along the length of a catalyst monolith [95]. Theoretical studies focused on oxidation reactions or NO_X reduction, have shown that an axial distribution of the active metal, with higher loading in the upstream section of the monolith and lower loading in the downstream, is superior to that of a uniform distribution, while utilizing the same amount of active metal [22, 81, 95-104]. Collins and colleagues optimized three-way catalyst performance by targeted zoning of precious metal [81]. They found that most pollutant conversion occurs in the front portion, and consequently the optimum catalysts have the majority of the precious metal content there [81]. Furthermore, through analysis of CO, HC, and NO_X conversion along the catalyst length, results have shown that CO and HC are converted in the front portion of the catalyst whereas NO_X conversion relies on the total volume of catalyst [81]. Based on a one-dimensional, two-phase model of the light-off behavior and cumulative emissions of a generic catalytic monolith, Ramanthan and his colleagues found that for a fixed amount of metal loading, redistribution of the active sites with more near the front section of the monolith can achieve higher conversion and lower ignition temperature [99-102]. If catalyst fouling is an issue, then multiple-zone distribution is the optimum design with more catalyst in the middle [100]. The optimal axial distribution of the active catalyst was also investigated to minimize cold start emissions [22, 102, 103]. Based on their numerical study, the authors found that a high concentration of the active metal in the upstream section of the monolith was optimal to

minimize cold start emissions because it ensured that the highest temperature is maintained at the inlet of the monolith and heat transfer by convection dominates [22, 103]. Similar results were observed in a separate study where different Pt distribution profiles along the reactor length were examined, and it was found that the best light-off performance was achieved with Pt concentrated in the upstream section of the monolith [104]. Similarly, precious metal usage in DPFs was optimized by non-uniform catalyst coating, with more catalyst in the front part showing improvements in CO and HC conversion as well as cold start emissions [101].

In addition to the light-off temperature performance, Tronci et al. [22] suggested that degradation due to sintering is more severe in the case of a uniform active site distribution. Even though the surface area loss in the front section of the non-uniform active site distribution catalyst (front-loaded catalyst) was larger than that of the uniform distribution, the remaining activity was high enough to maintain the minimum heat to keep a high solid temperature and avoid monolith cooling by the inlet gas [22]. Furthermore, based on a theoretical study of methane oxidation under steady-state and transient operating conditions, non-uniform catalyst distributions have the potential to achieve lower thermal stresses as the temperature gradient in the catalyst is lower than that for a uniform distribution [96]. In some conditions, catalyst distribution with high loading at the entrance has no effect on conversion improvement, such as when the space velocity is too high for high conversions to be achieved in the higher loaded region (above SV=1,000,000 hr^{-1} in this example) [105]. This suggests, as does other work, that there is a range of catalyst loadings in which the optimal design corresponds to having more catalyst at the front but not for all [98]. For example, in an adiabatic reactor, the optimal active component distribution profile was shown to be axially decreasing along the reactor length for first-order exothermic reactions and increasing for endothermic reactions, while a uniform active component distribution profile is optimal for first order reactions in an isothermal reactor [105].

Precious metal component zoning in lean NO_X trap system performance has shown that reverse precious metal zoning (zoned with low loading in the front section of the monolith followed by a zone with higher loading) can be used to reduce the cost of the LNT while essentially maintaining the NO_X reduction performance, compared to a similarly sized trap with a uniform, high precious metal loading [99]. After high temperature aging, the back half of the tested NO_X trap had better performance than the front half, because the front of catalyst was exposed to higher temperatures than the back due to the heat generated from exothermic HC and CO oxidation. Therefore, high loading at the back of the catalyst protects the active sites in that zone and better preserves the low temperature NO_X performance of the LNT [99]. In a more recent study of an aged diesel truck aftertreatment system, a Ford research team found that the back of a DOC deteriorated most significantly than the rest of the catalyst because the back is most affected by the heat generated from the exothermic reactions, specifically burning hydrocarbons during filter regeneration [39].

2.5 Hysteresis Behavior

As was mentioned earlier, CO, NO and C_3H_6 TPO experiments, with tests done with individual reactants and in mixtures, were conducted as a part of an Auto21 project. In these experiments outlet gas concentrations and temperatures, across the monolith length, were monitored during ignition and extinction processes. Preliminary results showed interesting hysteresis behavior in the case of gas mixtures, specifically CO inverse hysteresis behavior in a CO and C_3H_6 mixture. This phenomenon was characterized and therefore, the hysteresis behavior of CO is discussed in the following section.

The oxidation of CO on Pt has been investigated in numerous studies beginning with the classic work of Langmuir [35, 48, 106-109]. CO oxidation is known to occur through a Langumir-Hinshelwood (LH) dual-site mechanism, in which the reaction occurs between CO and O_2 after both molecules adsorb on the surface [47, 48, 56]. CO oxidation studies during a temperature ramp up and

then ramp down have shown hysteresis behavior, with higher conversion during extinction [47, 110-123]. This higher conversion during extinction is often called normal hysteresis behavior. Researchers have proposed different reasons to explain the higher activity of the catalyst during extinction, of which surface inhibition by CO adsorption, reaction exotherm, and thermal inertia of the catalyst are the most common. Carlsson and Skoglundh [111], explained normal hysteresis as a combination of three possible reasons: (1) inherent kinetics bistability, (2) interaction between reaction kinetics and diffusion phenomenon, and (3) local overheating of the catalyst surface. Hysteresis, or multiplicity, in CO oxidation on Pt was first observed by Beusch et al. [110] in 1972. In addition to the Beusch study, Wei and Becker [123], Schmitz et al. [118], Hegedus et al. [115], and Chakrabaty [112] have demonstrated that interaction between surface reaction and diffusion can lead to hysteresis behavior. Hegedus et al. [115] concluded that CO oxidation hysteresis behavior is due to the interaction of the negative-order kinetics for CO oxidation with the diffusive resistances of the catalysts. For example, the region of hysteresis could be broadened by increasing the diffusion resistance of the tested Pt/Al_2O_3 catalyst by partially aging the catalyst [115]. Oh et al. [116], who investigated the role of intrapellet diffusion resistance in hysteresis during CO oxidation over $Pt\text{-}Al_2O_3$, showed that the width of conversion-temperature hysteresis loop is a function of particle size and it could be eliminated if the catalyst particle size is very small. In addition to the reaction-diffusion interaction explanation, Chakrabaty et al. [112] stressed the effect of surface reaction-sorption interference. For example, multiple steady states were observed depending on whether CO, O_2, or CO and O_2 are preadsorbed on the catalyst [112]. The oscillations in CO conversion observed in the multiplicity region of CO oxidation were explained partly by switches in adsorbate concentrations [112], as mentioned above. Eigenberger proposed that two or more surface rate steps where CO is chemisorbed on Pt could result in multiple steady states without obvious changes in reaction conditions [124]. A transient, in-situ FTIR study of CO oxidation over a Pt/Al_2O_3 catalyst, by Carlsson et al. [56],

associated CO oxidation hysteresis with different rates by which Pt is oxidized and reduced as a function of gas-phase composition. Their results showed that a transition during the extinction process from an O_2 to a CO covered surface occurs on a much longer time scale than the reverse transition from a CO to O_2 covered surface during the ignition process. The authors concluded this was due to Pt oxide formation, during extinction, which changes the adsorption kinetics [56]. In their CO oxidation model, Salomons et al. [47] suggested multiple steady states with the hysteresis effect corresponding to two Pt states; predominantly CO covered during ignition and O_2 covered during extinction. The model was based on adsorption and surface reaction using a LH mechanism, with a dissociative chemisorption step for oxygen requiring two surface sites, whereby ignition and extinction processes correspond to the two states of predominantly CO covered or O_2 covered [47]. This idea of surface coverage is consistent with research by Langmuir and other researchers who observed that at high temperature and excess oxygen, active sites are entirely covered with oxygen and the reaction is limited by the rate at which CO adsorbs to the surface [106, 107, 109]. However, at low temperature the surface is covered with CO and the reaction is inhibited by strong adsorption of CO on the surface, a phenomenon known as CO self-poisoning [35, 106, 108, 109]. The effect of CO self-poisoning increases with increasing CO concentration [48], and decreases with increasing temperature, with negligible inhibition above 400 °C [35, 107].

Another explanation was put forward by Subbotin and Gudkov et al [113, 119-121, 125], who explained hysteresis by local "overheating" of the active sites on the catalyst, caused by relatively slow dissipation of the energy through dispersed catalyst particles. They proposed it is possible to explain the hysteresis behavior in exothermic reactions, such as CO oxidation, by overheating of the active sites of the catalyst via the exotherm. This conclusion was extended to another catalytic system by Subbotin et al. [121] who tested hysteresis in CO oxidation on both supported and unsupported catalysts. They concluded that CO conversion during extinction was higher than CO conversion

during ignition due to local overheating of an active center rather than a transition from one steady state to another [121]. This was supported by their observation that the higher the number of active sites of the catalyst, the larger the hysteresis loop became; and in the case of bulk metals, no hysteresis was observed due to their ability to disperse the reaction heat [121]. In an exothermic reaction, such as CO oxidation, the rate of heat being liberated is larger than the rate of heat being dissipated into the environment due to the low heat conductivity of the support or inactive catalytic mass in which heat is released. Therefore, during the extinction phase when the temperature of the inlet gas decreases, the temperature drop over the catalyst surface lags, staying warmer [113, 125]. Similar conclusions were made in another study, of the oxidation and methanation of CO and propylene hydrogenation, as temperature hysteresis was explained by overheating of the active sites due to slow removal of reaction heat [126]. In addition, it has been observed that the width of hysteresis loop increases with increasing active component and CO concentration in the reaction [119-121].

Unlike CO oxidation, Hauptmann et al. [114] have shown that NO oxidation on a Pt catalyst under excess oxygen conditions exhibits "inverse hysteresis" as the catalytic activity during ignition exceeds the activity during extinction. The reason for inverse hysteresis behavior is that at high temperature Pt is oxidized by NO_2 to form an oxide phase that is less catalytically active than metallic Pt and at low temperature Pt oxide is reduced back by NO to metallic Pt, a phenomenon known as reversible oxidation of Pt. Thus, during the extinction phase, which initiates at high temperature, Pt is in a less active state than that during ignition. In addition, in a $CO/NO/O_2$ mixture, CO hysteresis behavior switches from normal hysteresis to inverse hysteresis, which the authors suggested was due to reversible oxidation of the Pt surface [114].

Chapter 3: Methodology

The thesis work is divided into two main topics: (1) a comparison study between the performance of uniformly and non-uniformly distributed catalysts before and after thermal aging, and (2) reactant species interactions on a DOC, specifically CO oxidation hysteresis behavior in a mixture of CO and C_3H_6. In the first stage, fresh and aged homogeneous catalysts' performances were analyzed using TPO and spatially resolved experiments to study the reactions and active regions along the axial direction of the catalyst. Based on the analysis, a non-homogeneous catalyst with a distribution of active metal along the length was designed and tested using the same conditions that were previously used for the homogeneous catalyst. Characteristics including total loading and dispersion of the fresh and aged samples were measured. During my thesis work at UW, experiments were performed as part of an Auto21 project. A matrix of experiments was designed to study the interactions and effect of CO, C_3H_6, and NO on the overall performance of a DOC. These data were then used at University of Alberta in developing a predictive model to characterize DOC reactions during ignition and extinction processes. In this work, low catalytic activity were obtained during the extinction process, which is rarely characterized, leading to further investigation with the focus on understanding the hysteresis behavior of CO oxidation.

3.1 Catalyst Preparation

A cordierite substrate in monolithic form (400 cells per square inch – cpsi) with 1.59 g/in^3 (97.03 kg/m^3) γ–Al_2O_3 coating (donated by Johnson Matthey) was used to prepare Co-based catalysts, to practice, and Pt-based catalysts with various axial distributions along the catalyst length. The samples provided were 9" in diameter and 6" in length. The precursor for Co was cobaltous nitrate-hexahydrate ($CoN_2O_6.6H_2O$) purchased from Fluka and for Pt was tetraammine platinum (II) nitrate,

$Pt(NH_3)_4(NO_3)_2$, purchased from Alfa-Aesar. The monolithic samples were cut to 1" diameter and 2.4" length.

For the catalyst with a non-uniform distribution, the goal was to prepare a sample with more catalyst deposited in the front section of the monolith while keeping the overall loading the same as that of the uniform sample. This was not to suggest that such a distribution is the optimum – experimentation and modeling lead catalyst design, but the modeling studies discussed in the literature review overall suggest this leads to improved performance. The monolith was prepared using the wet impregnation method. Before impregnating the monolith, the water pore volume of the support was determined by immersing the monolith sample into DI water and measuring the weight difference between wet and dry samples.

The sample was then dried in an oven at 120 °C for 2 h before impregnation. For uniform distribution, based on the desired loading, a catalyst solution was prepared by dissolving a certain amount of the precursor into DI water. For example, water up-take was measured to be 5 g, and Pt tetra-ammine-platinum (II) hydroxide powder was dissolved in DI water to make the precursor solution. The precursor solution was diluted with 30 ml of DI water, so that each time the monolith is immersed in the solution, it would adsorb an amount of Pt equal to 0.5%. The monolith was dipped into the fresh solution, quickly removed, and an air line was used to blow excess solution out of the monolith channels. The sample was then air dried for 2 hrs and then in an oven at 120 °C overnight. For the uniform catalyst this process was repeated twice so that the total Pt loading equaled 1%, whereas for the non-uniform catalyst, the whole monolith was dipped once and the front 2 times to make a two-zone monolith with Pt loadings equal to 1.5% in the front and 0.5% in the back. Finally the sample was calcined for 4 hrs at 500 °C. Figure (3-1) shows the uniform and non-uniform catalysts after Pt loading.

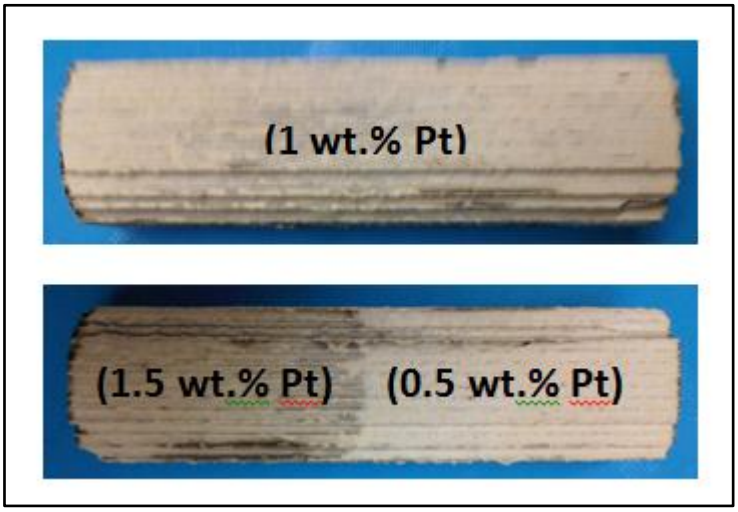

Figure 3-1: Monolith samples with uniform and non-uniform catalyst distribution.

In order to validate the procedure used in sample preparation and understand the results obtained, certain features of the catalyst samples were characterized before and after aging. There are many techniques to characterize catalysts; here, simply total loading and dispersion were used to validate the zone coated catalyst and examine the effects of degradation in each zone. For these characterizations, powder samples are required, so the monolith-supported samples were crushed for testing. For the non-homogeneous samples, the monolith was cut into two sections and each section was analyzed separately. Inductively coupled plasma (ICP) analysis was used to measure the total loading of active metal. The samples were prepared for ICP by dissolving the crushed monolith sample in a mixture of acids. 0.1g of the monolith sample was crushed to fine powder and dissolved in 4 ml of nitric acid (HNO_3), 3 ml of hydrochloric acid (HCl), and 3 ml of sulfuric acid (H_2SO_4) while heating to 150 °C and continuously stirring the mixture. The mixture was then diluted with DI water before running the ICP test. Samples from the uniform catalyst and the front and back part of the non-uniform catalyst were tested using a Prodigy High-Dispersion ICP Spectrometer. The uniform sample contains 1.01 wt.% Pt, and the front and back parts of the zoned sample contain

1.50% and 0.55% Pt, respectively. Due to the lower cost of Co-based catalysts compared to Pt-based catalysts, before preparing Pt-based catalysts, several Co-based catalysts were prepared and analyzed by ICP to ensure the validation of the procedures used. ICP results of the Co samples are shown in Appendix (A). The uniform Co-based sample before and after deposition of the active metal is shown in Figure (3-2).

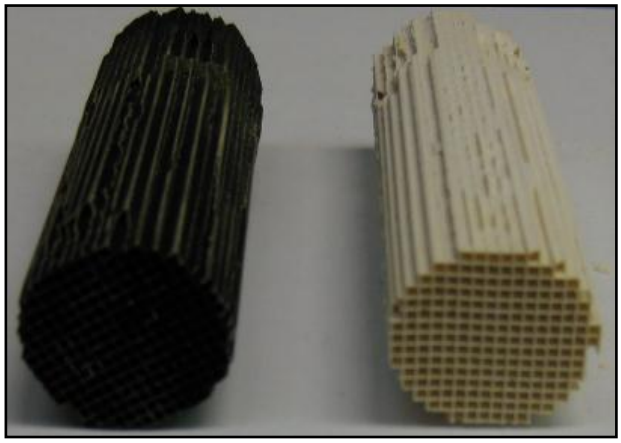

Figure 3-2: Monolithic sample before impregnating (white) and after impregnating (black) with the active metal.

The dispersion of the active sites over the catalyst before and after thermal aging was measured by H_2 chemisorption. The crushed powder of the tested sample was loaded into a Hiden Catlab micro-reactor. The catalyst was pretreated with H_2 at 450 °C for 30 minutes then the catalyst was exposed to 26 pulses of 100 µl of 5% H_2 with a He balance for 30 seconds with 1 minute of pure He between each pulse. The detailed reaction protocol for H_2 chemisorption is shown in Figure (3-3).

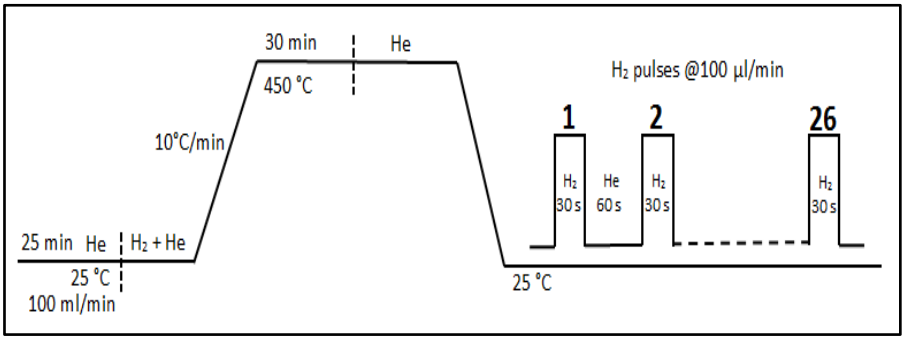

Figure 3-3: H_2 chemisorption protocol.

3.2 Catalyst Performance

Catalyst performance was tested by measuring the temperature and gas concentrations at the reactor outlet and along the axial direction of flow. To do that, two well-known methods were used: (1) temperature programmed oxidation and (2) spatially resolved capillary-inlet mass spectrometry (SpaciMS).

3.2.1 Temperature Programmed Oxidation (TPO) Experiments

This method was used to evaluate the effect of different flow conditions on the performance of the DOC as a function of temperature. In these experiments, the temperature of the catalyst was ramped up and/or down, while measuring the gas concentrations of the outlet flow. TPO of different reactant mixtures was utilized to test the catalytic activity of the fresh and aged samples with different axial distributions of the active metal. The tube reactor system used for such tests consists of a gas mixing unit, the actual tube reactor, and gas analyzers, as shown in Figure (3-4). Pure gases and gas mixtures were supplied by Praxair, except N_2, which was generated using a nitrogen generator manufactured by OnSite, and were metered with Bronkhorst mass flow controllers. Water was introduced downstream after the dry gas mixture had been heated. The water system consists of a water tank, carrier nitrogen gas, and a Bronkhorst controlled evaporator mixer. The wet gas mixture

was further preheated prior to entering the reactor. The pre-heater raised the temperature of the feed gas to a value close to the test temperature. The reactor system consists of a furnace, 26" quartz tube, small quartz tubes, and the catalyst sample. The sample was inserted into the larger quartz tube, which was placed inside a Lindberg Minimite temperature-controlled furnace as shown in Figure (3-5). The catalyst was wrapped with 3M insulation material to seal the catalyst in the tube, and ensure that no gas slips around the sample. To stabilize the temperature inside the reactor and better preheat the gases, smaller quartz tubes were placed in the front part of the reactor, while the catalyst sample was placed in the back. For temperature measurements, three K-type thermocouples were placed at different positions along the catalyst length.

The effluent gas of the reactor was analyzed using a MKS MultiGas 2030 FT-IR analyzer and a Hiden HPR20 mass spectrometer (MS). Both instruments measure the concentration of gases as a function of time. The FTIR instrument was used to measure the concentrations of CO, CO_2, NO, NO_2, N_2O, C_3H_6, and H_2O. The MS was used to measure O_2 and H_2, and also used in spatial resolution experiments to measure the concentrations of C_3H_6, NO, NO_2, CO_2, H_2O, O_2, and H_2. In the spatial resolution experiments, the composition of the gas at different locations inside the sample was measured by moving the capillary inlet of the MS to the specified location.

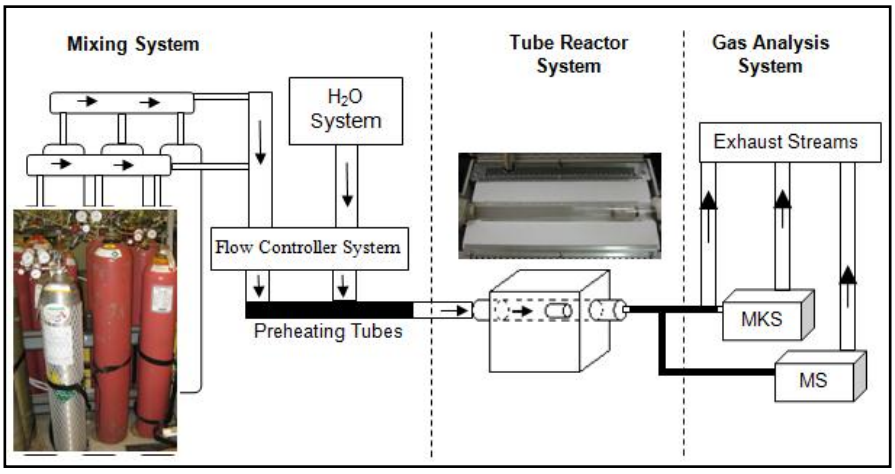

Figure 3-4: Flow diagram of the tubular reactor system.

Figure 3-5: Furnace portion of the tube reactor system, with a DOC catalyst inserted.

Isothermal inlet and TPO experiments were conducted. For TPO, the concentrations of gases at the catalyst outlet and temperature along the catalyst were measured as a function of time. For the isothermal inlet experiments, the temperature was set to some nominal value, using an upstream thermocouple, and the concentrations of gases at different locations in the catalyst were measured once steady-state was achieved. These measurements were repeated at different temperatures. In all experiments the feed stream contained O_2, H_2O, CO_2, He, and reactant gas(es), with N_2 as the balance gas. Table (3-1) describes the set of TPO experiments that was used to test each catalyst.

Table 3-1 : Experiment Matrix.

Run	CO [ppm]	C_3H_6 [ppm]	NO [ppm]	Flow rate [L/min]
1	1000			10
2		1000		10
3			200	10
4		1000	200	10
5	1000			28
6		1000		28
7			200	28
8		1000	200	28

3.2.2 Spatially Resolved Capillary-Inlet Mass Spectrometry (SpaciMS) Experiments

Spatially resolved capillary-inlet mass spectrometry (SpaciMS) was used to measure the gas concentrations at different locations along the monolith, at a constant upstream temperature. Due to reaction exotherms, and decreasing reactant species concentrations and increasing product concentrations down the length of catalyst, the activity and kinetics varied along the catalyst length. This technique provided information about the progress and behavior of different reactions, and the change of reaction rates as a function of position along the catalyst, which is critical in understanding the effects or activity of not only a normal, homogeneously distributed catalyst, but even more critical in understanding catalysts with different active site densities. These experiments were run at different temperatures and a variety of feed gas compositions. Figure (3-6) shows the configuration of the SpaciMS technique. A silica capillary, I.D. = 0.3 mm and O.D. = 0.34 mm, with a throughput of 20 mL/min was connected to the Hiden HPR20 MS and placed inside one of the central channels of the monolith. The capillary was heated along its entire length to avoid condensation. 1000 ppm C_3H_6, 200 ppm NO, 120 ppm He (added for calibration), 5% H_2O, 10% O_2, and N_2 as a balance were fed to the

reactor at 80 °C. The temperature was then raised to 220 °C. After reaching steady state, the capillary was moved from the inlet (0 cm) to the back (7 cm) of the monolith in 1 cm increments in order to measure the gas composition at 8 different locations along the catalyst length. This was also done at 270 °C. The pretreatment protocol before each experiment was: the sample was heated to 450 °C while flowing 10% H_2O, 5% CO_2, and balance N_2; then 10% O_2 was added to the mixture for 5 minutes followed by 2000 ppm of H_2 for 5 minutes; and then the temperature was decreased to 80 °C before starting the experiment.

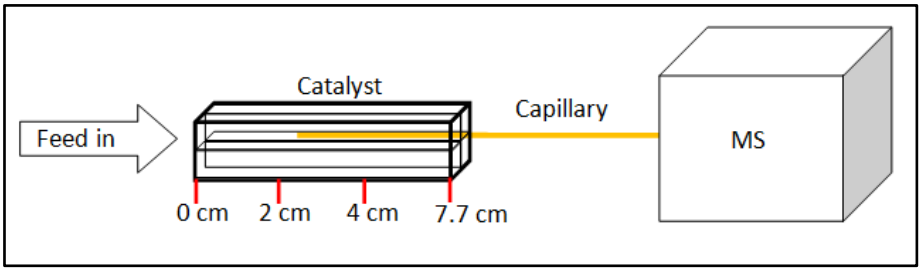

Figure 3-6 : SpaciMS configuration.

3.3 Catalyst Aging

After collecting data using the fresh sample, the monolith was thermally deactivated and the experiment methods described above were again used to characterize the aged sample. For thermal degradation, two methods were used, homogeneous and heterogeneous thermal aging, both representing different conditions in real application. In the first method, the sample was heated slowly in a furnace to a chosen temperature so that no temperature gradients exist in the catalyst. This method represents the case where the catalyst is exposed to constant and high temperatures, such as when exhaust gas temperature is the only source of heat. In the second method, the sample was thermally degraded using the heat generated during an exothermic reaction. The heat released from the exothermic reaction causes an increase in the temperature of the zone where the reaction takes

place, which causes a gradient in temperature along the catalyst. These temperature gradients lead to different degrees of thermal degradation along the axial length. This method represents the case when exothermic HC or CO oxidation occurs on the catalyst causing an increase in temperature at distinct locations. In real application degradation is a combination of both exhaust gas temperature and exothermic reactions. First, the samples were heterogeneously aged using the exothermic heat of propylene oxidation. Then the samples were placed in an oven at higher temperature to further deactivate the whole sample; homogeneous aging. The temperature of the homogeneous aging, 750 ℃, was higher than that of the heterogeneous aging to ensure that the all parts of the sample were equally affected. Using a lower temperature, i.e. close to that of the heterogeneous aging, would not necessarily result in "homogeneous" aging.

For the homogeneous aging, the sample was placed in a 47900 Barnstead Thermolyne furnace at 750 ℃ for 4 hours. For heterogeneous aging, the inlet gas stream was cycled between an inert composition and a phase containing O_2 and C_3H_6, with C_3H_6 oxidation being exothermic and acting as the heat source. The catalyst, at approximately 500 ℃, was exposed for 10 seconds to the exotherm phase, which consisted of 7000 ppm C_3H_6, 10% O_2, 5% H_2O, and balanced by N_2, and 150 seconds to the inert phase, which consisted of 5% H_2O and balanced by N_2. This cycle was repeated 50 times. The same TPO and steady-state experiments were repeated after thermally aging the catalyst. Figures (3-7) and (3-8) show the temperature profile inside the standard and zoned samples. The heterogeneous aging protocol resulted in the front temperature reaching around 550 ℃, and the back about 680 ℃.

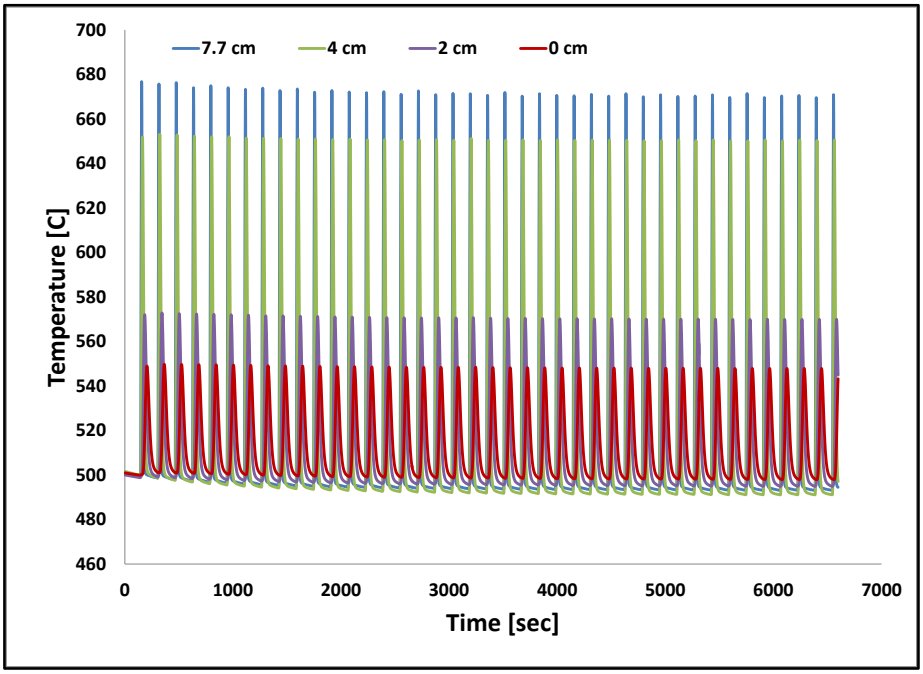

Figure 3-7 : Temperature data at different locations of the standard sample during heterogeneous aging.

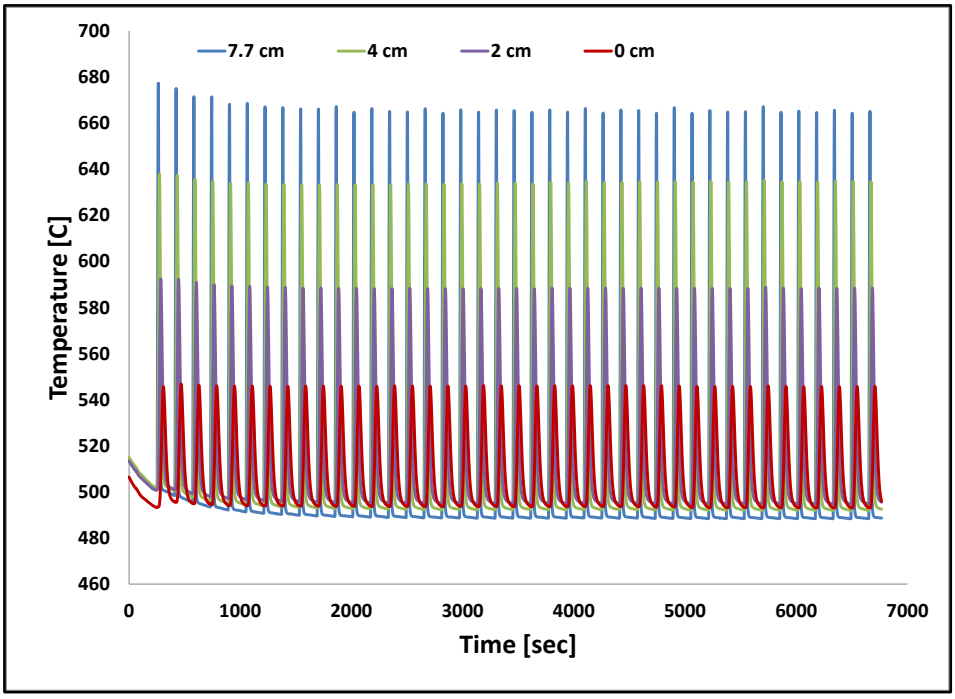

Figure 3-8 : Temperature data at different locations of the zoned sample during heterogeneous aging.

Chapter 4: Improved CO, Hydrocarbon and NO Oxidation Performance Using Zone-Coated Pt-Based Catalysts*

4.1 Abstract

The effect of an axial Pt distribution along a diesel oxidation catalyst (DOC) was investigated by comparing a standard catalyst, with a homogeneously distributed Pt amount along the length, with a non-homogeneously distributed catalyst (zoned). The zoned catalyst had more Pt located at the upstream portion, and less downstream, while maintaining the same total amount of Pt as the standard case. The effects of flow rate on NO, CO or C_3H_6 oxidation, and during oxidation of NO and C_3H_6 as a mixture, were used for the comparison. The reaction details along the catalyst were also resolved using spatially-resolved, capillary inlet mass spectrometry (Spaci-MS). Results showed that the performance of the two catalysts are similar at low flow rate and with a single reacting gas, while the zoned sample works better for CO and C_3H_6 oxidation as the flow rate increases, and better for NO oxidation in a NO/C_3H_6 gas mixture. With CO oxidation or C_3H_6 oxidation, the superior performance of the zoned sample is due to a larger, localized exotherm and a decreased self-poisoning effect. The exothermic reaction heat produced in the front part of the zoned catalyst allows it to reach higher temperature at the front faster than the homogeneous/standard sample and it also lowers the effect of self-poisoning by converting most of the reactants in the front part. NO oxidation, being kinetically more challenging, occurs along the entire length of catalyst at low temperature, not achieving near 100% conversion in these tests. Spatially-resolved experiments during C_3H_6 and NO oxidation, as a mixture, show that NO oxidation starts after C_3H_6 is consumed. Therefore, for the zoned sample, C_3H_6 is oxidized closer to the inlet portion of the catalyst, where a higher density of Pt is located, leaving the rest of the catalyst for NO oxidation. However, with the standard sample, C_3H_6 oxidation utilizes a larger part of the catalyst leaving a smaller portion of the monolith for NO oxidation.

*See Appendix C for permission.

4.2 Introduction

The diesel oxidation catalyst (DOC) has been used in many heavy duty applications since the 1970's. DOCs are used to convert, or help convert, carbon monoxide (CO), hydrocarbon (HC), and nitrogen oxide (NO_X) emissions from diesel engines into less harmful components. Today, DOCs can remove CO and HCs from diesel emissions with efficiencies reaching more than 90% [1]. However, with increasingly strict environmental regulations for vehicle emissions, more research is needed to improve the performance of DOCs to meet the new standards, especially at low temperature. Even though CO and HC oxidation on a DOC are seemingly uncomplicated reactions, the low temperature of diesel engine exhaust impacts catalyst efficiency during low-speed driving or the cold start emissions period, i.e. the first 1-2 minutes after starting the engine [127].

Many sources in the literature have observed that the CO oxidation reaction is inhibited by CO adsorption at low temperature, a phenomenon known as CO self-poisoning [47, 56]. This inhibition by CO decreases as temperature increases [35]. Similarly, the C_3H_6 oxidation reaction is also self-inhibited by C_3H_6 chemisorption on the catalyst surface at low temperature [35]. In a study of three-way catalysis, Collins et al. found that CO and HC oxidation reactions occur in the front portion of catalyst once light off has occurred [81]. Similar results were observed for C_3H_6 oxidation over Pt/Al_2O_3 [128]. Evidence shows that C_3H_6 oxidation under certain test conditions occurs via back-to-front light-off and the reaction zone moves closer to the inlet as the temperature increases [128, 129]. This is due to a combination of conduction along the monolith and associated decreased self-poisoning. NO oxidation to NO_2 is an important reaction over a DOC, as the presence of NO_2 can enhance the performance of other downstream catalysts in the emissions control system, such as selective catalytic reduction, lean NO_X traps and diesel particulate filters (DPF) [24, 130]. However, NO oxidation is kinetically limited at low temperature and thermodynamically limited at high temperature, with conversions typically lower than those of CO and HC species [131].

Reducing the cost of the DOC is a common target for catalyst manufacturers. A major contributor to the DOC cost is of course the precious metal component, usually Pt or Pt/Pd blends; therefore, efficient use of the catalyst can reduce the cost while maintaining the same performance. Preliminary research, based on mathematical modeling, has shown that an axial distribution of the active metal, with higher loading in the upstream section of the monolith and lower loading in the downstream, is superior to that of a uniform distribution, while utilizing the same amount of active metal [22, 95-97, 101-103, 105, 132]. Collins et al. optimized three-way catalyst performance by targeted precious metal zoning [56]. As mentioned above, they found that most CO and HC conversion occurs in the front portion, and consequently the optimum catalysts have the majority of the precious metal content there. Optimal axial distribution of the active catalyst has been investigated to minimize cold start emissions [95, 102, 133]. Tronci et al. numerically investigated the effect of catalyst distribution on cold start emissions in a monolithic catalyst converter. Based on their model, they predicted that a high concentration of the active metal in the upstream section of the monolith was optimal to minimize cold start emissions because it ensured that the highest temperature is maintained at the inlet of the monolith and heat transfer by convection dominates [22]. Kim et al. [95] used a one-dimensional catalyst model to predict the optimal design of axial noble metal distribution on the performance of a Pt/Rh-based catalytic converter. Based on their model, lower light-off and CO emissions were achieved with a design that contained more catalyst in the upstream section and lower catalyst in the downstream section, compared to that with a uniform distribution. In another study, Khanaev et al. [133] also predicted that in order to lower the CO oxidation light-off temperature while maintaining the same performance as an uniformly distributed catalyst, the active component should be concentrated in the inlet section of the monolith. Ramanathan and colleagues [102] simulated the cumulative cold start emissions of a monolithic catalyst converter with a non-uniform catalyst loading. Based on their mathematical model, they found that cold start emissions

were reduced by redistributing the catalyst with more catalyst near the inlet. Similarly, Koltsakis et al [97] found that catalyst zoning with more catalyst in the front is favorable for CO and HC conversion in a DPF.

In this work, the performance of uniformly distributed catalyst was compared to that of a zone-coated catalyst. Both samples contained the same amounts of Pt, but the zoned sample had more located at the inlet and less at the outlet. This represents a first experimental study of these non-uniform distributions.

4.3 Experimental Procedures

An Al_2O_3 washcoated cordierite honeycomb monolith brick, with a 1.59 g/in^3 (97.03 kg/m^3) Al_2O_3 loading, and a 325 cell/in^2 (cpsi) cell density, was provided by Johnson Matthey. Samples were cut to 1" in diameter with a length of 3". 5 g of tetraammine platinum (II) nitrate ($Pt(NH_3)_4(NO_3)_2$, Alfa Aesar), was first dissolved in 250 ml of water. To make the uniform catalyst with 1% Pt loading, the sample was dipped twice in the Pt-solution, and each time 0.5% Pt was loaded. Between impregnations, the sample was dried in air overnight, and heated in an oven to 300°C for 1 hr to evaporate H_2O and fix Pt. The zoned catalyst with 1.5% Pt loading in the front and 0.5% at the back was prepared by dipping the whole catalyst once and the front half two more times. Similarly, after each dipping the sample was dried in air overnight, and heated to 300°C for 1 hr. Finally, both samples were calcined at 500°C for 4 hrs.

The amounts of Pt in both samples were measured using the inductively-coupled plasma (ICP) technique. Samples from the homogeneous catalyst and the front and back part of the zoned catalyst were tested using a Prodigy High-Dispersion ICP Spectrometer. The homogeneous/standard sample contains 1.01 wt.% Pt, and the front and back part of the zoned sample contains 1.50% and 0.55% Pt, respectively.

The schematic of the monolith test reactor used is shown in Figure (4-1). The sample was wrapped with 3M insulation, to prevent gas bypass around the sample, and placed in a horizontal quartz tube with three thermocouples; two to measure the inlet and outlet temperatures and one placed 2 cm from the inlet face inside one the central channels. CO, C_3H_6, NO, CO_2 and He, were supplied as compressed gas cylinders by Praxair, and N_2 was generated using a nitrogen generator manufactured by OnSite Gas Systems. The gases were fed to the reactor with Bronkhorst mass flow controllers. Water was introduced using a Bronkhorst CEM system. The feed gases were mixed and heated before entering the reactor. All inlet and outlet lines were heated and insulated to prevent water condensation. The composition of the outlet gas was analyzed using an MKS MultiGas 2030 FT-IR. A Hiden HPR20 MS connected to a capillary for gas sampling within the reactor, known as spatially-resolved capillary inlet mass spectrometry (Spaci-MS), was also used to spatially resolve reaction patterns inside the monolith sample. More detail about the Spaci-MS set-up can be found in previous work [134-136]. Before running experiments, the temperature gradient across the catalyst was checked by flowing inert gas, N_2, and ramping the temperature from 80°C to 500°C at 5°C/min. The maximum temperature difference between the front and the back of the catalyst was about 5°C. To avoid the effect of exothermic reactions on the temperature, the front thermocouple was used to compare data.

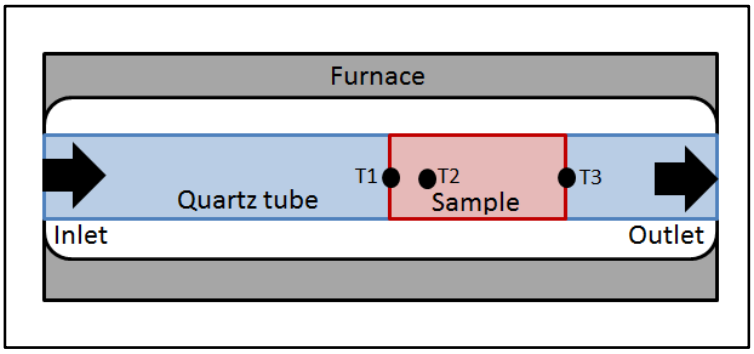

Figure 4-1: Diagram of the monolith reactor.

The gas compositions and flow rates during the experiments run are described in Table (4-1). Temperature-programmed oxidation (TPO) was used as the test technique. The feed stream consisted of CO, C_3H_6 or NO, or a combination of C_3H_6 and NO, always in the presence of 10% O_2, 5% H_2O, 5% CO_2, and N_2 as the balance. Performance was tested under low and high flow rate conditions: 10 and 28 L/min, corresponding to space velocities of 19200 and 53700 hr^{-1}, respectively, at STP (273K and 1atm). The TPO experiments were performed by ramping the temperature from 80°C to 500°C at a rate of 5°C/min.

For Spaci-MS, a silica capillary, I.D. = 0.3 mm and O.D. = 0.34 mm, was connected to the Hiden HPR20 MS and placed inside one of the central channels of the monolith. The capillary was heated along its entire length to avoid condensation. 1000 ppm C_3H_6, 200 ppm NO, 120 ppm He (added for calibration), 5% H_2O, 10% O_2, and N_2 as a balance were fed to the reactor, initially set at 80°C. The temperature was then raised to 220°C. After reaching steady state, the capillary was moved from the inlet (0 cm) to the back (7 cm) of the monolith in 1 cm increments in order to measure gas composition at 8 different locations along the catalyst length. This was also done at 270°C.

The sample was pretreated prior to each experiment: the sample was heated to 450°C while flowing 10% H_2O, 5% CO_2, and balance N_2; then 10% O_2 was added to the mixture for 5 minutes followed by 2000 ppm of H_2 for 5 minutes; and then the temperature was decreased to 80°C before starting the experiment.

Table 4-1 : Experiment matrix for TPO.

Run	CO [ppm]	C_3H_6 [ppm]	NO [ppm]	Flow rate [L/min]
1	1000			10
2		1000		10
3			200	10
4		1000	200	10
5	1000			28
6		1000		28
7			200	28
8		1000	200	28

4.4 Results and Discussion

4.4.1 CO Oxidation

The results of the TPO experiment with 1000 ppm CO over both the zoned and homogeneous samples at different flow rates, 10 L/min and 28 L/min, are shown in Figure (4-2). CO conversion, in both samples, started instantaneously around 80°C, the onset of the TPO experiment, and identical trends were observed up to 30% conversion during the temperature ramp. However, with a further increase in temperature, the zoned catalyst showed better performance at the higher flow rate. The light-off temperature, $T_{(50)}$, of the zoned catalyst was 2°C lower than the homogeneous catalyst in the case of the lower flow rate, and 4°C lower in the case of the higher flow rate. This difference in performance increased as the conversion approached 100%. To validate the results and ensure reproducibility, experiments at high flow rate were repeated and the data were reproducible with a <2°C maximum difference between data sets. Therefore, at low flow rates the performance of the zoned and homogeneous samples could be considered the same as the small difference in $T_{(50)}$ falls within the margin of error of the data. However, there was a real difference between zoned and homogeneous sample performance at the higher flow rate. The superior performance of the zoned

catalyst is due to a higher localized exothermic heat of reaction and lower CO self-poisoning during the warm up period. CO oxidation in DOCs follows a back-to-front ignition pattern under these conditions, a common trend in heterogeneous catalyst systems with exothermic reactions [21, 137-139]. During the cold start emission period, CO oxidation is inhibited by CO self-poisoning due to strong CO adsorption on Pt at low temperatures. The zoned catalyst, with a higher Pt concentration in the front section, oxidizes more CO in the front and therefore accumulates more exothermic heat near the inlet of the monolith. This exothermic heat lowers the effect of CO self-poisoning downstream, plus as more CO is converted in the upstream this lowers it further [22]. Figure (4-3) shows the temperature difference (ΔT) between the inlet temperature and the temperature at 2 cm from the inlet, of the homogeneous and zoned catalysts as a function of CO conversion at high flow rate. The temperature rise is larger in the front section of the zoned sample, indicating that the exothermic heat of CO oxidation is greater thereby reaching a higher temperature faster than the homogeneous sample, especially at the lower temperatures. Even though the reaction is back-to-front and the homogeneous sample has more Pt in the back, the conversion rates of both samples are equal below 30% conversion. This is because below 30% conversion the exotherm is still forming and is apparently not significant enough to result in an integral difference (i.e. show a difference between the two when considering the entire catalyst length) and the rate of heat transfer from the back to the front by conduction is slow; thus CO conversion rates of both samples are similar. As conversion increased and as the reaction zone moves toward the front, the zoned sample with more Pt in the front section generated more heat via the exothermic reaction and reaches 100% conversion faster than the homogeneous sample, and the temperature difference between the zoned and homogeneous samples increased with increasing CO conversion as shown in Figure (4-3). The different stages of the reaction can also be reflected in the slopes of the lines, which correlate to the reaction rates, in Figure (4-2).

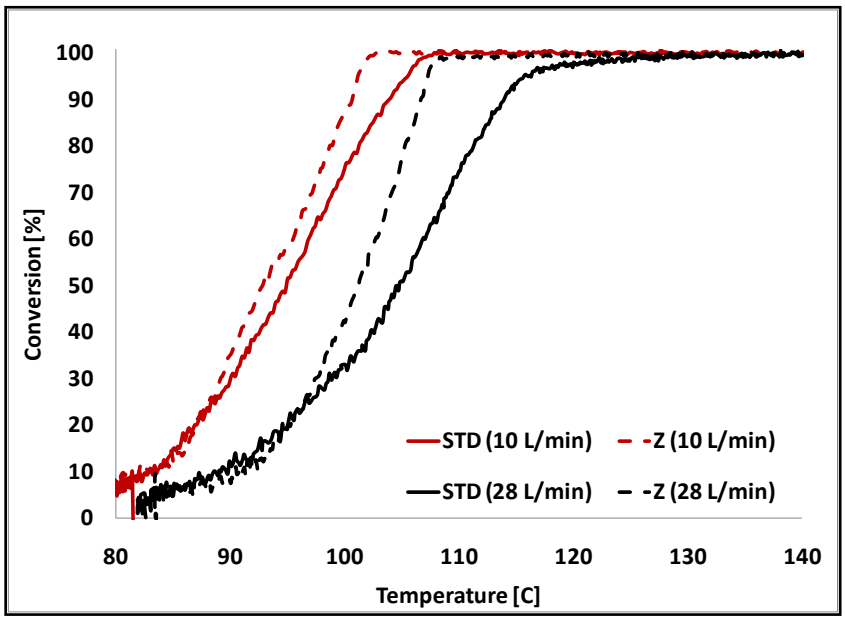

Figure 4-2 : CO conversion as a function of temperature. The feed gas consisted of 1000 ppm CO, 10% O_2, 5% CO_2, 5% H_2O, balanced with N_2.

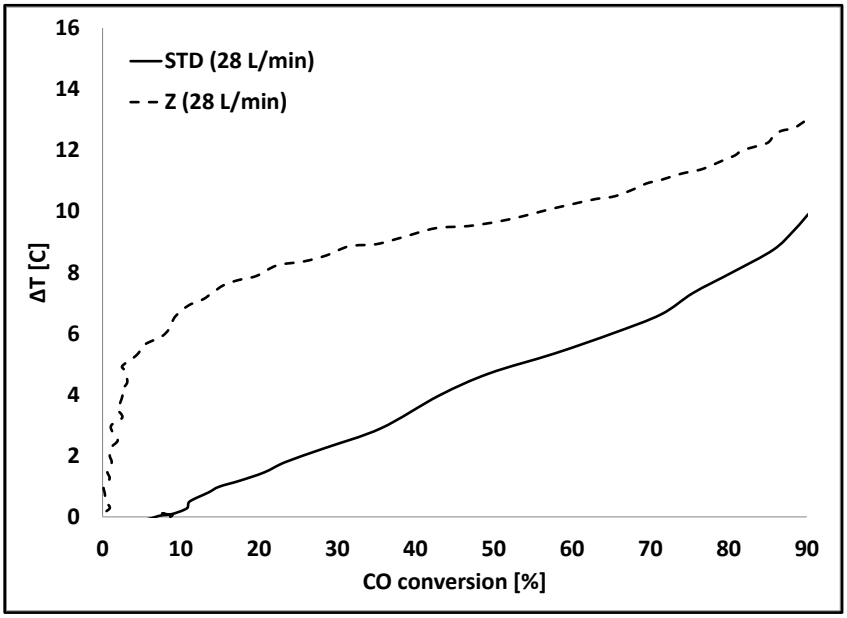

Figure 4-3 : Temperature rise at 2 cm from the inlet of the catalyst relative to the inlet temperature as a function of CO conversion at a feed flow rate of 28 L/min with the inlet conditions as listed in Figure 4-2.

4.4.2 C_3H_6 Oxidation

TPO of C_3H_6 experiments were also carried out on both catalysts. The results were somewhat similar to CO oxidation as shown in Figure (4-4). However, unlike CO oxidation, at low and high flow rates the difference between the homogeneous and zoned samples was observable even at low conversion. At the higher flow, the difference between the homogeneous and zoned samples was still more significant. For example, the difference in $T_{(50)}$ between the zoned and homogeneous samples was 5°C at the lower total flow rate and 8°C at the higher. This is related to the larger exothermic heat generated by C_3H_6 oxidation relative to CO oxidation; therefore, the differences between the zoned and homogeneous catalysts were more significant and observable even at lower conversion. Figure (4-5) shows the temperature rise in the front 2 cm section as a function of C_3H_6 conversion for both samples at high flow rate. As expected, the temperature rise is higher compared to CO oxidation due to the larger exothermic heat generated. As the conversion increases, the reaction zone moves toward the front and the temperature rise in the front section reaches its maximum at 100% conversion. Due to higher Pt concentration in the front section of the zoned sample, the temperature rise in the front part of the zoned sample was higher than that of the homogeneous sample. Again, the higher temperature rise indicates a larger exotherm produced in the front part of the zoned catalyst, which helps prevent the effect of C_3H_6 self-poisoning downstream by oxidizing most of the C_3H_6 in the front. The higher exotherm also lowered the light off temperature of the catalyst.

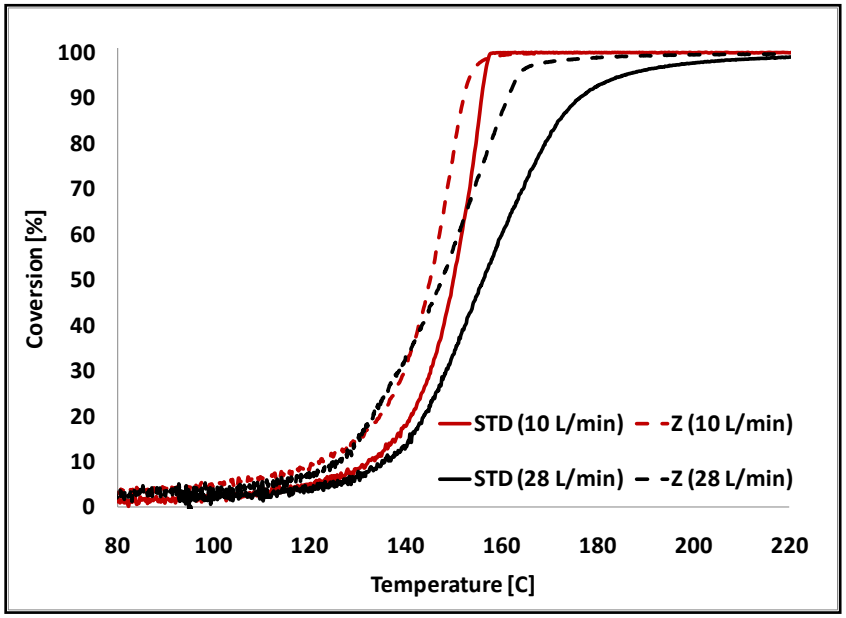

Figure 4-4: C_3H_6 conversion as a function of temperature. The inlet gas consisted of 1000 ppm C_3H_6, 10% O_2, 5% CO_2, 5% H_2O, balanced with N_2.

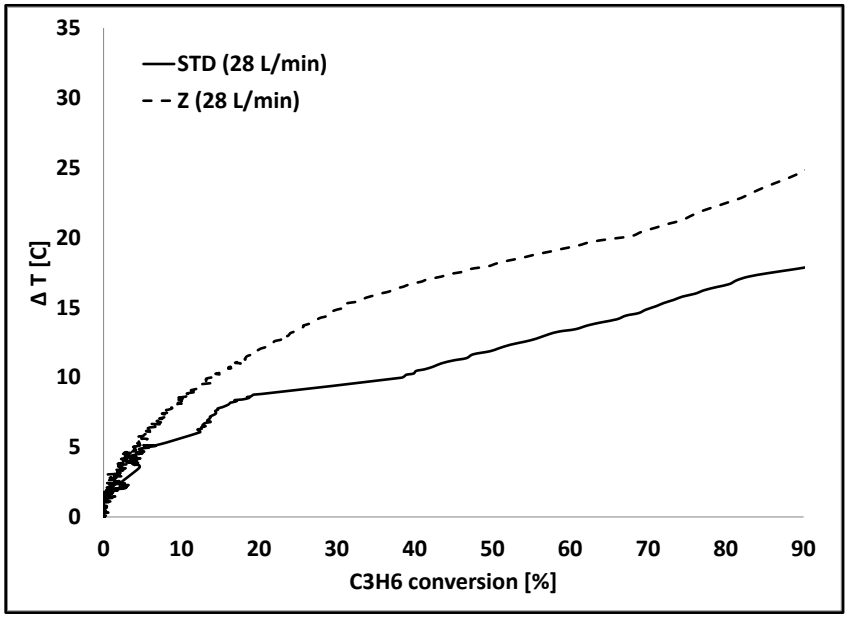

Figure 4-5: Temperature rise at 2 cm from the inlet of the catalyst, relative to the inlet, as a function of C_3H_6 conversion at 28 L/min with the inlet gas described in Figure 4-4.

4.4.3 NO Oxidation

The results of the NO TPO are shown in Figure (4-6). NO oxidation kinetics are slower than those of CO and C_3H_6, and are also thermodynamically limited in the higher end of the temperature range of interest. Both the homogeneous and zoned samples showed similar trends in terms of light-off temperature, $T_{(50)}$, and maximum conversion at low and high total flow rates. In NO oxidation, unlike CO and C_3H_6 oxidations, increasing the total flow rate did not result in any difference between the homogeneous and zoned catalysts. These results were expected since in the case of NO oxidation, there is negligible exothermic heat and significant NO_2 poisoning [43]. Figure (4-7) shows the temperature difference between inlet temperature and the temperature at 2 cm from the inlet of the two catalysts at the higher total flow rate. As shown, NO oxidation produced an insignificant amount of heat in the front section of both catalysts. In addition, analysis of the NO oxidation activity is complicated here, as NO oxidation is known to depend on Pt particle size, where NO oxidation rates increase with increasing particle size [140-145]. The zoned sample with more Pt particles concentrated in the front of the catalyst has larger Pt particles in the front, with a dispersion of 8.5%, and the homogeneous sample had a higher dispersion, 11.7% (with the back of the zoned sample having a 39% dispersion – all measured with H_2 chemisorption). So, although the zoned sample has larger particle sizes in the front section, the NO conversion was still similar to that of the homogeneous sample, which may be due to the homogeneous sample having larger particles at the outlet section, combined with the less significant heat of reaction. Furthermore, NO oxidation is product inhibited, with NO_2 having a significant poisoning effect. This is due to the high sticking coefficient of NO_2 on Pt, with the NO_2 "over-oxidizing" the Pt, making it less active [21, 42]. Because of these many factors, it is not clear which effects were more dominant and may have cancelled each other, resulting in the similar conversions observed.

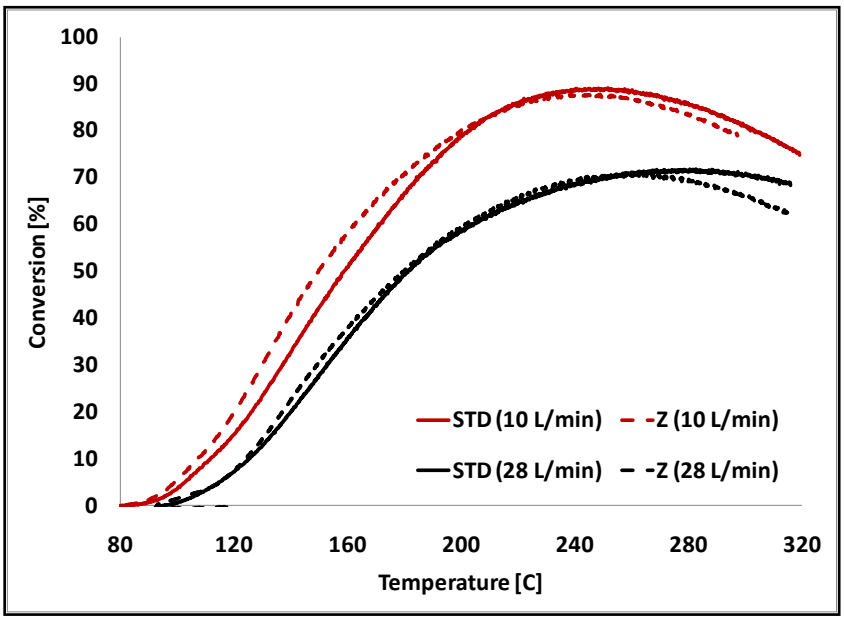

Figure 4-6 : NO conversion as a function of temperature. The inlet gas consisted of 200 ppm NO, 10% O_2, 5% CO_2, 5% H_2O, balanced with N_2.

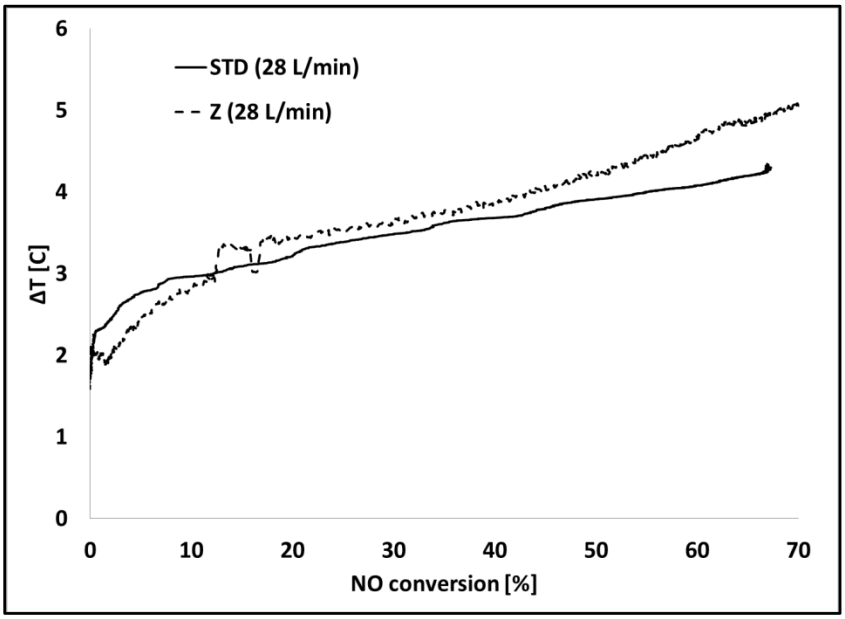

Figure 4-7: Temperature rise at 2 cm from the front of the catalyst, relative to the inlet, as a function of NO conversion at 28 L/min with the inlet gas described in Figure 4-6.

4.4.4 Oxidation of C_3H_6 and NO as a Mixture

The performances of the homogeneous and zoned samples in the oxidation of a mixture of C_3H_6 and NO were also evaluated. Results of the TPO experiments are shown in Figures (4-8) and (4-9). For both low and high total flow rates, the performance of the zoned sample was better than the performance of the homogeneous. In Figure (4-8), again the difference in C_3H_6 light off temperature $T_{(50)}$ between the homogeneous and zoned samples was greater at higher flow rate than the lower. Likewise, Figure (4-9) shows that at the higher flow rate, the NO light off temperature of the zoned sample was lower and reached higher conversion than that of the homogeneous sample. For C_3H_6 oxidation, the difference in $T_{(50)}$ between the zoned and homogenous samples was similar to that observed when just C_3H_6 oxidation was evaluated (in the absence of NO). For NO oxidation however, the difference in $T_{(50)}$ between the zoned and homogeneous samples for the mixture was more pronounced, more than twice as large, relative to the results from the experiments where just NO oxidation was evaluated (i.e. in the absence of C_3H_6). The zoned sample, with more Pt at the front, was oxidizing most of the C_3H_6 in the front section of the catalyst when noticeable NO oxidation was measured (as will be shown below), leaving the rest available for NO oxidation. In addition, the zoned catalyst can utilize the exothermic heat in the front, caused by C_3H_6 oxidation, to heat the catalyst faster and initiate NO oxidation earlier. This conclusion is initially based on literature evidence which shows that hydrocarbon and CO oxidation conversion, including C_3H_6, takes place in the front part of the catalyst, whereas NO oxidation requires the entire volume of the monolith [56]. Further, Irani et al. [21] studied the effect of hydrocarbons on NO oxidation over a model DOC. Using SpaciMS, they found that in a C_3H_6/NO mixture, C_3H_6 inhibits NO oxidation by preferentially consuming NO_2, the product of NO oxidation, relative to O_2, as an oxidant in C_3H_6 oxidation. Therefore, NO_2 was observed in the outlet after C_3H_6 was almost completely oxidized. Therefore, for the C_3H_6 and NO mixture, C_3H_6 is oxidized in the front zone of monolith, then after it is completely

oxidized any NO_2 formed will not react with C_3H_6, resulting in observed NO oxidation in the remaining part of the catalyst. The zoned catalyst, with more Pt particles in the front, makes the active C_3H_6 oxidation zone shorter leaving a larger volume for NO oxidation. To further investigate this, spatially resolved experiments were used to measure C_3H_6 and NO concentrations as a function of catalyst length.

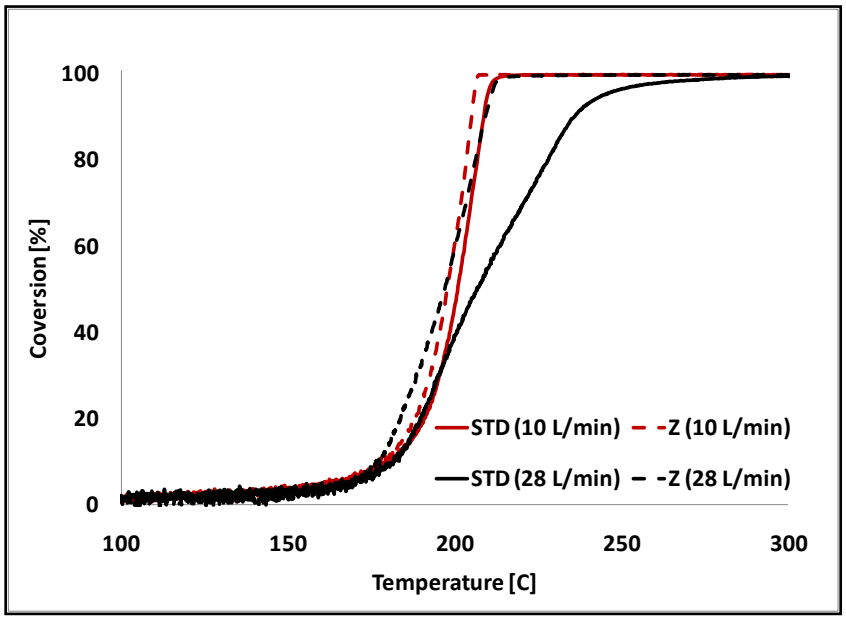

Figure 4-8: C_3H_6 conversion as a function of temperature. The inlet gas consisted of 1000 ppm C_3H_6, 200 ppm NO, 10% O_2, 5% CO_2, 5% H_2O, balanced with N_2.

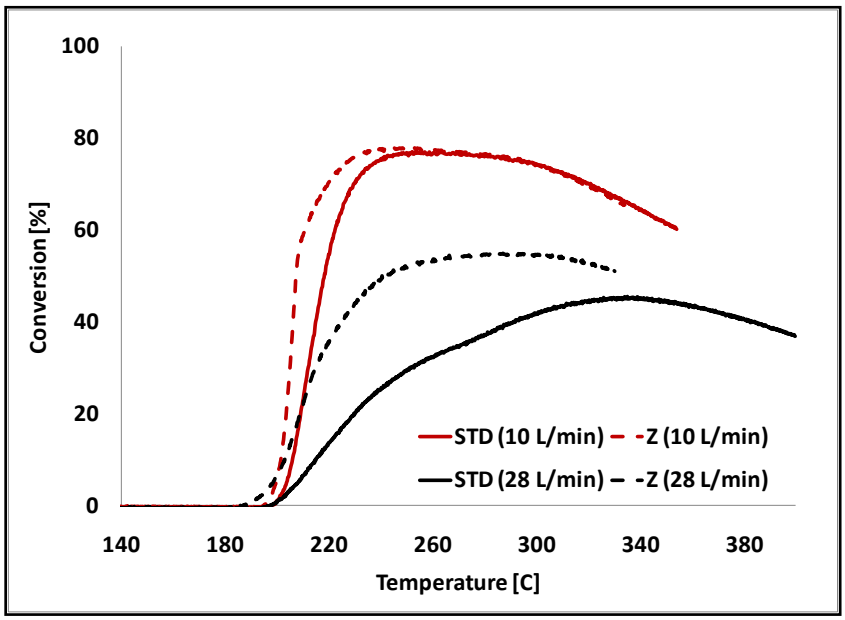

Figure 4-9: NO conversion as a function of temperature. The inlet gas consisted of 1000 ppm C_3H_6, 200 ppm NO, 10% O_2, 5% CO_2, 5% H_2O, balanced with N_2.

4.4.5 Spatially Resolved Experiments

The gas species were spatially resolved at 220°C and 270°C under the same low and high total flow rates: 10 L/min and 28 L/min. The furnace temperature was ramped to 220°C, and then after reaching steady state, gas compositions were measured at 8 different positions along the catalyst length by moving the capillary from the front of the catalyst to the back in 1 cm increments. The temperature was ramped to 270°C and the process repeated. Figures (4-10) and (4-11) show the results of C_3H_6 and NO oxidation at 220°C. In comparing the zoned catalyst with the homogeneous catalyst at the lower flow rate, the zoned catalyst converted most of the C_3H_6 within 2 cm, whereas the homogeneous catalyst took 4 to 6 cm to achieve a similar conversion. Thus, as suggested above, for NO oxidation, the zoned sample indeed had more volume available for NO oxidation compared to the homogenous sample. For example, the zoned catalyst catalyzed 63 ppm of NO_2 formation at 2 cm, while the homogeneous catalyst only 5 ppm at the same position. At the back of the monolith, both

samples were able to oxidize all of the C_3H_6, however, the zoned sample was still slightly better than the homogeneous catalyst in terms of NO oxidation, with the difference only 16 ppm. Thus for the low flow rate and mixture case, both catalysts were capable of reaching 100% C_3H_6 conversion and the difference in the overall NO conversion was relatively small, but the trends in the C_3H_6 and NO oxidation conversions inside the catalysts were significantly different and support the conclusion that having more volume available for NO oxidation, by oxidizing the HC species in a smaller zone, results in higher NO oxidation conversions.

At higher flow rates and 220°C, the differences were again more evident. For example, the zoned sample reached 70% C_3H_6 conversion within half of the catalyst length, however, the homogeneous sample required the entire length of the catalyst to reach the same conversion. Consequently, NO oxidation on the zoned sample reached higher conversions as it had more volume with lower C_3H_6 concentration available. Overall, for the C_3H_6/NO mixture case, the zoned sample with more catalyst in the front generates a larger exotherm in the front that heats up the catalyst faster resulting in more of the C_3H_6 oxidized in a smaller volume leaving more volume for NO oxidation.

Figures (4-12) and (4-13) show the results of C_3H_6 and NO oxidation at 270°C. At the lower flow rate, the trends in C_3H_6 and NO oxidation along catalyst length are similar for both samples because the active zones of both samples have moved close to the front of the catalyst at this higher temperature condition and only a small portion of the catalyst is required to oxidize C_3H_6. At the lower flow rate, both samples oxidized most or all the C_3H_6 using the first 1 cm. NO conversion also started in this region. However, at the higher flow rate, there was a small difference between zoned and homogeneous samples in C_3H_6 oxidation as shown in Figure (4-12). The C_3H_6 conversion in the zoned sample reached 99% within 2 cm, while it was 90% at the same position in the homogeneous sample. The difference in performance was also seen in NO oxidation. Overall, these results suggest

that under conditions where the catalyst is "stressed", for example at high flow rate and lower temperature, the differences in performance become more significant.

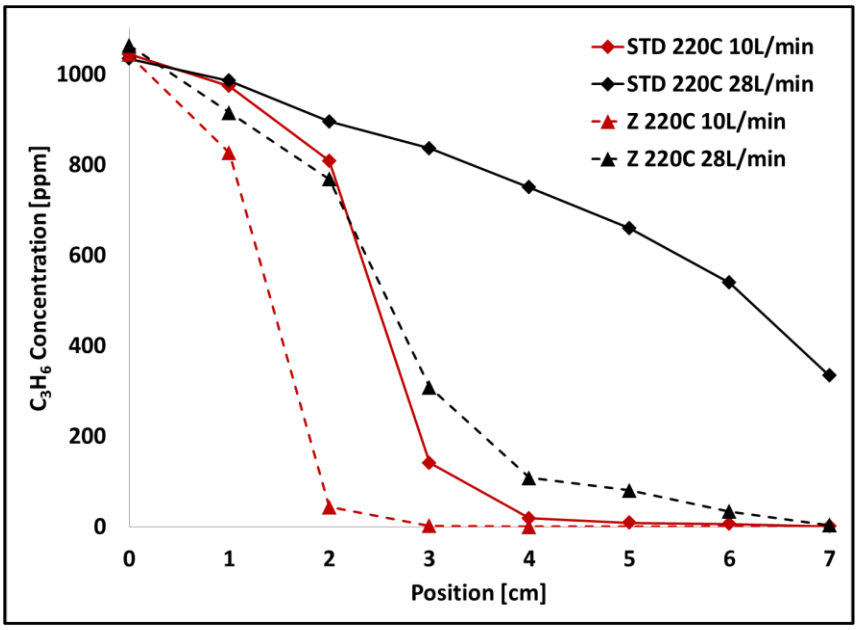

Figure 4-10: C_3H_6 concentration as a function of position at 220 °C measured using SpaciMS. The inlet gas consisted of 1000 ppm C_3H_6, 200 ppm NO, 100 ppm He, 10% O_2, 5% H_2O, balanced with N_2.

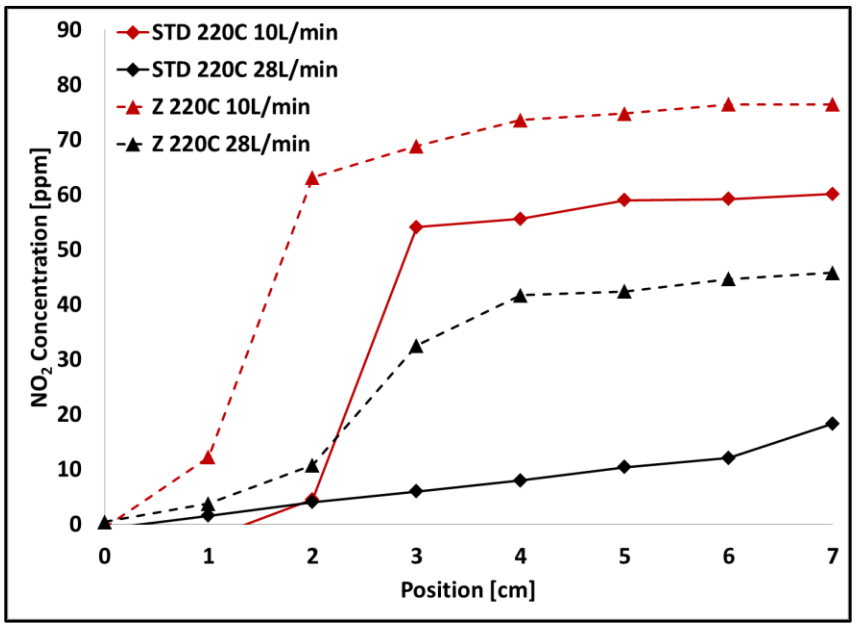

Figure 4-11: NO_2 concentration as a function of position at 220 °C measured using SpaciMS. The inlet gas conditions are described in Figure 4-10.

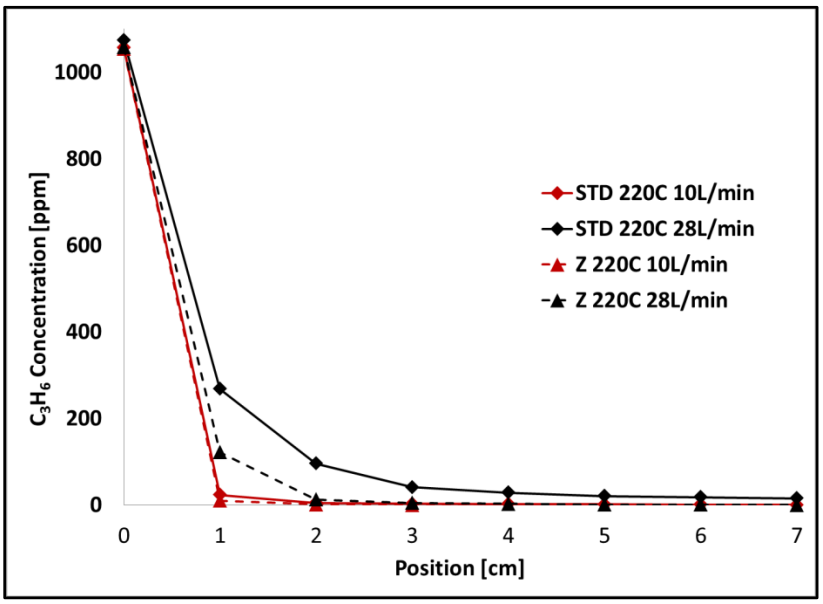

Figure 4-12: C_3H_6 concentration as a function of position at 270C measured using SpaciMS. The inlet gas consisted of 1000 ppm C_3H_6, 200 ppm NO, 100 ppm He, 10% O_2, 5% H_2O, balanced with N_2.

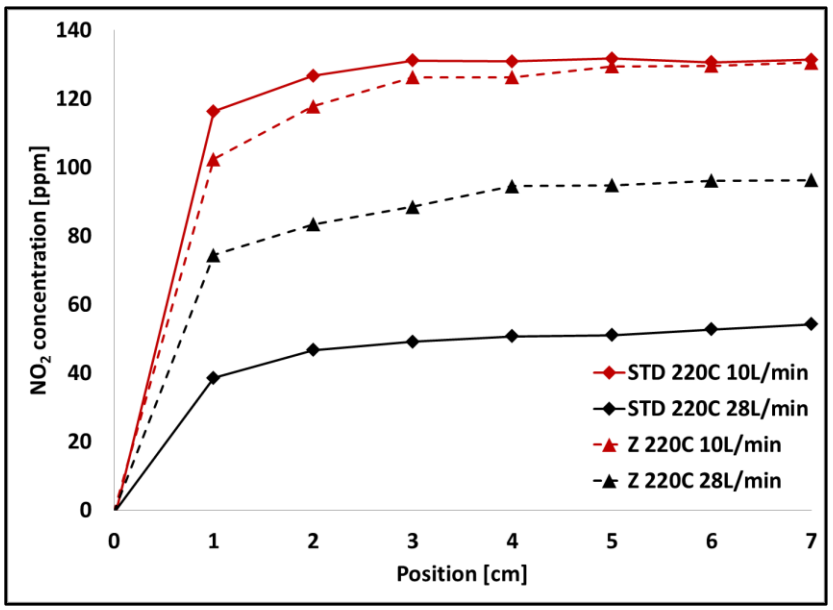

Figure 4-13: NO_2 concentration as a function of position at 270 °C measured using SpaciMS. The inlet conditions are described in Figure 4-12.

4.5 Conclusions

The effect of a catalyst axial distribution on the performance of a diesel oxidation catalyst was studied. Two Pt catalysts were prepared, containing the same amount of Pt; one with a homogeneous distribution, and one with more Pt concentrated in the upstream section. Results show that the zoned catalyst performed better for CO and C_3H_6 oxidation, but the two samples were similar for NO oxidation. The difference in performance between the zoned and homogeneous samples was less significant with a lower total flow rate and more significant when a mixture of reactions was tested and at a higher total flow rate. For CO and C_3H_6 oxidation, the better performance of the zoned sample was due to a higher catalyst upstream temperature resulting from a larger exothermic heat of reaction, generated nearer the front of the catalyst and a coincident decreased self-poisoning effect. Spatially resolved gas measurements showed that in a C_3H_6/NO mixture, the zoned catalyst oxidizes C_3H_6 in a smaller volume at the front part of the monolith sample leaving a larger volume available for NO oxidation; therefore, the zoned catalyst had better performance than the homogeneous catalyst in mixtures especially for NO oxidation at low temperature.

4.6 Acknowledgments

The authors gratefully acknowledge the Province of Ontario's Early Researcher Award and Auto21 for funding.

Chapter 5: Investigation of Thermal Degradation on the Performance of Zone-Coated Pt-Based Catalysts

5.1 Abstract

Temperature-programmed oxidation (TPO) experiments were used to evaluate the performance of uniformly (standard) and non-uniformly (zoned) distributed Pt/Al_2O_3 catalysts after homogeneous and heterogeneous thermal degradation. Both catalysts were homogeneously aged in an oven by exposing the entire catalyst to 750 °C in air for 4 hours at atmospheric pressure. In heterogeneous aging, only the back of the catalysts were exposed 680 °C, while the temperature at the inlet section did not exceed 550 °C. This was accomplished by pulsing in C_3H_6 and O_2, with an inert gas between each pulse, for 50 cycles, and using the heat generated via the exothermic oxidation reaction to thermally age zones of the samples. In all cases the performances of both catalysts after heterogeneous aging were better than those after homogeneous aging, because only part of the catalyst was damaged in heterogeneous aging, and the homogeneous aging temperature was higher. The zone-coated catalyst, with more Pt concentrated in the front of the monolith, showed better performance than the standard sample after heterogeneous aging. The reason is that most of the Pt in the zoned sample, which is located in the front half, was not affected by the more significant aging at the back of the monolith. On the other hand, at a higher total flow rate and higher temperature, the performance of the homogenously aged zoned catalyst was worse than that of the standard, because the effect of the Pt-rich upstream area of the zoned catalyst is lost through formation of larger particles widening the reaction zone into the less Pt-rich downstream region.

5.2 Introduction

It is commonly known that all catalysts deactivate. In diesel engine exhaust aftertreatment, catalyst deactivation results in a gradual decrease in performance, resulting in increased emissions from the vehicle. Catalysts can deactivate via a variety of mechanisms, including sulfur poisoning, mechanical deterioration, and thermal aging [16]. With the new restrictions on sulfur content in diesel fuel, new generation ultra-low sulfur fuels are expected to contribute less than 1 ppm to the total sulfur content of the exhaust gas [16], although accumulation over time still poses a serious issue. Thermal degradation occurs when the catalyst is exposed to high temperatures, via a hot inlet exhaust gas or from exothermic oxidation reactions occurring on the catalyst surface. The focus of this study is catalyst degradation by thermal aging.

Even though diesel engine exhaust temperature is relatively low, the DOC can be exposed to higher temperatures due to heat generation via exothermic hydrocarbon oxidation, and during the regeneration of diesel particulate filters (DPF) [69], where the filter requires temperatures in excess of 550 °C for soot oxidation to commence. For example, during the regeneration of a DPF, the DOC bed temperature can reach 850 °C [146]. In addition, during the lean NO_X trap (LNT) desulfation process, the DOC can be exposed to temperatures around 650 °C, with temperatures in excess of 600 °C required to remove sulfur from an LNT [16, 69]. When the catalyst is exposed to such a high temperature, catalyst atoms, molecules and particles aggregate to form larger particles on the surface of the catalyst [71, 72, 147]. This sintering effect results in a decrease in catalytic activity due to a loss of active surface area. With sintering, DOC performance drops, typically expressed as an increase in reaction light-off temperature, and ultimately resulting in reduced conversion of key species. In addition, DOC thermal deactivation can influence the performance of aftertreatment components downstream of the DOC, such as the selective catalytic reduction (SCR) and LNT catalysts. For example, a decrease in NO to NO_2 conversion over a DOC can reduce the SCR

efficiency since the fast SCR reaction requires an NO:NO_2 ratio of 1:1 [28] and reduce LNT efficiency as LNT catalysts trap NO_2 more readily than NO [16].

Homogenous aging, by placing the monolith in a furnace so that the entire monolith is exposed to a constant temperature, is a common laboratory thermal degradation technique. However, several studies have shown that, in real applications, thermal degradation is non-uniform [39, 128, 139]. Lambert et al. [39] found that the outlet of the DOC deteriorated the most significantly, after aging a Tier 2 light-duty diesel truck aftertreatment system to an equivalent of 120,000 miles. This is because the outlet of the DOC is exposed to the highest temperatures over time, being relatively adiabatic and catalyzing a variety of exothermic reactions. On the other hand, Winkler et al [72], who also tested the catalytic activity of an engine aged DOC, found that the degradation was non-uniform with the front section more affected than the rest of the catalyst. However, in the analysis performed, the authors showed that the particle sizes at the back of the catalyst were larger than in the front, indicating more thermal degradation had indeed occurred at the outlet section of the DOC. The reason for the poorer performance of the catalyst front was directly related to chemical poisoning by S, Zn, P, Mg and Ca. Using IR-thermography and spatially resolved capillary-inlet mass spectrometry (SpaciMS), Shakir el al. [139], observed that C_3H_6 oxidation follows back-to-front light-off, and the ignition front of the thermally aged sample moved more slowly toward the inlet relative to the non-thermally degraded sample. Using the same technique and methodology, Shakir et al. results were confirmed by Russell et al. [128], who observed an increase in time for the temperature and concentration waves to travel though the catalyst during back-to-front ignition. Furthermore, the reaction zones were spread farther into the catalyst relative to those observed before aging.

This chapter focuses on the influence of homogeneous and heterogeneous thermal degradation on the performance of a uniformly distributed catalyst (standard) and a non-uniformly distributed catalyst (zoned). Using the same amount of Pt for both samples, the Pt was

homogeneously distributed on the standard sample, whereas the zoned sample had more Pt in the front section and less Pt in the back. To compare the performances of the two samples under different thermal aging situations, two aging protocols were used, homogeneous and heterogeneous thermal aging, both representing different conditions in real application. In homogeneous aging, the sample is heated in a furnace to a chosen temperature so that no temperature gradients exist in the catalyst. This method represents the case where the catalyst is exposed to constant and high temperatures, such as when exhaust gas temperature is the only source of heat. In heterogeneous aging, the sample is thermally degraded by the heat of exothermic reactions. The heat released from the exothermic reaction causes an increase in the temperature of the zone where the reaction takes place, which will cause a gradient in temperature in the catalyst. These temperature gradients will lead to different degrees of thermal degradation along the axial length. This method represents the case when exothermic HC or CO oxidation occurs on the catalyst causing an increase in temperature where the reaction occurs, thus in distinct catalyst zones. In real applications degradation is a combination of both exhaust gas temperature and exothermic reactions.

In our previous study, fresh zoned and standard catalysts were compared [37]. The zoned catalyst with more Pt located in the upstream portion and less downstream showed better performance for CO and C_3H_6 oxidation at higher flow rates due to larger heat generated at the front via the exothermic reaction and a decreased self-poisoning effect downstream. In a NO/C_3H_6 mixture, the zoned catalyst showed higher NO conversion than the standard catalyst because most of the C_3H_6 was oxidized in a small volume in the front of the catalyst leaving the rest of the catalyst available for NO oxidation; whereas the standard catalyst utilized a larger area to oxidize C_3H_6 thus leaving a smaller volume for NO oxidation.

5.3 Experimental Procedures

The uniformly (standard) and non-uniformly (zoned) distributed catalysts used in this study were prepared using the same method described in previous work [38]. The Pt/Al_2O_3 monolith samples, with a 1.59 g/in^3 (97.03 kg/m^3) Al_2O_3 loading, 325 cell/in^2 (cpsi) cell density, 1" in diameter and a length of 3", were thermally aged using two different aging protocols, representing heterogeneous and homogenous aging of a DOC. The same protocols were used for both the standard and zoned samples. In the first aging protocol, in order to heterogeneously age the back of the sample, the front of the monolith was exposed to 50 pulses of 7000 ppm C_3H_6, 10% O_2, 5% H_2O, balanced with N_2 for 10 s at 500 °C with a gas hourly space velocity (GHSV) of 25 000 hr^{-1}. To avoid over heating the catalyst, an inert phase consisting of 5% H_2O and balanced with N_2 was pulsed into the reactor for 150 s after each C_3H_6-containing pulse. As a result, the exothermic C_3H_6 oxidation increased the temperature of the front section of the monolith to 680 °C after 50 cycles, while the temperature of the back of the catalyst did not exceed 550 °C. The reactor used is non-adiabatic, thus we had to thermally damage the front, switch the position of the sample in the reactor (flipped) to simulate a sample that is more heavily aged on the downstream section, as was noted by Lambert [39]. In the second aging protocol, homogeneous aging, the samples were placed in an oven at atmospheric pressure and 750 °C for 4 hours to age the whole sample.

For reaction performance testing, the sample was wrapped with 3M insulation and placed in a horizontal quartz tube with two thermocouples, one in the front and one in the back of the monolith, each about 1 mm inside the sample. The performances of the heterogeneously and homogenously aged samples were tested using temperature-programmed oxidation (TPO) experiments. The inlet gas consisted of CO, C_3H_6, or NO, or a mixture of C_3H_6 and NO, in the presence of 10% O_2, 5% H_2O, 5% CO_2 and N_2 as the balance gas. At 80 °C, the inlet gas was fed into the reactor then the temperature was ramped at 5 °C/min to 500 °C. TPO experiments were run with two flow rates: 10 L/min and 28

L/min. To ensure the consistency of the experimental conditions, the catalyst was pretreated before each experiment by flowing 10% O_2, 5% CO_2, and 5% H_2O with a N_2 balance at 500 °C for 20 minutes, then the temperature was cooled down to 80 °C with N_2 only.

The dispersion of the active sites over the surface area of the catalyst before and after homogeneous aging was measured using the H_2 chemisorption method. For the fresh sample, two were prepared simultaneously and we assume that they had the same initial dispersions. No measurements were taken between heterogeneous and homogeneous aging protocols as the same sample was used and the measurements required sample destruction. For the measurement, different portions of the monolithic sample were crushed to fine powder. Then the powder was loaded into a Hiden Catalab micro-reactor and was exposed to 26 pulses of 100 µl of 5 % H_2 with a He balance for 30 seconds with 1 minute of pure He between each pulse. Before each measurement, the catalyst was pretreated in 100 ml/min He at 25 °C for 25 minutes, then 5% H_2 was added and the temperature was ramped at 10 °C/min to 450 °C. The catalyst was exposed to 450 °C for 30 minutes, then the H_2 was turned off and the temperature was cooled down to 25 °C before starting the H_2 pulses. H_2 chemisorption was measured based on irreversible H_2 adsorption on a Pt site with a H_2:Pt ratio assumed to be 1:2. H_2 chemisorption results showed that before aging, the dispersion of the zoned sample was 8.5% at the front and 39% at the back, while the standard was 11.7%. After the homogeneous thermal aging protocol, the Pt dispersion of the standard sample was 2.4%, whereas the dispersion of zoned sample was 1.1% at the front and 3.8% at the back.

5.4 Results and Discussion

5.4.1 CO Oxidation

The results of temperature programmed CO oxidation experiments from the fresh, heterogeneously aged, and homogeneously aged samples with 1000 ppm CO are shown in Figures (5-

1) and (5-2). In general, the zoned sample showed better performance than the standard sample, except after homogeneous aging with the higher total flow rate and at high temperature conditions. Table (5-1) shows the light-off temperature corresponding to 50% conversion, T_{50}, for both samples before and after thermal aging.

Table 5-1 : T_{50} of CO oxidation for the standard (STD) and zoned (Z) samples before and after thermal aging.

Sample	FR [L/min]	Fresh	HT* Aged	HM* Aged
Standard	10	95 °C	109 °C	142 °C
Zoned	10	93 °C	104 °C	137 °C
Standard	28	105 °C	123 °C	156 °C
Zoned	28	101 °C	111 °C	146 °C

*HT=heterogeneously, HM=homogeneously.

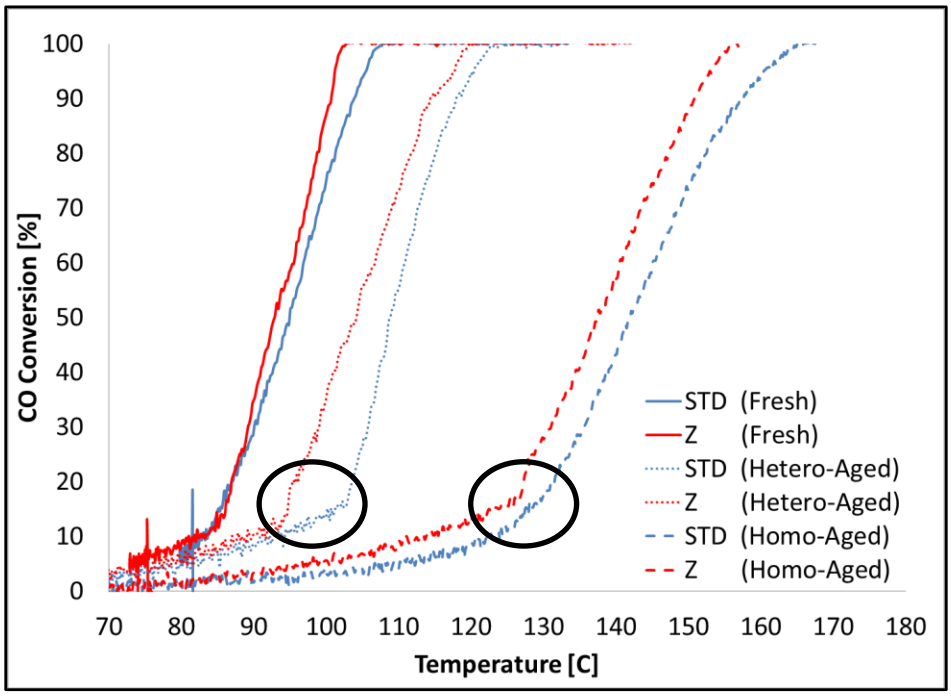

Figure 5-1: CO conversion as a function of temperature after homogeneous and heterogeneous aging. The feed gas consisted of 1000 ppm CO, 10% O_2, 5% CO_2, 5% H_2O, balanced with N_2 at 10 L/min.

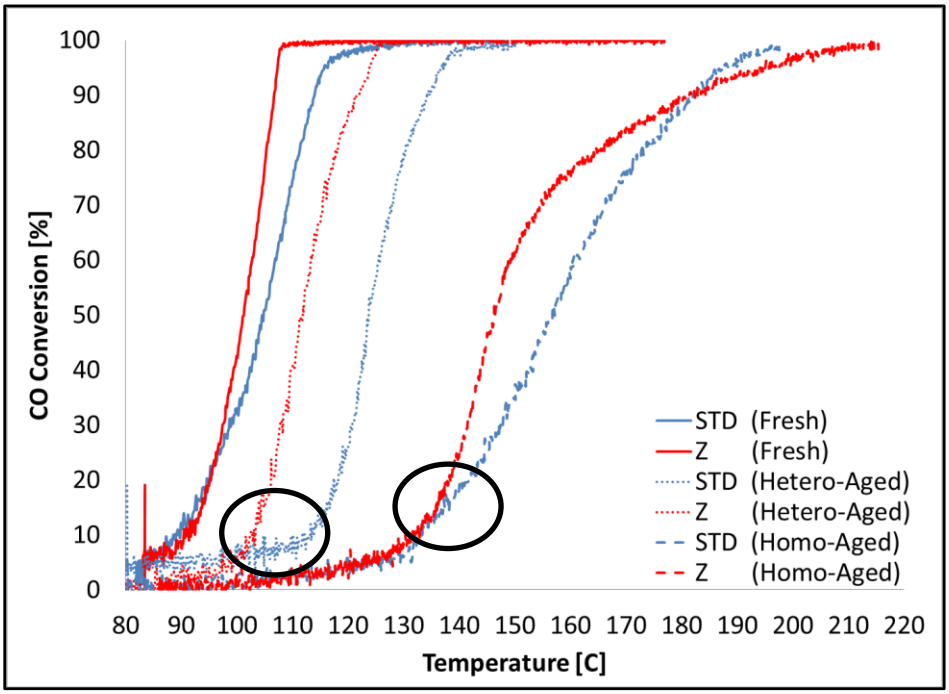

Figure 5-2: CO conversion as a function of temperature after homogeneous and heterogeneous aging. The feed gas consisted of 1000 ppm CO, 10% O_2, 5% CO_2, 5% H_2O, balanced with N_2 at 28 L/min.

At the lower total flow rate, as shown in Figure (5-1), CO conversions after homogeneous aging were more negatively affected than those after heterogeneous aging, or just aging the back of monolith. For example, in the case of standard sample the difference in T_{50} between the heterogeneously aged sample and fresh sample, ΔT_{50}, was 14 °C, whereas the ΔT_{50} between the homogeneously aged and fresh was 47 °C. These differences in T_{50} after heterogeneous and homogeneous aging were lower in the case of zoned sample. The reason for the better performance of the heterogeneously aged sample compared to the homogeneously aged sample is that: (1) during the homogeneous aging the sample was exposed to higher temperature than during heterogeneous aging and (2) during heterogeneous aging only the back of the catalyst was affected by exposure to high temperature, whereas as in homogeneous aging the whole catalyst was exposed to high temperatures.

Therefore, in all cases, the light-off temperature of the heterogeneously aged sample was about 33 ℃ lower than that of the homogeneously aged sample. It has been reported in the literature that a DOC is likely to suffer more extensive thermal degradation (sintering) at the outlet compared to the front [39]; therefore, these results suggest that a zoned sample, with more catalyst concentrated in the front part, can enhance catalytic performance and durability if heterogeneous thermal aging is the primary degradation mode, at least to the temperatures studied.

In addition, there is a region at low temperature when the CO conversions of both the standard and zoned samples are identical. For example, CO conversion trends overlap at temperatures below 86 ℃ for the fresh samples, 95 ℃ after heterogeneous aging, and 127 ℃ after homogeneous aging. During this period, the catalyst temperature is low, below the light-off temperature of CO, and the catalyst surface is dominated by CO adsorption, or CO self-poisoning, thus inhibiting the CO oxidation reaction. As the catalyst temperature increases, more CO is oxidized, and consequently more exothermic heat is generated, thereby the effect of CO self-poisoning decreases and the reaction proceeds faster, which is sometimes called light off. This change in reaction rate is shown by the black circles in Figures (5-1). This shift in the reaction rate of the zoned sample occurs at lower temperature than the standard, thus the cold start period was shorter. Our previous study of the performance of a standard and zoned DOC has shown that the zoned catalyst, with a larger amount of Pt concentrated at the inlet, lights-off at lower temperature due to the greater amount heat released via the exothermic reaction and a lower CO self-poisoning effect during the cold start period. Hence in the case of zone coated catalyst, the cold start period was shorter and CO lit off at lower temperature [38]. The performance of the zoned catalyst after heterogeneous aging was more similar to the fresh than that after homogeneous aging in terms of a short cold start period. The reason for the shorter cold start period associated with the zoned sample after heterogeneous aging is that heterogeneous aging primarily damaged the back of the monolith, which contains a smaller amount of active sites

with most of the active sites in the front of the monolith being less affected. Therefore the zoned catalyst oxidizes more CO in the front, producing more heat in the front compared to the standard catalyst, thus increasing the temperature of the catalyst faster and coincidentally lowering the effect of CO self-poisoning. On the other hand, more catalyst (sintering of the precious metal) in the downstream section was damaged on the standard sample with the uniform distribution. As a result, the zoned catalyst lights-off at lower temperature and reaches higher conversion faster than the standard sample after heterogeneous aging. For this reason, the zoned catalyst, after heterogeneous aging, can maintain good performance in terms of low light-off temperature, which is critical for the cold start period, when most of the pollutants leave the DOC unreacted [148-150].

In the case of homogeneous aging, the light-off temperatures of both samples were higher and the cold start period was longer than those of the heterogeneously aged catalysts. This is due to exposing the entire catalyst to high temperature, thus forming larger Pt particles and lowering catalyst activity. For example, after homogeneous aging, the dispersion of the standard sample decreased by 20% and that of the zoned sample decreased by 13% at the front and 10% at the back. It is observed that during the warm up period, below 20% conversion, the difference between the standard and zoned catalyst was smaller after homogeneous aging than that after heterogeneous aging as shown by the black circle in Figure (5-1). However, as the temperature increases the difference between both catalysts becomes similar to that after heterogeneous aging, with the zoned catalyst having a lower T_{50} by 5 °C. Studies have shown that at low conversion the reaction occurs at the back and it moves toward the front as temperature increases [38, 128, 151]. Even though the back of the standard catalyst contains more catalyst compared to the back of the zoned catalyst, the dispersion was higher at the back of the zoned catalyst, 3.8%, than that of the standard, 2.4%. Therefore, at low conversion and temperature, when the reaction occurs in the back, the standard and zoned samples showed similar performance. However, as the temperature increased and the reaction zone propagated toward

the front, the zoned sample showed slower CO conversion than the standard sample especially at higher flow rate. For example, in Figure (5-2), it is observed that the CO conversion with the homogeneously aged zoned sample slowed down, when the CO conversion reached 70%. This is because at higher temperature and conversion, the reaction zone is located within the front section of the monolith, where the zoned sample had lower dispersion, 1.1%, compared to 2.4% for the standard sample. Therefore, the zoned sample exhibits lower activity than the standard, when the reaction zone reaches the front of the monolith.

At higher total flow rate, as shown in Figure (5-2), the differences between the standard and zoned samples after heterogeneous and homogeneous aging were greater than those at the lower total flow rate in Figure (5-1). For example, after heterogeneous aging the difference in light-off temperature between the zoned and standard sample was 6 °C higher than that at the lower total flow rate. Previous modeling work has shown that the differences between zoned and standard catalysts become more evident when the catalyst is operating under more severe conditions, such as higher flow rates, higher levels of reactants, low precious metal content, slow ramp rates, etc. [151], consistent with the observations here. The reasons given were related to front-loaded catalysts, such as the zoned sample in this study, catalyzing more oxidation at the front, resulting in more heat generated, thus less CO self-poisoning and a more rapid warm up, all relative to a standard sample. Furthermore, there was a longer period of similar CO conversion in the low temperature region, 5 °C higher than that at the lower total flow rate. This is ultimately due to a greater CO self-poisoning effect. During the warm up period, prior to light-off, the effect of heat transfer by convection is more significant than that by conduction because of the higher total flow rate and smaller exotherm produced. This leads to CO conversions for both cases being similar at low temperature [151].

Similarly, after homogeneous aging, the overlap period was longer and the difference in light-off temperature between both samples was higher than that at the lower total flow rate. However, as

the conversion reached 70% in the zoned sample, the rate of increase in CO conversion slowed, whereas the CO conversion of the standard sample continued to increase rapidly with temperature. This could be attributed to more significant agglomeration of the Pt particles in the front section of the zoned sample, which contains more Pt particles in the front section than the standard sample does. As mentioned before, chemisorption results showed that Pt dispersion in the front of the zoned sample was 1.1% compared to 2.4% in the front of standard sample. Thus bigger particles were formed in the front of the zoned sample after homogeneous aging relative to the standard sample. So, as the temperature increased the reaction zone moved toward the front of the monolith [128, 152, 153], where for the zoned sample more of the active sites are located. High conversions are observed when the reaction zone is located at the inlet portion [128]. If more damage was done to the higher density Pt on the zoned sample, then the reaction zone cannot shift as far to the front, leaving the back to do more of the catalysis, which has less active site density. This is also consistent with previous observations made where thermally degrading the catalyst widens the reaction zone and slows down its movement from back to front [128]. After homogeneous aging, the Pt-rich section of the zoned sample will suffer more extensive agglomeration, and as the reaction zone becomes wider it will spread to areas with less and less Pt, and the movement from back to front becomes slower and may not reach the front. Thus the rate of CO conversion slows as the reaction zone moves closer to the front of the monolith. This effect was more evident when the catalyst was operating under the higher total flow rate.

5.4.2 C_3H_6 Oxidation

The results of TPO experiments with 1000 ppm C_3H_6 after homogeneous and heterogeneous aging at lower and higher total flow rates are shown in Figures (5-3) and (5-4), respectively. Like CO oxidation, the C_3H_6 oxidation catalytic performance of the standard and zoned samples was more

affected by homogeneous aging than by heterogeneous aging as expected. Table (5-2) shows the T_{50} for C_3H_6 oxidation before aging and after heterogeneous and homogeneous aging.

Table 5-2: T_{50} of C_3H_6 oxidation for the standard (STD) and zoned (Z) samples before and after thermal aging.

Sample	FR [L/min]	Fresh	HT* Aged	HM* Aged
Standard	10	150 °C	167 °C	198 °C
Zoned	10	145 °C	154 °C	178 °C
Standard	28	156 °C	179 °C	221 °C
Zoned	28	147 °C	162 °C	191 °C

*HT=heterogeneously, HM=homogeneously

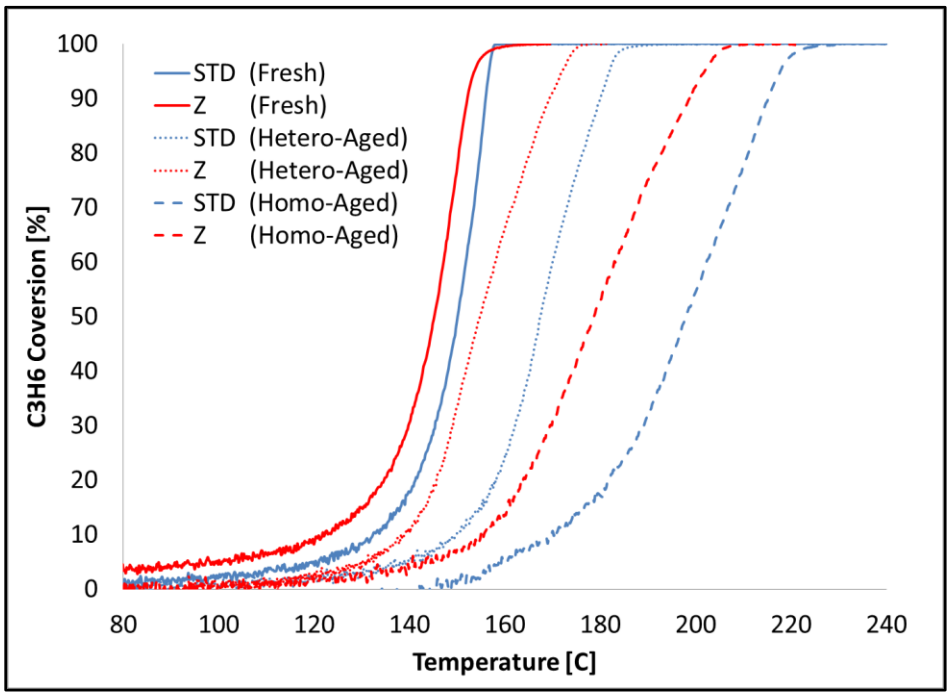

Figure 5-3: C_3H_6 conversion as a function of temperature after homogeneous and heterogeneous aging. The feed gas consisted of 1000 ppm C_3H_6, 10% O_2, 5% CO_2, 5% H_2O, balanced with N_2 at 10 L/min.

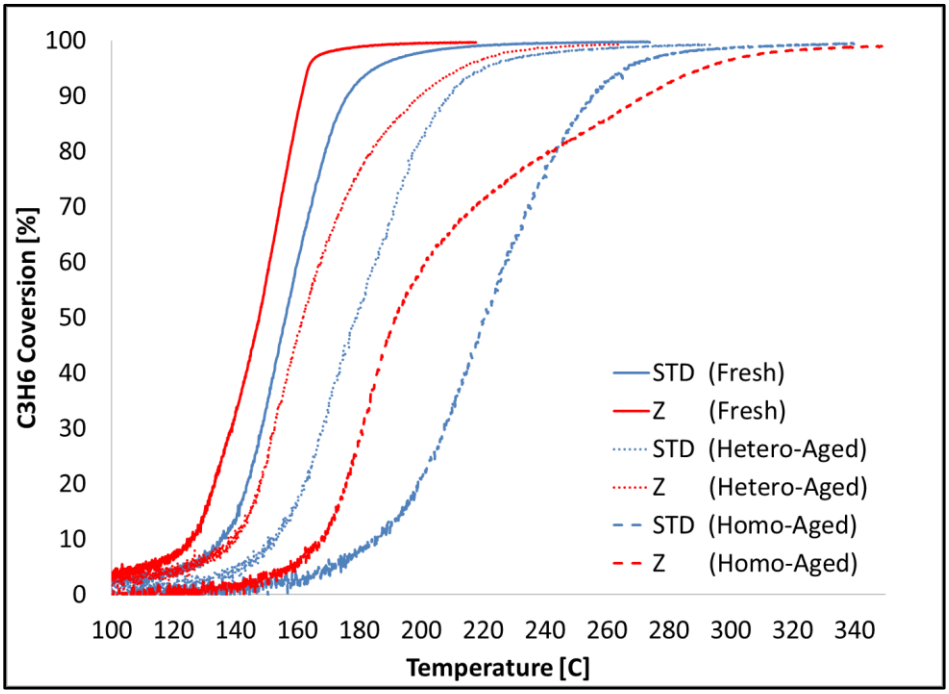

Figure 5-4: C_3H_6 conversion as a function of temperature after homogeneous and heterogeneous aging. The feed gas consisted of 1000 ppm C_3H_6, 10% O_2, 5% CO_2, 5% H_2O, balanced with N_2 at 28 L/min.

Like the CO conversion trends, the thermally deactivated zoned sample showed better performance than that of the standard sample except at the higher temperature/higher total flow rate conditions. For example, at the lower total flow rate, the light-off temperature of the zoned sample after heterogeneous aging was 13 ℃ lower than the light-off temperature of the heterogeneously aged standard sample. The same reasoning for the superior performance of the zoned sample over the standard sample applies here: heterogeneous aging affected the back of the catalyst, thus the zoned sample, which contains less catalyst in the back and more catalyst in the front, was less affected by the heterogeneous aging. Similar to CO oxidation, the performance of the zoned sample, after homogeneous aging, was better than the performance of the standard sample at the lower total flow rate. For example, at lower total flow rate, the light-off temperature T_{50} of the homogeneously aged

zoned sample was 9 °C higher than the fresh, whereas the standard sample was 17 °C higher. At higher total flow rate, 28 L/min, the trend for C_3H_6 conversion was similar to that at the lower flow rate, but the ΔT_{50} was greater between the fresh and aged samples because the catalyst was operating under higher flow rates. As mentioned before, at higher flow rate more heat is transferred by convection than that at the lower flow rate, thus there is also less impact of conduction. Therefore the light-off temperature moves to a corresponding higher inlet temperature, and the difference between the fresh and aged samples becomes greater than that at lower flow rates. Again, as the reaction proceeded to higher temperature and conversions above 70%, the rate of C_3H_6 oxidation conversion increase becomes slower because the reaction zone reaches the front of the monolith, which contains larger particles than those at the front of the standard sample.

5.4.3 NO Oxidation

The results for NO TPO before and after thermal aging at the lower and higher flow rates are shown in Figures (5-5) and (5-6), respectively. The performance of the zoned catalyst in NO oxidation in all cases was better than the standard, especially at the lower flow rate and after heterogeneous aging. Table (5-3) shows the temperatures corresponding to 10% NO conversion, T_{10}, of the standard and zoned samples before and after heterogeneous and homogeneous aging.

Table 5-3: T_{10} of NO oxidation for the standard (STD) and zoned (Z) samples before and after thermal aging.

Sample	FR [L/min]	Fresh	HT Aged	HM Aged
Standard	10	112 °C	119 °C	126 °C
Zoned	10	107 °C	112 °C	113 °C
Standard	28	125 °C	135 °C	150 °C
Zoned	28	124 °C	125 °C	140 °C

*HT=heterogeneously, HM=homogeneously

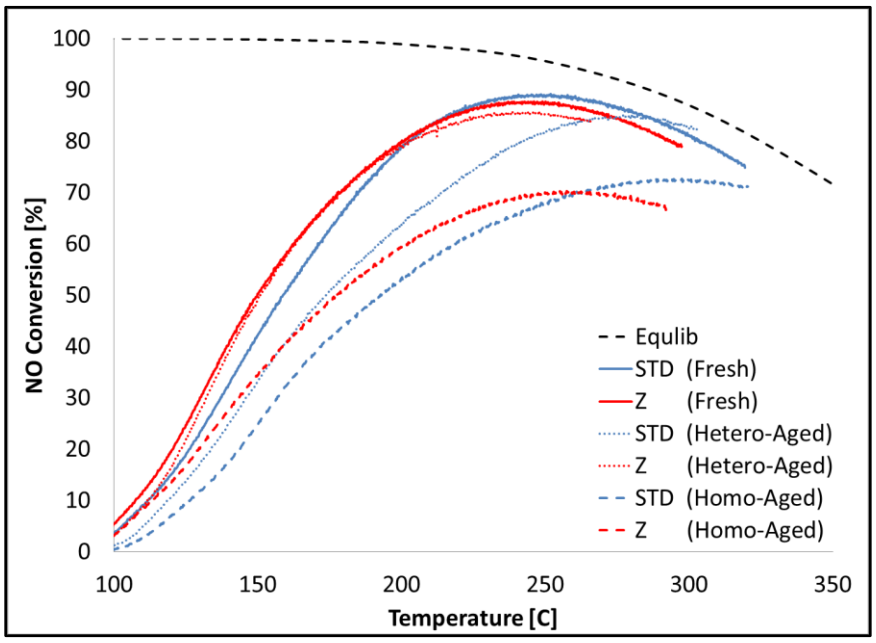

Figure 5-5: NO conversion as a function of temperature after homogeneous and heterogeneous aging. The feed gas consisted of 200 ppm NO, 10% O_2, 5% CO_2, 5% H_2O, balanced with N_2 at 10 L/min.

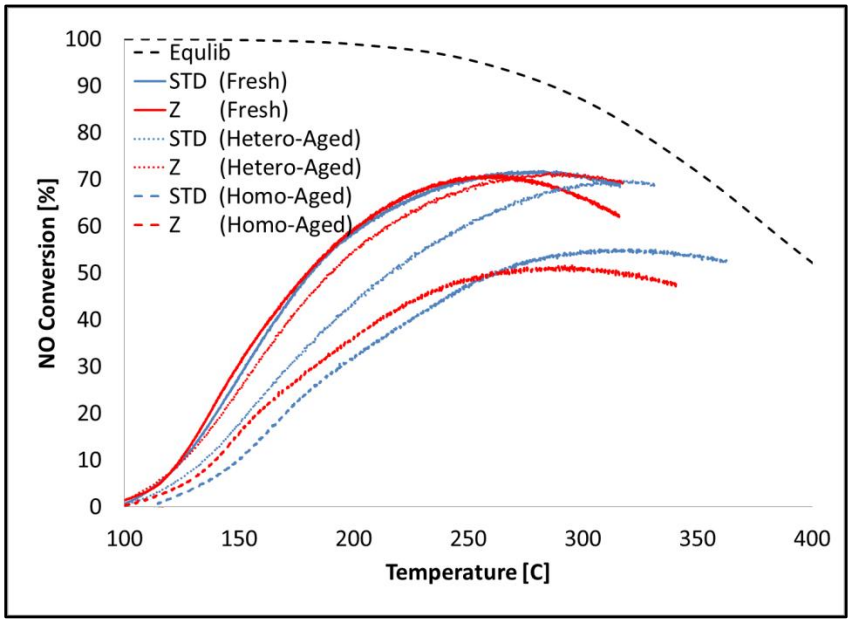

Figure 5-6: NO conversion as a function of temperature after homogeneous and heterogeneous aging. The feed gas consisted of 200 ppm NO, 10% O_2, 5% CO_2, 5% H_2O, balanced with N_2 at 28 L/min

Like CO and C_3H_6 oxidation, NO oxidation after homogeneous aging was affected more than that after heterogeneous aging. At the lower total flow rate, Figure (5-5), the temperature to reach 10% conversion, T_{10}, of the zoned sample was slightly affected by the heterogeneous and homogeneous aging procedures, with the differences between the fresh and heterogeneously aged samples being 5 °C and fresh and homogeneously aged samples being 6 °C. As the temperature increased, the NO conversion profile of the heterogeneously aged zoned sample converged to that of the fresh zoned sample. This indicates that at the lower NO oxidation conversions, or at lower temperatures, the reaction rate was influenced by aging the back of the catalyst, but as the temperature increased, the performance of the catalyst became similar to the fresh. The performance of the standard sample was worse than the performance of the zoned sample after thermal aging, especially after heterogeneous aging as T_{10}, and more evidently T_{50}, were higher than those of the zoned sample. For example, at the lower flow rate, the NO conversion of the heterogeneously aged standard sample reached 64% at 200 °C, whereas over the heterogeneously aged zoned sample the conversion reached 80% at the same temperature. On the other hand, the homogeneous aging more significantly affected both samples. For example, at the lower total flow rate, the T_{10} difference between the fresh and homogeneously aged standard sample was 23 °C. This difference increased to 33 °C for T_{50}. Similarly the difference between fresh and homogeneously aged zoned sample was 6 °C for T_{10} and 28 °C for T_{50}. NO oxidation requires the entire length of the monolith under the conditions tested [81]. And therefore the changes noted cannot be explained based on the width of a reaction zone. However, similar logic can be applied. The influence of heterogeneous aging was less significant for the zoned sample because more Pt particles were damaged by homogeneous aging than heterogeneous aging, and the zoned catalyst, with a higher Pt concentration in the front was less affected by heterogeneously aging the back of the monolith.

5.4.4 Oxidation of C_3H_6 and NO in a Mixture

The results of TPO of a C_3H_6 and NO mixture at the lower and higher total flow rates after thermal deactivation are shown in Figures (5-7), (5-8), (5-9), and (5-10). Tables (5-4) and (5-5) list the 50% C_3H_6 conversion temperatures, T_{50}, and 10% NO conversion temperatures, T_{10}.

Table 5-4: T_{50} of C_3H_6 oxidation in C_3H_6 +NO mixture for the standard (STD) and zoned (Z) samples before and after thermal aging.

Sample	FR [L/min]	Fresh	HT Aged	HM Aged
Standard	10	201 ℃	218 ℃	246 ℃
Zoned	10	197 ℃	202 ℃	216 ℃
Standard	28	206 ℃	241 ℃	268 ℃
Zoned	28	201 ℃	217 ℃	235 ℃

*HT=heterogeneously, HM=homogeneously

Table 5-5: T_{10} of NO oxidation in C3H6 +NO mixture for the standard (STD) and zoned (Z) samples before and after thermal aging.

Sample	FR [L/min]	Fresh	HT Aged	HM Aged
Standard	10	207 ℃	221 ℃	253 ℃
Zoned	10	202 ℃	203 ℃	213 ℃
Standard	28	214 ℃	250 ℃	296 ℃
Zoned	28	203 ℃	223 ℃	260 ℃

*HT=heterogeneously, HM=homogeneously

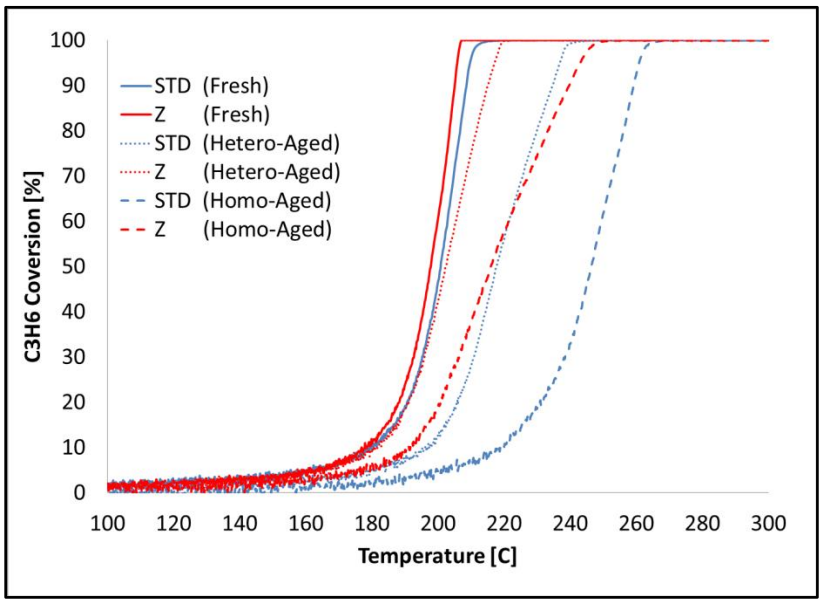

Figure 5-7: C_3H_6 conversion as a function of temperature after homogeneous and heterogeneous aging. The feed gas consisted of 1000 ppm C_3H_6, 200 ppm NO, 10% O_2, 5% CO_2, 5% H_2O, balanced with N_2 at 10 L/min.

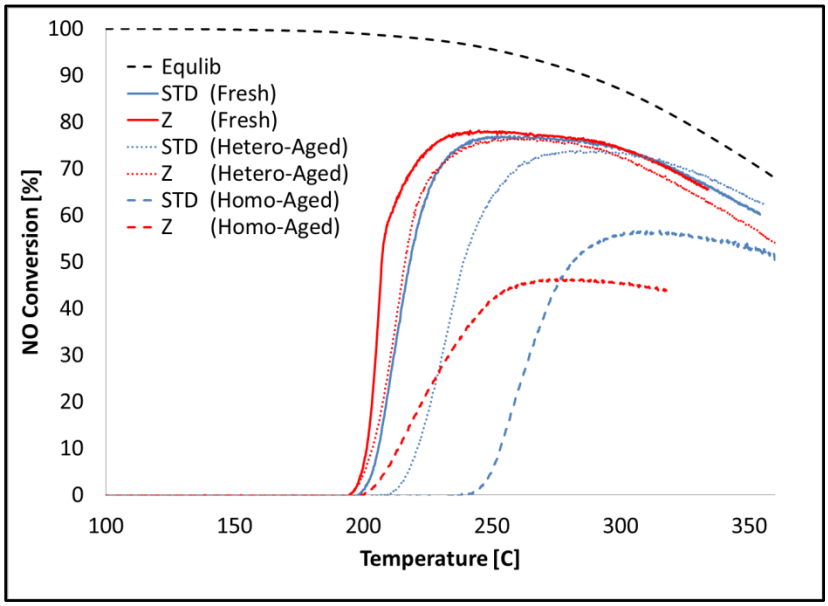

Figure 5-8: NO conversion as a function of temperature after homogeneous and heterogeneous aging. The feed gas consisted of 1000 ppm C_3H_6, 200 ppm NO, 10% O_2, 5% CO_2, 5% H_2O, balanced with N_2 at 10 L/min.

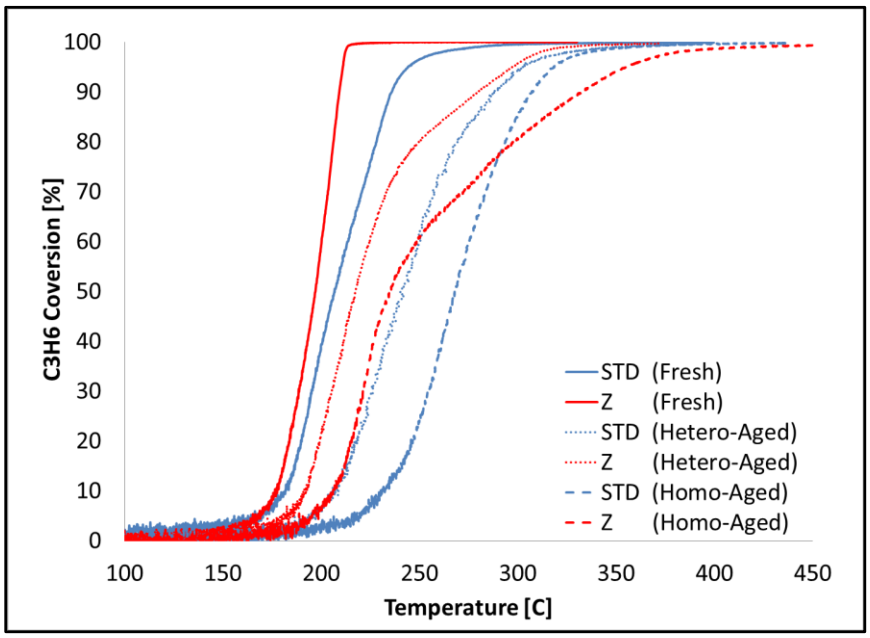

Figure 5-9: C_3H_6 conversion as a function of temperature after homogeneous and heterogeneous aging. The feed gas consisted of 1000 ppm C_3H_6, 200 ppm NO, 10% O_2, 5% CO_2, 5% H_2O, balanced with N_2 at 28 L/min.

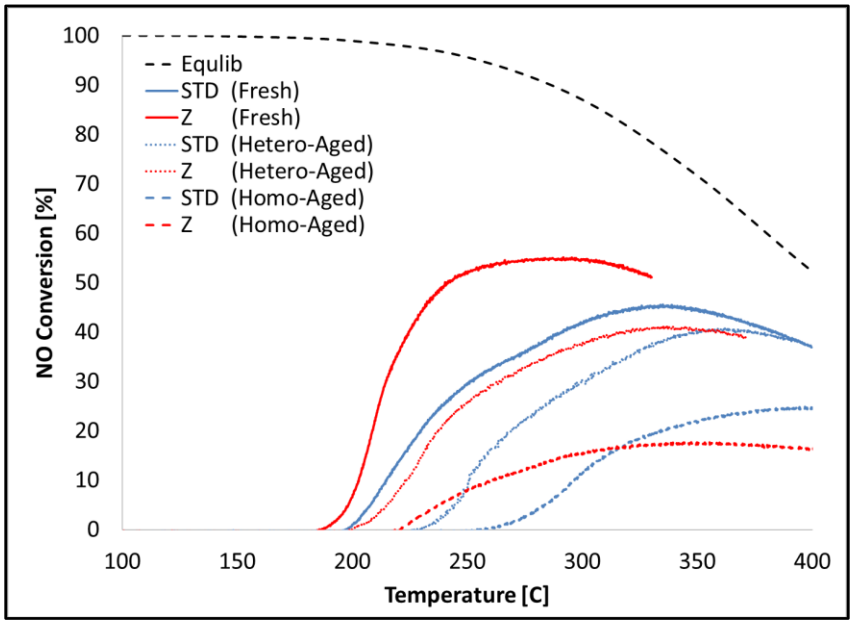

Figure 5-10: NO conversion as a function of temperature after homogeneous and heterogeneous aging. The feed gas consisted of 1000 ppm C_3H_6, 200 ppm NO, 10% O_2, 5% CO_2, 5% H_2O, balanced with N_2 at 28 L/min.

Like the experiments with only C_3H_6 or NO, in the combined C_3H_6 and NO mixture the zoned sample showed better performance than the standard sample at the two flow rates, and the effect of heterogeneous aging was less significant than that of homogeneous aging. As explained in detail above, heterogeneous aging impacted the back section of the catalyst more than the front; therefore the zoned sample with the lower Pt concentration at the back was less affected. Comparing the zoned and standard samples at the lower total flow rate, the difference in C_3H_6 oxidation light-off temperature was higher between the fresh and heterogeneous and homogeneous aging with the standard sample, as shown in Figure (5-7). At higher total flow rate, the differences in the C_3H_6 and NO oxidation light-off temperatures between the fresh samples and after heterogeneous and homogeneous aging were larger than those at lower flow rate, because the catalysts are working under harsher conditions, i.e. higher flow rate. Aging the front of the monolith, where C_3H_6 is oxidized, would increase the width of the C_3H_6 reaction zone, hence decreasing the available area for NO oxidation [38, 128]. This drop in NO oxidation in a mixture with C_3H_6 is due to the large Pt particles formed throughout the monolith that reduce the active site surface area and activity of the catalyst.

5.4.5 Conclusions

TPO experiments were used to compare the performance of standard and zone-coated Pt/Al_2O_3 catalysts after heterogeneous and homogeneous aging. In most cases the zone-coated catalyst showed better performance than the standard sample; however, after homogeneous aging, at the higher flow rate and at higher temperatures, the zone-coated catalyst was poorer due to more loss of the effect of the Pt rich zone at the inlet, which is key to high conversions, and resulting slow movement of the reaction front toward the catalyst inlet under harsher conditions. The performance of the zoned sample after heterogeneous aging was similar to that of the fresh catalyst, because most of Pt particles, concentrated in the front section, were not affected by damaging the back of the sample, which contains less Pt. In the case of the C_3H_6 and NO mixture, the difference between the standard

and zoned catalysts was greater at higher flow rate because of a more significant effect of convective heat transfer, where the light off temperature is higher and thus when it does occur, the hotter particles at the front of the zoned catalyst result in higher conversions more quickly. Like the single reactant reactions, after heterogeneous aging, the performance of the zoned catalyst was better than the standard because the damage was less significant in the upstream volume where most of C_3H_6 was oxidized, thus leaving a larger volume available for NO oxidation.

Chapter 6: The Effect of CO/H_2, C_3H_6, and NO on the Oxidation of Each Other over a Pt-based Diesel Oxidation Catalyst

6.1 Abstract

Diesel oxidation catalyst (DOC) reactions were investigated, with H_2/CO, C_3H_6 or NO added separately and added as mixtures, to further understand the effect of different reactants on the performance of a DOC under various inlet gas component conditions. Experimental sets of different compositions and concentrations of these reactants were designed to evaluate the performance of the DOC (Pt/Al_2O_3) catalyst. Results show an inhibition effect of CO, C_3H_6, and NO on CO and C_3H_6 oxidation. The light-off temperatures of CO and C_3H_6 were higher in a mixture than that when individually tested. When not in a mixture, CO and C_3H_6 inhibited their own oxidation by adsorbing to the active sites, known as "self-poisoning", especially at low temperature. In a mixture, CO and C_3H_6 oxidation reactions were also inhibited by each other due to competition for active sites. The inhibition effect of CO, C_3H_6, and NO increased with increasing concentrations of each in the feed gas. On the other hand, hydrogen enhanced CO oxidation, where literature suggests this is due to H_2 lowering the activation energy of CO desorption.

6.2 Introduction

In this chapter, some of the data obtained during the course of an Auto21 project are presented. The project was conducted in conjunction with the University of Alberta (U of A) and Umicore, to further understand DOC reactions, in order to develop a more comprehensive and accurate model. A matrix of experiments was constructed to test the performance of two commercial catalysts, Pt/Al_2O_3 and $Pt\text{-}Pd/Al_2O_3$, with different compositions of inlet gases. The reactants of interest were CO, C_3H_6, NO, and H_2. Different combinations of these reactants were fed to the reactor with 10% O_2, 10% H_2O, 10% CO_2, 1% or 300 ppm He and N_2 as a balance always added. Inverse

hysteresis behavior was observed with the CO and C_3H_6 mixture during ignition/extinction experiments, thus more investigations were done for this specific system and are discussed in the next chapter. In this chapter, part of the Pt/Al_2O_3 data is shown. Extra results can be found in Appendix B.

6.3 Experimental Procedures

A Pt/Al_2O_3 monolith sample, supplied by Umicore AG with a total Pt loading of 95 g/ft^3 (3.35 kg/m^3) based on total volume, was used to test the performance of the catalyst with different inlet gas compositions. The sample was cut to 0.9" diameter with a length of 2.4" and had a cell density of 400 cpsi. A matrix of different combinations and concentrations of the reactants was constructed to test the performance of the catalysts. The reactants of interest were CO, H_2, C_3H_6, and NO. In all of these experiments, the feed stream was introduced to the reactor at temperatures below 80˚C, to try to avoid any reaction before ramping. Then the temperature was ramped at a rate of approximately 3˚C/min. When complete oxidation was achieved, the reactor was cooled down by decreasing the furnace temperature. In all experiments the feed stream consisted of 10% O_2, 10% H_2O, 10% CO_2, 300 ppm or 1% He, the CO, C_3H_6 and/or NO reactant gas(es), and N_2 as the balance gas. The gas flow rate was 9.34 L/min, equivalent to a space velocity of 25,000 hr^{-1} at STP (298K and 1 atm). The outlet gas was measured using a MultiGas 2030 FT-IR analyzer (MKS) and a HPR20 mass spectrometer (MS). Before running any experiment, a test with N_2 only (no reactant) was performed to check the temperature difference between the front and the back of the catalyst as well as the radial direction. The test showed that the maximum difference was less than 5˚C between the front and the back and 4˚C in the radial direction.

6.4 Results and Discussion

6.4.1 CO Oxidation

The results of CO TPO experiments at different CO and H_2 concentrations are shown in Figure (6-1). The catalyst was tested with different CO concentrations in the inlet gas: 500 ppm, 1000 ppm, and 2000 ppm, while maintaining a 3:1 ratio of CO: H_2 in all experiments. An increase in CO concentration in the feed increased the CO light-off temperature, $T_{(50)}$. The CO oxidation light-off temperatures are listed in Table (6-1). This increase in light-off temperature, with increasing CO concentration, was due to CO self-inhibition. The self-poisoning phenomenon primarily occurs at low temperature, for example in Figure (6-1) at temperatures below 101°C, in the case of 1000 ppm CO, and 111°C, in the case of 2000 ppm CO. As the temperature increases above these temperatures, the CO reaction rate increases rapidly indicating a shift from a CO-dominated surface, to O_2 dominated, at high temperature [106, 107, 109]. The effect of different species on CO oxidation was investigated by adding H_2, C_3H_6, and NO to the feed gas. Figure (6-2) and Table (6-2) show the results. In all cases 2000 ppm CO was introduced to the reactor with different concentrations of other species. C_3H_6 and NO inhibited CO oxidation, while H_2 promoted the reaction. For example, the light-off temperature of CO in the presence of H_2 was 16℃ lower that in the absence of H_2. This positive effect of H_2 on CO oxidation is due to H_2 lowering the effect of CO self-poisoning by reducing the activation energy of CO desorption [46]. On the other hand, C_3H_6 inhibited CO oxidation, with the CO oxidation light-off temperature increased by 30 ℃ when 750 ppm C_3H_6 was added to the CO + H_2 mixture. This inhibition was greater when 600 ppm NO was introduced to the previous mixture as the CO oxidation light-off temperature further increased by 21 ℃. The negative effects of C_3H_6 and NO on CO oxidation are due to competition between these species and CO for active sites [35].

Table 6-1: CO oxidationT_{50} values with different CO concentrations in the feed.

CO/H_2 [ppm]	T_{50} [°C]
500/167	92
1000/333	106
2000/666	115

Table 6-2 : CO oxidation T_{50} values with different feed gas compositions.

Experiment	CO [ppm]	H_2 [ppm]	C_3H_6 [ppm]	NO [ppm]	T(50) [°C]
1	2000				131
2	2000	666			115
3	2000	666	750		145
4	2000	666	750	600	166

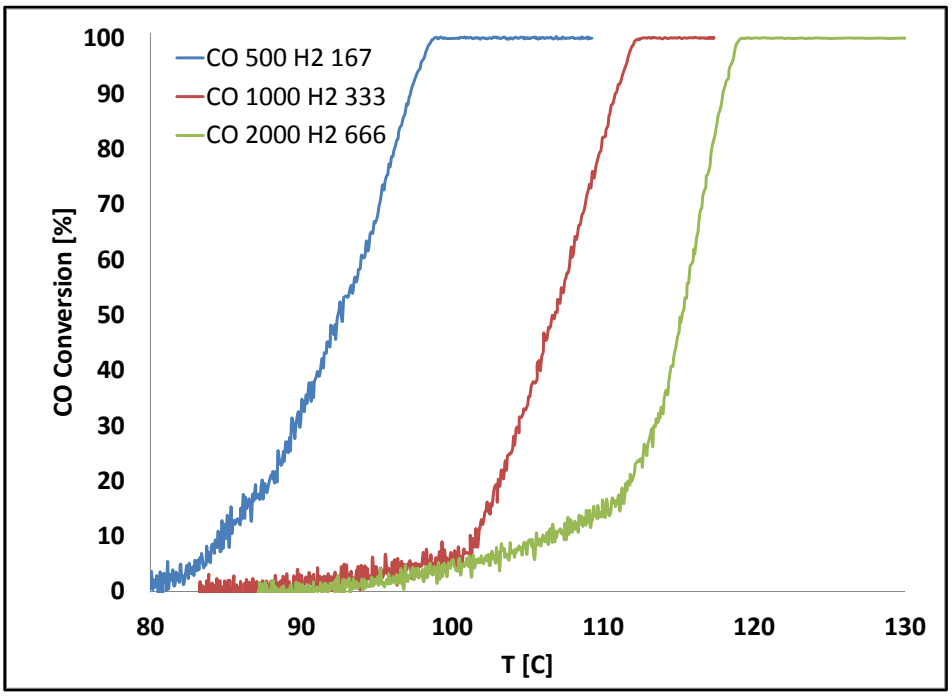

Figure 6-1: CO conversion as a function of temperature with different CO and H_2 concentrations in the feed.

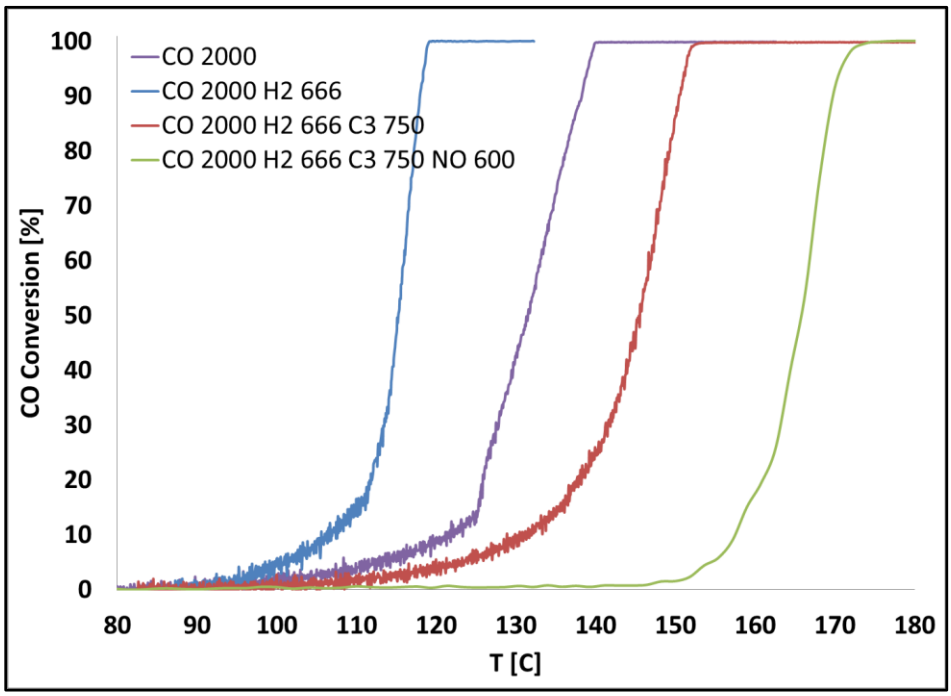

Figure 6-2: CO conversion as a function of temperature with different inlet gas composition.

6.4.2 C_3H_6 Oxidation

The results of C_3H_6 TPO at different C_3H_6 concentrations are shown in Figure (6-3). Like CO oxidation, the light-off temperature of C_3H_6 increased with increasing C_3H_6 concentration in the feed. Table (6-3) lists light-off temperatures for different C_3H_6 concentrations in the feed. The kinetics of C_3H_6 oxidation are similar to CO, as both follow the Langmuir-Hinshelwood mechanism [35, 36, 67, 154], in which the reaction occurs after CO or C_3H_6 and O_2 molecules are adsorbed on the surface at two different sites [47, 48, 56]. The increase in C_3H_6 light-off temperature with increasing C_3H_6 concentration is due to C_3H_6 self-poisoning. As the temperature increased, the desorption rate of C_3H_6 increased and the surface became dominated by O_2 instead, just as in the case of CO. To study the effect of CO on C_3H_6 oxidation, CO was added to the inlet gas with the following concentrations: 500 ppm, 1000 ppm, 2000 ppm, while the C_3H_6 concentration was maintained at 250 ppm. Figure (6-4)

shows the resulting CO and C_3H_6 conversions. The C_3H_6 oxidation light-off temperature increased with increasing CO in the mixture. This inhibition effect of CO on C_3H_6 oxidation was again due to competition between CO and C_3H_6 for active sites. CO molecules have a higher affinity in adsorbing to Pt and block active sites making the sites unavailable for C_3H_6 oxidation. Once CO oxidation begins, sites become free, leading to C_3H_6 oxidation onset. The influence of NO on C_3H_6 oxidation was also investigated, with results shown in Figure (6-5). The concentration of NO was doubled in each run, while maintaining the C_3H_6 concentration at 500 ppm. Table (6-4) shows the C_3H_6 oxidation light-off temperatures with NO in the mixture. The light-off temperature of C_3H_6 increased with increasing NO concentration in the mixture. NO_2 was not observed until the C_3H_6 was completely oxidized, because C_3H_6 reacts with produced NO_2 [21]. HC oxidation has been shown to preferentially consume the NO_2 relative to O_2, thus NO_2 was not observed until all C_3H_6 was completely reacted. Figure (6-6) compares the effect of CO and NO on C_3H_6 oxidation and Table (6-5) lists the light-off temperatures with different inlet gas compositions. The C_3H_6 oxidation light-off temperature increased with the addition of both CO and NO to the mixture. This inhibition increases with increasing CO and NO concentrations in the mixture [35].

Table 6-3: C_3H_6 T_{50} oxidation values with different C_3H_6 concentrations in the feed.

C_3H_6 [ppm]	T_{50} [°C]
250	102
500	121
750	136

Table 6-4: C_3H_6 and NO oxidation T_{50} values with different feed gas compositions.

C_3H_6 [ppm]	NO [ppm]	C_3H_6 T_{50} [°C]	NO T_{50} [°C]
500	150	165	174
500	300	177	186
500	600	184	194

Table 6-5 : C_3H_6 light-off temperatures T_{50} at different feed gas compositions.

Experiment	CO [ppm]	H_2 [ppm]	C_3H_6 [ppm]	NO [ppm]	T_{50} [°C]
1			500		121
2	1000	333	500		145
3	1000	333	500	150	150

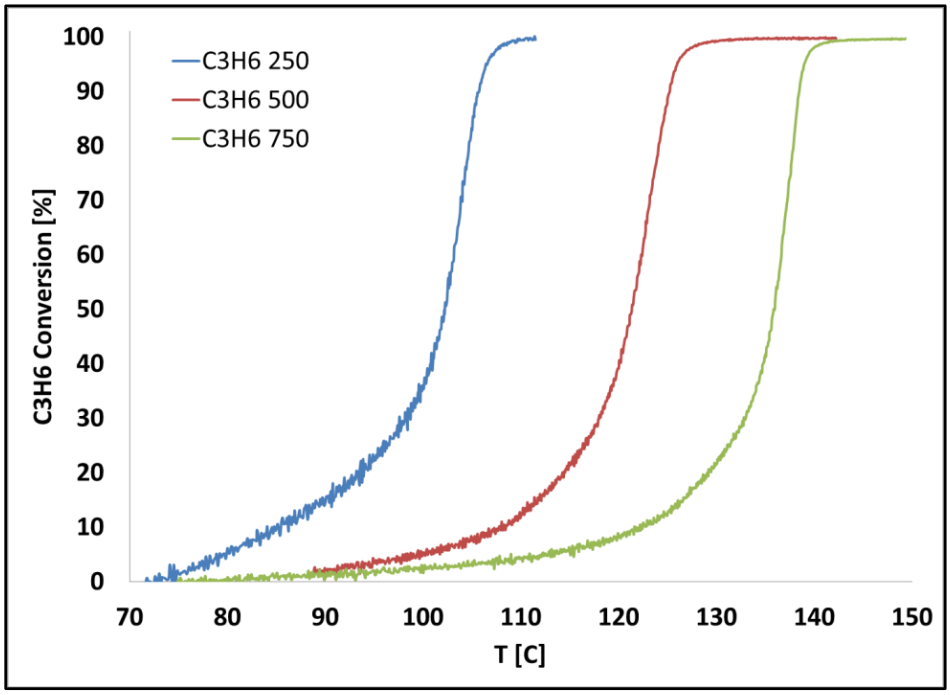

Figure 6-3: C_3H_6 conversion as a function of temperature with different C_3H_6 concentrations in the feed.

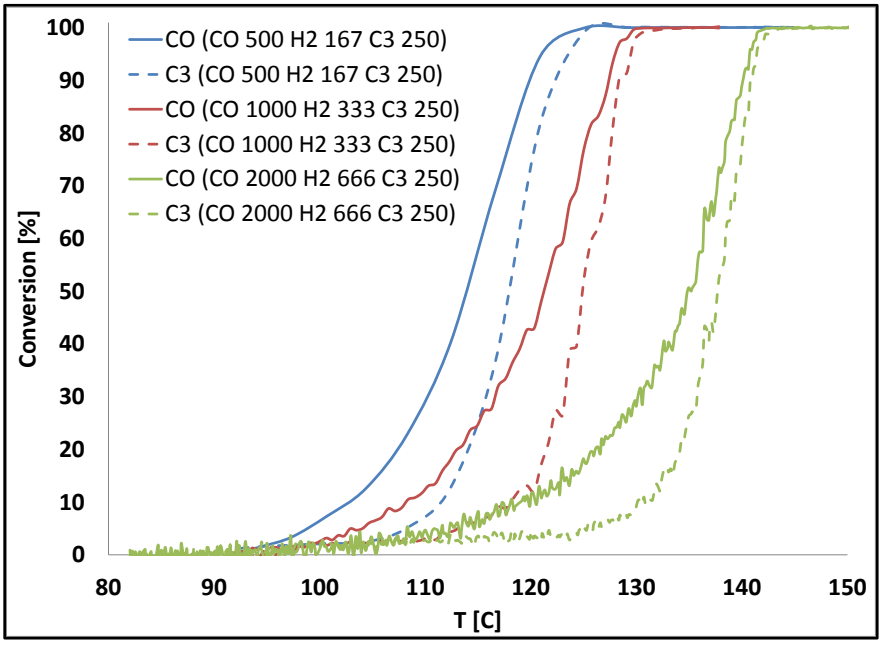

Figure 6-4: C_3H_6 and CO conversions as a function of temperature with 250 ppm C_3H_6 and different CO and H_2 concentrations in the feed.

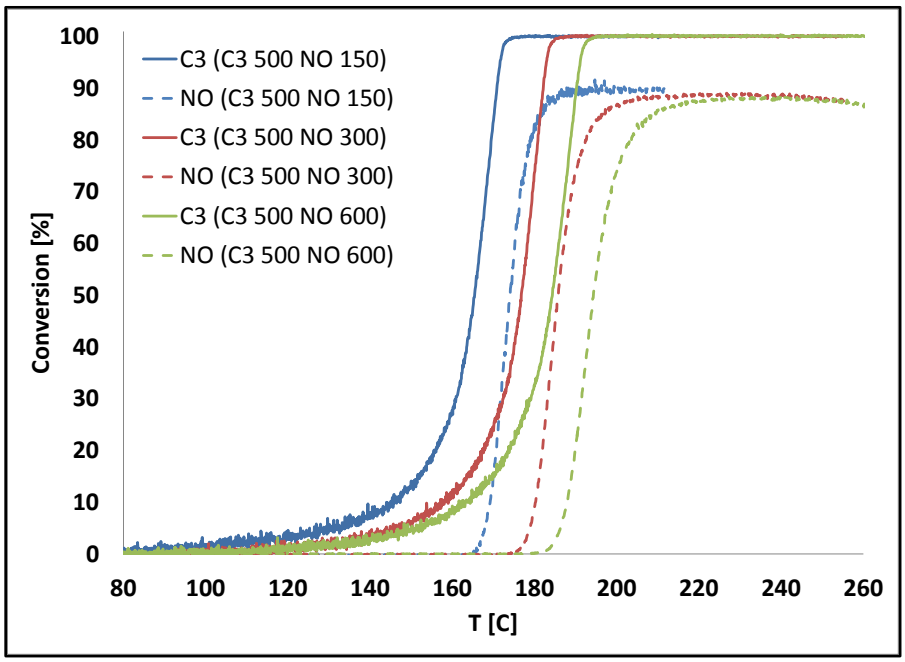

Figure 6-5: C_3H_6 and NO conversions as a function of temperature with 500 ppm C_3H_6 and different NO concentrations in the feed.

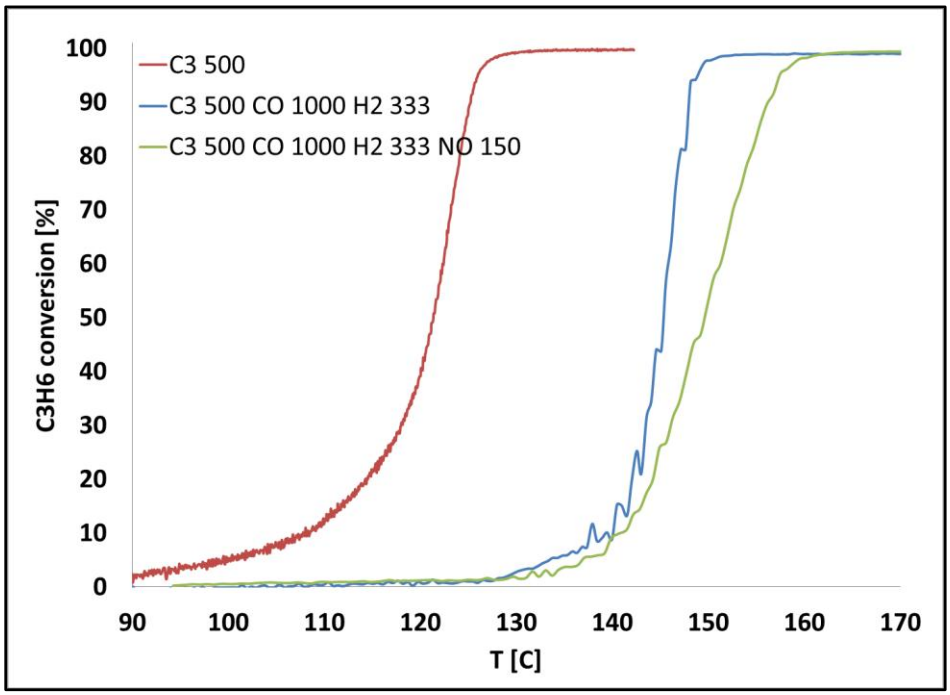

Figure 6-6: C_3H_6 conversion as a function of temperature with and without CO, H_2 and NO added.

6.5 Conclusions

The oxidation performance of a Pt/Al_2O_3 catalyst when different inlet gas compositions were fed was investigated using temperature-programmed oxidation experiments to better understand the effect of different species on the overall conversion. TPO results showed that CO, C_3H_6, and NO inhibited CO and C_3H_6 conversions by increasing the oxidation reaction light-off temperatures. The CO and C_3H_6 oxidation light-off temperatures, when tested separately, increased with increasing CO and C_3H_6 concentrations due to a self-poisoning effect. When present in a mixture, C_3H_6 and NO inhibited CO oxidation by competing with CO for active sites. For the same reason, C_3H_6 oxidation was inhibited by CO and NO.

These experiments actually included both ignition (shown) and extinction, where the temperature is ramped downward while the reaction is still being evaluated. The conversions as a

function of temperature differ between these two phases, with the activity during CO and C_3H_6 oxidation being higher during extinction than ignition, as will be explained in the following chapter. However, when these two were added together, the opposite was observed under certain conditions, i.e. activity during ignition was higher than extinction. This phenomenon was investigated further.

Chapter 7: Inverse Hysteresis Phenomenon during CO and C_3H_6 Oxidation over a Pt/Al_2O_3 Catalyst*

7.1 Abstract

It is well known that conversion as a function of temperature hysteresis can occur in exothermic reaction experiments, such as CO oxidation over Pt/Al_2O_3, with the activity during the ignition process not matching that during the extinction process. Conversions being higher during extinction than that during ignition are often observed. Several explanations have been proposed in which heat effects, different catalyst surface states, and different Pt oxidation states are the most common. In this work CO oxidation hysteresis behavior, when in a mixture with C_3H_6, was investigated. The results show that when C_3H_6 was absent, CO oxidation followed normal hysteresis behavior; however, when C_3H_6 was added to the mixture, the catalytic activity during the extinction phase decreased. As the C_3H_6 concentration in the mixture increased, the hysteresis loop became smaller and ultimately reverse hysteresis was observed. The decrease in catalytic activity during extinction was due to the formation of C_3H_6 oxidation intermediate species. These species competed with CO for active sites, thus inhibiting CO oxidation, and were not present during ignition as CO was the dominant adsorbed species when starting at low temperature.

7.2 Introduction

Carbon monoxide (CO) and hydrocarbons (HCs) are pollutants emitted from vehicle engines. For diesel engines, diesel oxidation catalysts (DOCs) are used in aftertreatment systems to convert CO and HC species to CO_2 and H_2O.

*See Appendix C for permission.

Even though DOCs provide very effective control of CO and HC emissions at higher temperatures, during the cold start period significant amounts of CO and HCs pass unconverted through the catalyst [22, 127]. During the cold start period the catalyst temperature is too low for the reactions to take place. The oxidation of CO on Pt has been investigated in numerous studies, including in the classic work of Langmuir [35, 48, 106-109, 129]. CO oxidation is known to occur through a Langumir-Hinshelwood dual-site mechanism, in which the reaction occurs between CO and O_2 after both molecules adsorb on the surface [47, 48, 56]. Langmuir and others observed that at high temperature and excess oxygen, active sites are entirely covered with oxygen and the reaction is limited by the rate at which CO adsorbs to the surface [106, 107, 109]. However, at low temperature the surface is covered with CO and the reaction is inhibited by strong adsorption of CO on the surface, a phenomenon known as CO self-poisoning [35, 106, 108, 109]. The effect of CO self-poisoning increases with increasing CO concentration [48] and decreases with increasing temperature, with negligible inhibition above 400 °C [35, 107]. Voltz et al. [35] found that at low temperature, CO and C_3H_6 are both self-inhibiting. Furthermore, in a CO + C_3H_6 mixture, CO inhibits C_3H_6 oxidation and vice versa due to competitive adsorption over catalytically active sites [35].

CO oxidation ignition and extinction studies show hysteresis behavior, with higher conversion during extinction [47, 56, 110-123]. Carlsson and Skoglundh [111] explained normal hysteresis as a combination of three possible reasons: (1) inherent kinetic bistability, (2) interaction between reaction kinetics and diffusion phenomena, and (3) locally high temperatures on the catalyst surface. Hysteresis, or multiplicity, in CO oxidation on Pt was discussed by Beusch et al. [110] who argued that the multiplicity exists when the intrinsic rates of the reaction and chemisorption steps are of equal size. An alternative explanation of hysteresis [115, 117, 118, 123] is the interaction between surface reaction and diffusion. Hegedus et al. [115] concluded that CO oxidation hysteresis behavior

is due to the interaction of the negative-order kinetics for CO oxidation with the diffusive resistances of the catalysts. For example, the region of hysteresis was broadened by increasing the diffusion resistance of the tested Pt/Al_2O_3 catalyst by partially aging the catalyst [115]. Oh et al. [116], who investigated the role of intrapellet diffusion resistance in hysteresis during CO oxidation over $Pt-Al_2O_3$, also showed that the width of conversion-temperature hysteresis loop is a function of particle size and it could be eliminated if the catalyst particle size is very small. However, Carlsson et al. [56] concluded that CO oxidation hysteresis is associated with different rates at which Pt is oxidized and reduced as function of gas-phase composition, which could also be related to the different oxidation and reduction rates associated with different particle sizes. Another explanation was put forward by Gudkov and et al. [113], who explained hysteresis as local "overheating" of the active sites on the catalyst, caused by relatively slow dissipation of the energy through dispersed catalyst particles. This was supported in other studies by Subbotin et al. [119-121]. According to their results, in an exothermic reaction, such as CO oxidation, the rate of heat liberated is larger than the rate of heat dissipated in the environment due to the support's (or inactive catalytic mass) low thermal conductivity in which heat is released. Therefore, during the extinction phase, when the temperature of the inlet gas decreases, the temperature drop over the catalyst surface lags, staying warmer. In addition, it has been observed that the width of hysteresis loop increases with increasing CO concentration [119-121]. In terms of Pt state, Salomons et al. [47] modeled CO oxidation during ignition and extinction using a LH mechanism, with a dissociative chemisorption step for oxygen requiring two surface sites, whereby ignition and extinction processes corresponded to the two states of predominantly CO covered or O_2 covered.

Unlike CO oxidation, Hauptmann et al. [114] have shown that NO oxidation on a Pt catalyst under excess oxygen conditions exhibits "inverse hysteresis" as the catalytic activity during ignition exceeds the activity during extinction. The reason for this inverse hysteresis behavior during NO

oxidation is that Pt is oxidized by NO_2, and the oxide is less catalytically active than metallic Pt. As the temperature drops during extinction, the Pt is more highly oxidized than it was during ignition, leading to poorer performance. In addition, in a $CO/NO/O_2$ mixture, CO hysteresis behavior switches from normal hysteresis to inverse hysteresis, which the authors attributed to reversible oxidation of Pt [114].

In this study, the hysteresis behavior of CO oxidation in a CO + C_3H_6 mixture over a Pt/Al_2O_3 monolith catalyst was investigated. Specifically, it was observed that C_3H_6 had a negative effect on CO oxidation during extinction. To explain the impact, TPO experiments and in situ DRIIFTS were used, during ignition and extinction, to determine if this was due to temperature or surface changes as a function of the C_3H_6 exposure.

7.3 Experimental Procedures

The Pt/Al_2O_3 sample used, with a total Pt loading of 95g/ft^3 (3.35kg/m^3) based on total monolith volume, was provided in monolithic form by Umicore AG. The sample was 1" in diameter with a length of 2.5". The sample was inserted into a horizontal quartz tube, which was placed inside a Lindberg Minimite temperature controlled furnace. The temperature was measured with 2 K-type thermocouples located at radial centers of the catalyst; the front one placed 1mm upstream of the catalyst and the back one just inside outlet face of the catalyst. CO, C_3H_6, CO_2 and O_2, were supplied from compressed gas cylinders by Praxair, and N_2 was generated using a nitrogen generator manufactured by OnSite Gas Systems. The flow rates of the various gases were controlled by Bronkhorst mass flow controllers and water was introduced using a Bronkhorst CEM system. The effluent gas from the reactor was analyzed using a MKS MultiGas 2030 FTIR analyzer. A matrix of experiments with different CO and C_3H_6 concentrations was run, shown in Table (7-1), and in all experiments the feed also contained 10% O_2, 10% H_2O, 10% CO_2, and a balance of N_2, at a space velocity of 25,000 hr^{-1} at standard conditions. In all CO + C_3H_6 mixture experiments, the temperature

was ramped from 90°C to 160°C at a rate of 3°C/min. Then the ramping was stopped and the reactor was cooled by decreasing the temperature of the furnace back to 90°C. Before each experiment the catalyst was treated with 10% O_2 in N_2 for 20 minutes at 200°C, then the catalyst was cooled down under N_2 to 90°C for the next experiment.

Table 7-1: CO and C_3H_6 concentrations during TPO experiments

Run	CO [ppm]	C_3H_6 [ppm]
1	500	0
2	1000	0
3	1000	300
4	1000	500
5	1000	800

7.4 Results and Discussion

7.4.1 CO Oxidation

Figure (7-1) shows the results from temperature programmed CO oxidation of 500 ppm and 1000 ppm CO during the temperature ramp up (solid lines) and the temperature ramp down (dashed lines). The inlet gas temperatures corresponding to 50% CO conversion, $T_{(50)}$, during ignition and extinction are listed in Table (7-2). These data show normal hysteresis behavior. Also, the temperature difference (ΔT) at 50% conversion between the ignition and extinction increased with increasing CO concentration. Thus, the width of the hysteresis loop was larger with higher CO concentration. Such a trend has been previously observed in several studies [16-20, 22, 23] for the reasons explained in the Introduction section. A potential explanation, based on the possibilities listed in the Introduction section, for the increase in activity during extinction is the catalyst surface or active sites being at a higher temperature than the measured temperature due to the heat generated by

the exothermic reaction and thermal inertia of the catalyst (the catalyst temperature change lags behind the inlet temperature change during the ramp down) [114]. Data in Figure (7-1) and temperature differences listed in Table (7-2) support this theory. It can also be related to Pt surface coverage and Pt chemical state [56, 111, 115], or a combination of these effects. As mentioned above, during ignition catalytic activity increases, but initially the Pt surface is predominantly covered with CO and the reaction is CO self-poisoned [56, 111, 155]. At higher temperature, once the reaction reaches complete conversion, all adsorbed CO is converted and the Pt surface becomes predominantly covered with O_2. Therefore, during extinction, as the temperature decreases below the temperature of complete conversion, the catalyst can remain active until adsorbed CO builds up, which is slowed due to the locally high temperatures of the active sites. The data in Figure (7-1) indicate that CO coverage inhibited the reaction at low temperature, CO self-inhibition, and this affected the reaction during ignition of course, but only affects the extinction phase once the inlet gas temperature was much lower.

Table 7-2: Ignition and extinction $T_{(50)}$ CO oxidation values in a gas mixture including 10% O_2, 10% H_2O, 10% CO_2, balanced by N_2 at a GHSV 25,000 h^{-1}.

CO [ppm]	Ignition T [°C]	Extinction T [°C]	Δ T [°C]
500	95	87	8
1000	120	108	12

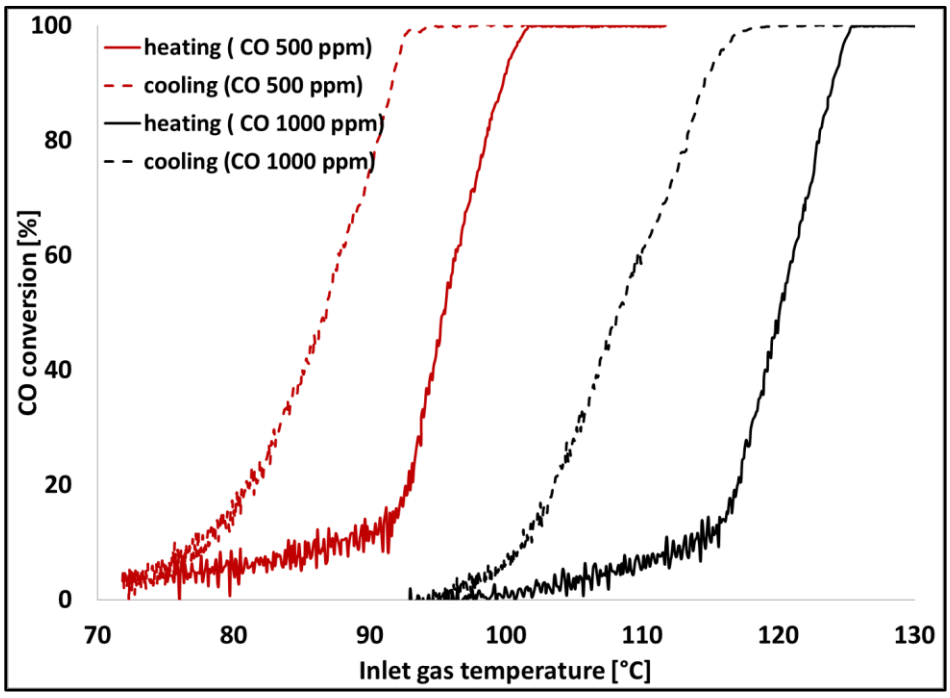

Figure 7-1: Temperature-programmed CO oxidation with the following inlet conditions: 1000 ppm or 500 ppm CO, 10% H_2O, 10% CO_2, and 10% O_2 over a Pt/Al_2O_3 monolith.

7.4.2 CO + C_3H_6 Oxidation

The results of TPO, during heating and cooling, with a CO and C_3H_6 mixture are shown in Figures (7-2) and (7-3). The inlet gas mixture consisted of different C_3H_6 concentrations (300 ppm, 500 ppm, 800 ppm), 1000 ppm CO, 10% H_2O, 10% O_2, 10% CO_2, and balanced by N_2. Figure (7-2) shows CO conversion as a function of inlet gas temperature at different C_3H_6/CO ratios. When C_3H_6 was not present in the inlet mixture, CO conversion exhibited normal hysteresis behavior as the ignition temperature at lower conversions was higher than those for extinction. However, when C_3H_6 was added to the mixture, the temperatures required to achieve certain conversions during the extinction phase increased and the hysteresis loop became smaller. Table (7-3) shows temperature differences between ignition and extinction corresponding to 20%, 50%, and 80% conversion. As the C_3H_6/CO ratio increased, the extinction conversions continued to shift to higher temperature. At a 0.8

C_3H_6/CO ratio, the extinction temperatures, for conversions less than 100%, became higher than the ignition temperatures, reverse hysteresis, as shown in Table (7-3) (with a negative difference between the ignition and extinction temperatures representing reverse hysteresis). C_3H_6 conversion as a function of inlet temperature is shown in Figure (7-3). Like CO conversion, increasing the C_3H_6 concentration increased the temperatures to reach a certain conversion during the extinction phase and the hysteresis loop became smaller. Table (7-4) lists the temperature differences between the front and the back of the monolith at maximum conversion for the CO + C_3H_6 mixtures. The difference between front and back temperature, ΔT, increased with increasing C_3H_6 in the mixture, however, the hysteresis loop became smaller as the temperature required to sustain maximum conversion increased during extinction. This is therefore not explained by the heat generated by the exothermic reactions or overheating theory that was proposed in many studies. Based on the overheating theory, the higher the concentration of reactant in the feed, the higher the exothermic heat released, and the larger the hysteresis loop should have become. However, these results with the CO/C_3H_6 mixture showed that the hysteresis loop became smaller when C_3H_6 concentration, and consequently exothermic reaction heat generated, increased.

Table 7-3: ($T_{Ignition}$ - $T_{extinction}$) at $T_{(20)}$, $T_{(50)}$, and $T_{(80)}$, of different inlet C_3H_6 concentrations, 1000 ppm CO, 10% O_2, 10% H_2O, 10% CO_2, balanced N_2 at a GHSV 25,000 h^{-1}.

CO [ppm]	C_3H_6 [ppm]	ΔT_{20} [°C]	ΔT_{50} [°C]	ΔT_{80} [°C]
1000	0	13	11	10
1000	300	2	5	5
1000	500	0	2	3
1000	800	-3	-3	-4

Table 7-4: Difference between back and front temperatures, ΔT, at maximum conversion with different combinations of CO and C_3H_6 with 10% O_2, 10% H_2O, 10% CO_2, and balanced N_2 at a GHSV 25,000 h^{-1}.

CO [ppm]	C_3H_6 [ppm]	Δ T [°C]
1000	0	23
1000	300	30
1000	500	38
1000	800	56

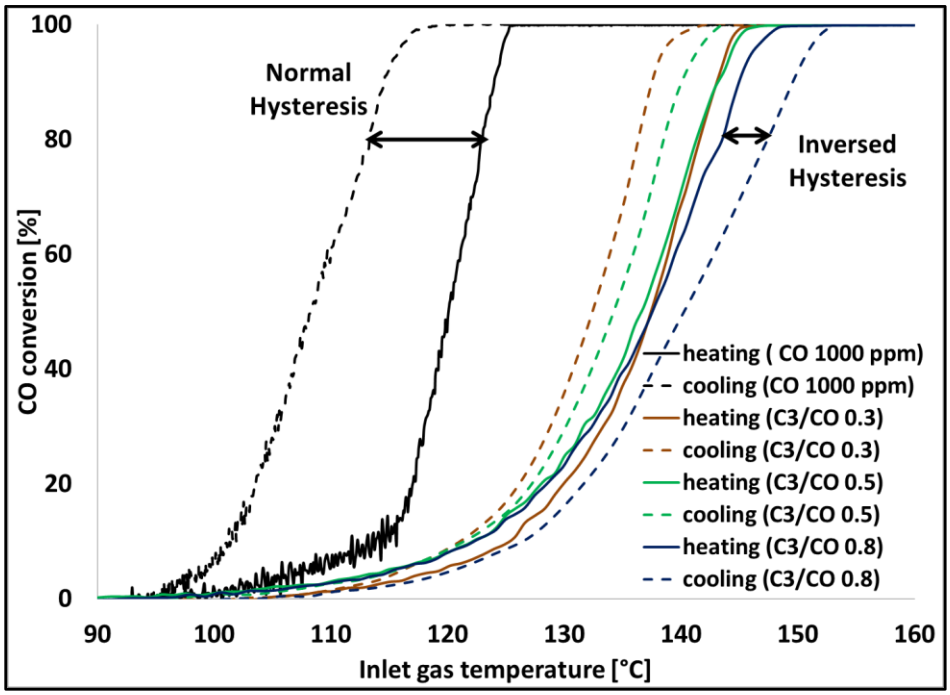

Figure 7-2: Temperature-programmed oxidation of CO/C_3H_6 mixture at the following inlet conditions: 1000ppm CO, 10% H_2O, 10% CO_2, 10% O_2, with different amounts of C_3H_6 over the Pt/Al_2O_3 monolith.

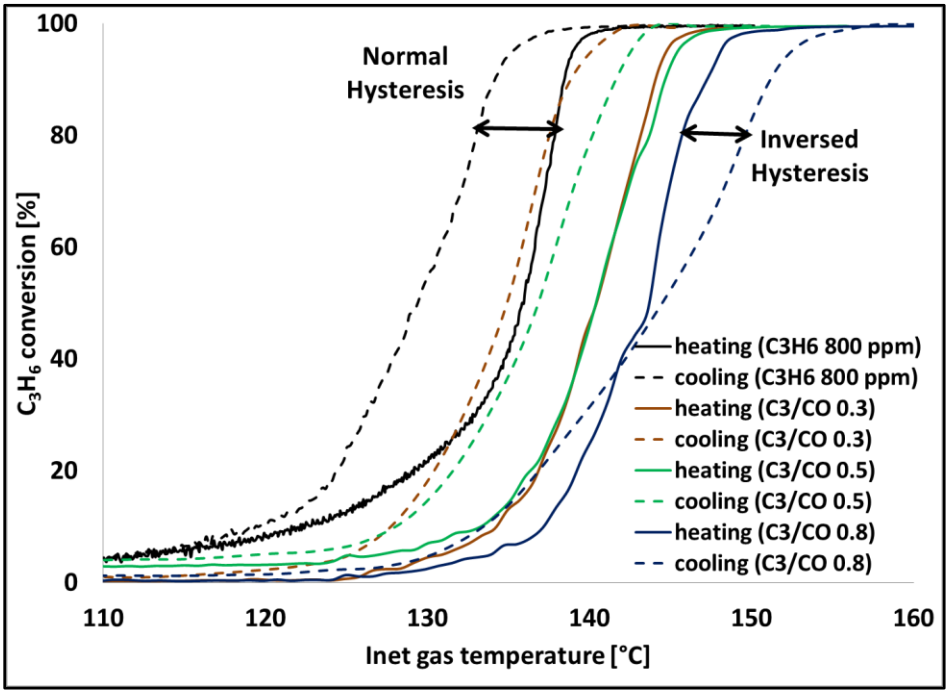

Figure 7-3: Temperature-programmed oxidation of CO/C_3H_6 mixture at the following inlet conditions: 1000ppm CO, 10% H_2O, 10% CO_2, 10% O_2, and different amount of C_3H_6 over a Pt/Al_2O_3 monolith.

7.5 DRIFT Spectroscopy

In situ diffuse reflectance infrared Fourier transform spectroscopy (DRIFTS) was used to investigate species formation on the catalyst surface in the presence of the CO/C_3H_6 mixture during ignition and extinction tests. DRIFTS spectra were recorded at 100, 120, 140, and 160°C, first increasing from 100 to 160°C, as in ignition, then decreasing back to 100°C, as in extinction. In order to understand the difference between what occurred during ignition versus extinction, in terms of catalyst surface coverage, DRIFTS spectra obtained with exposure of the Pt/Al_2O_3 powder to 1000 ppm CO and 0 or 600 ppm C_3H_6 are shown in Figure (7-4). In the absence of C_3H_6, the species formed on the surface, CO_2 at 2300-2400 cm^{-1}, blue circle, CO at 2000-2200 cm^{-1}, red circle, and carboxylate groups at 1500-1700 cm^{-1} [156-159], green circle, during ignition are similar to the those present during extinction, with the spectra overlapping, Figure (7-4-(A)), except for the peak at 1596

cm^{-1} which corresponds to the presence of bidentate carbonate species on the surface during extinction. This peak indicates that bidentate carbonate species are CO oxidation intermediates or byproducts that built up on the surface as the temperature decreased during the extinction phase.

On the other hand, in the case of exposure to the CO + C_3H_6 mixture, Figure (7-4-(B)), more species are present during extinction than during ignition. The peaks between 2300-2400 cm^{-1} are assigned to CO_2 bound to Pt and CO_2 gas, and were present in both ignition and extinction and they follow the same trend in terms of intensity. Similarly, in both phases, the peak at 2067 cm^{-1}, assigned to Pt bound CO, was seen at low temperature, but it disappeared at temperatures above 140°C. Unlike Figure (7-4-(A)), at temperatures below 120°C, the peak at 2067 cm^{-1} (Pt-CO) was present and the peaks at 2300-2400 cm^{-1} (CO_2) were absent in Figure (7-4-(B)). The absence of the CO_2 peak, and the CO peak being present at higher temperatures, albeit this may be associated with C_3H_6 oxidation as discussed below, is consistent with C_3H_6 inhibition of CO oxidation [35]. Furthermore, CO is an intermediate product of C_3H_6 oxidation during the extinction process, as discussed below; therefore, in the presence of C_3H_6 the peak at 2067 cm^{-1} appeared at higher temperatures and with greater intensity than in the absence of C_3H_6. The peaks increased in intensity as the C_3H_6 concentration increased. As verification, in tests with only C_3H_6 (i.e. with no CO in the mixture, data not shown), peaks in this range also appeared during extinction, demonstrating that these were associated with C_3H_6 oxidation intermediates. For this reason, the CO peak in Figure (7-4-(B)) is related to C_3H_6 oxidation rather than CO in the feed. In addition, between 1700 and 1300 cm^{-1} more peaks were observed with C_3H_6 in the mixture relative to in its absence, as shown in green circles in Figure (7-4). For example, in the presence of C_3H_6 the peaks at 1662 to 1560, 1456, and 1388 cm^{-1}, associated with different carboxylic groups [156, 157, 159-162], were higher in intensity during extinction, relative to ignition. During extinction, as the temperature decreased, the oxidation of these intermediate species slowed, allowing them to remain longer and therefore build up. The peaks at 1652 and 1456 cm^{-1} are

assigned to surface and bulk bicarbonates [156-159], respectively. The peaks at 1585 and 1388 are attributed to formate species [156, 160]. This indicates that in the presence of C_3H_6, more bicarbonate and formate species are present during the extinction process. At high temperatures these intermediates were easily oxidized, but as the temperature dropped, they built-up on the surface and compete with CO for active sites, thus inhibiting CO oxidation during extinction process.

Overall, these results show that intermediate species form during C_3H_6 oxidation and that the amounts on the surface during ignition and extinction differ. The data suggest that during the extinction phase, these intermediates compete with CO for, or block CO from, active sites. For this reason, CO oxidation during the extinction phase was inhibited. The inhibition stems from the build-up of different carboxylic, bicarbonate, and formate species as the temperature dropped. Thus, as the C_3H_6 concentration increased in the mixture, more intermediate species were present on the surface and CO oxidation during extinction moved to higher temperature.

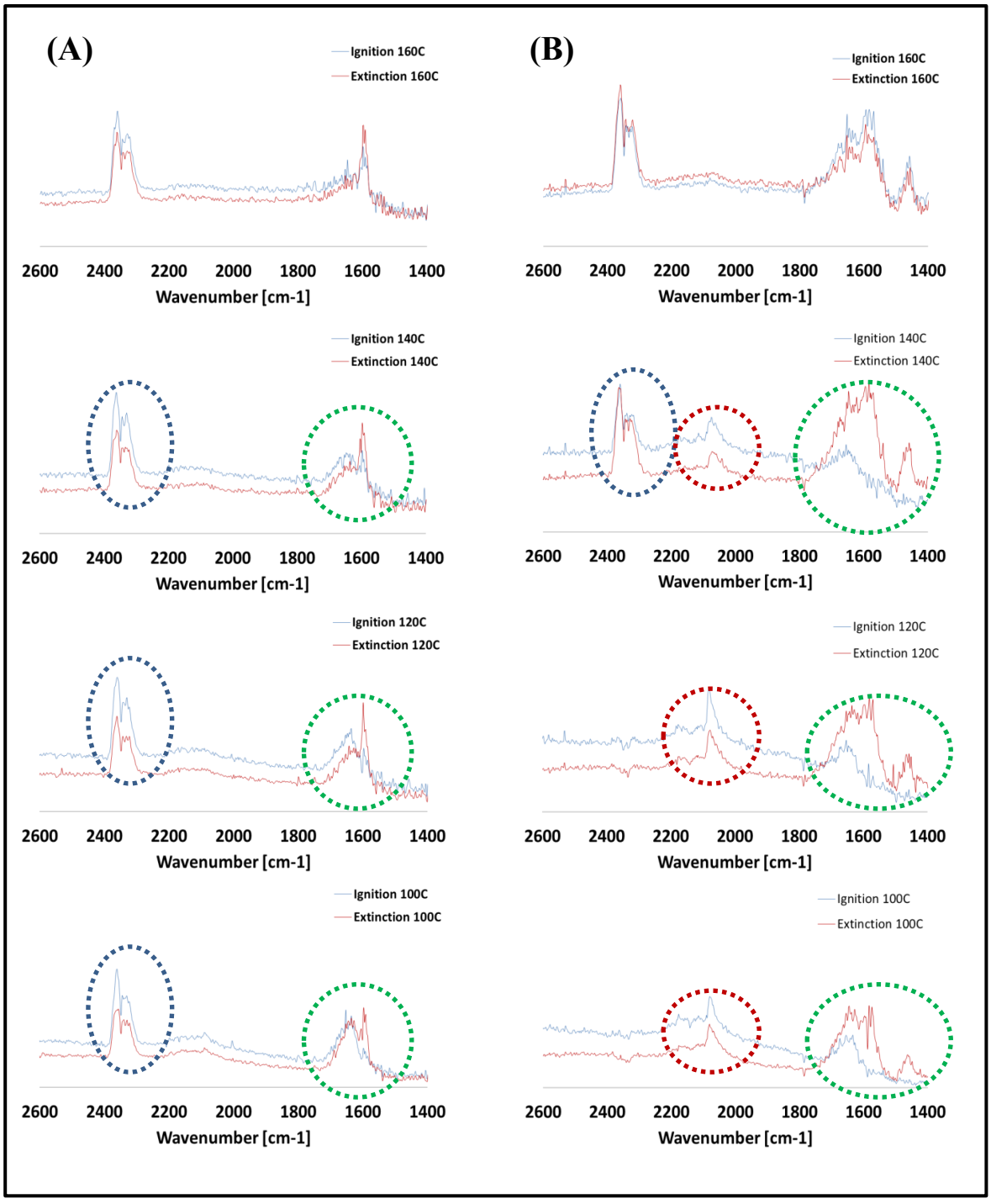

Figure 7-4: DRIFTS spectra recorded during ignition and extinction phases at different steady state temperatures with 1000 ppm CO and (A) 0 ppm C_3H_6 and (B) 600 ppm C_3H_6.

7.6 Conclusions

The oxidation of CO and CO + C_3H_6 over Pt/Al_2O_3 was studied, during both ignition and extinction. The results show that CO oxidation exhibits normal hysteresis in the absence of C_3H_6. However, in a CO + C_3H_6 mixture, as the C_3H_6 concentration increased in the mixture, CO and C_3H_6 normal hysteresis behavior shifted to inverse hysteresis, with the catalytic activity during extinction phase lower than that during ignition. The decrease in catalytic activity during the extinction phase in the CO + C_3H_6 mixture was due to the formation of intermediate C_3H_6 oxidation species. These intermediate species, carboxylic groups, carbonates, and formates, compete with CO for active sites, thus inhibiting CO oxidation during extinction.

Chapter 8: Conclusions and Recommendations

8.1 Conclusions

In this study different aspects of Pt/Al_2O_3 oxidation catalysis were studied, including the effect of axial distribution of the catalyst and species interaction on the overall performance. The first part focuses on the performance and durability of a uniformly distributed catalyst (standard) and a non-uniformly distributed catalyst (zoned), with more Pt concentrated at the inlet of the catalyst, with different inlet gas compositions and total flow rates. Results showed that the performance of the zoned catalyst was superior to that of the standard for CO and C_3H_6 oxidation reactions, whereas the two samples were similar for NO oxidation. At a higher total flow rate and with a mixture of reactants (i.e. C_3H_6 and NO), the difference between the zoned and standard samples was more significant; however, at a lower total flow rate and a single reactant case the difference was less significant. For CO and C_3H_6 oxidation, the temperature profile inside the catalyst showed that the zoned sample produced more heat in the front via the exotherm generated during the oxidation reaction and there was a coincident lower self-poisoning effect. Hence, the performance of the zoned sample was better than that of the standard sample. In a C_3H_6/NO mixture, spatially resolved gas measurements showed that the zoned sample utilizes a smaller volume at the front of the monolith to oxidize C_3H_6 leaving a larger volume for NO oxidation. The zoned sample, therefore, had better performance than the standard sample in this mixture especially at low temperature. Catalyst durability was tested by thermally degrading the whole catalyst (homogeneous aging) and the back part only (heterogeneous aging) to simulate different conditions that the catalyst experiences in a real application. Thermal aging results showed that the performance of the zoned catalyst was better than that of the standard catalyst. The performance of the zoned sample was not greatly affected after heterogeneous aging because most of the Pt particles, located in the front part, remained unaffected by exposing the back, which contains less Pt particles, to high temperature. At a high total flow rate, the rate of conversion

increase with temperature for CO and C_3H_6 oxidation in the zoned sample slowed down as the reaction zone moved toward the front, which contains larger Pt particles, thus Pt sintering was greater in the front of the zoned sample compared to that of the standard sample.

In the second part of this work, the effect of reactant species interactions on a commercial Pt/Al_2O_3 catalyst was investigated using a matrix of experiments with different inlet gas compositions. Results show that in a reaction involving only one of the species of interest, CO and C_3H_6 inhibit their own oxidation due to an increasing self-inhibition effect. When there is a mixture of the key species, CO, C_3H_6, and NO inhibit each other oxidation because of competitive adsorption on active sites. In contrast, H_2 promotes CO oxidation because it reduces the effect of CO self-inhibition. Studying the CO + C_3H_6 reactions during ignition and extinction produced an interesting hysteresis phenomenon as C_3H_6 concentration increased in the mixture. In the absence of C_3H_6, CO oxidation exhibits normal hysteresis as CO conversion during extinction occurred at lower temperature than the conversion during ignition. In the presence of high levels of C_3H_6, however, normal hysteresis behavior shifts to inverse hysteresis. As the C_3H_6 concentration increased in the CO+ C_3H_6 mixture, CO conversion during extinction occurred at higher temperature than CO conversion during ignition. DRIFTS results show that this inhibition effect on CO conversion during extinction is due to the presence of C_3H_6 oxidation intermediates including carboxylic groups, carbonates and formates that compete with CO for active sites, thereby inhibiting CO oxidation during extinction.

8.2 Recommendations

A main goal of this thesis research was to improve the performance of a DOC by utilizing the catalyst more efficiently. In addition, studying the interactions between different species help us understand the mechanism and chemistry on the DOC surface. Based on the experience gained in this work, several recommendations are proposed for the future work to improve the design and performance of DOC:

- The effect of Pt loading on the performance of the standard and zoned catalyst should be studied – as more significant differences may be observed.
- The effect of chemical degradation (i.e. SO_2 poisoning) should be tested on the zoned-based catalyst and compared with the homogeneously distributed catalyst. If the performance of standard catalyst shows better performance than the two-zoned catalyst after SO_2 poisoning, the two-zoned catalyst can be retailored to overcome the effect of SO_2 poisoning by possibly including an upstream "buffer" zone.
- The performance of catalysts should be tested under a larger variety of thermal degradation conditions so the effect of different sintering rates on different zones of the monolith can be more fully understood.
- The effect of hydrocarbons on the CO hysteresis behavior could be further investigated by turning off the inlet flow of C_3H_6 at high temperature and running TPR with H_2 in order to change in extinction process in a clean surface.
- The inverse hysteresis phenomenon was observed at different combinations of CO + NO and C_3H_6 + NO, thus more investigation on the extinction phase of these reactions can better explain the behavior of catalytic converters during accelerating and decelerating.

Appendix A
Statistical Analysis

A.1 ICP Results

The validation of preparation methods used to make the standard and zone-coated catalyst was checked by measuring the total loading of active metal. ICP was used to measure the loading on the standard and zoned catalysts. The sample was prepared for ICP analysis by crushing the monolith sample into fine powder, then dissolving the powder into different acids in order to make liquid solution of the tested metal. These procedures were described earlier in detail in Chapter 3. Due to the high cost of Pt-based catalysts, Co-based catalysts were prepared to practice catalyst preparation. ICP results of the Co-based catalysts, 2 standard and 2 zoned, are show in Table (A-1). The error associated with the standard catalyst loading was very low, less than 3% for both samples. Similarly, the error associated with the loading measurement of the back of the zoned catalyst was about the same for both samples, less than 7%. The calculated error for the front section loading was higher, but still less than 10%. This variation of the front loading, from 3.5% up to 9.2%, is likely due to the need for multiple dips of the front part, potentially compounding the error. Overall the errors were judged to be low and the methods used acceptable.

Table A- 1: ICP results of Co-based samples.

Sample No.	Type	Loading %	ICP results	Error %
1	Standard	5	4.887	2.26
2	Zoned (F)	4	3.630	9.26
3	Zoned (B)	1	0.931	6.94
6	Standard	5	4.895	2.10
7	Zoned (F)	4	3.860	3.51
8	Zoned (B)	1	0.934	6.64

A.2 TPO Results

In the experiments several variables were measured including the temperatures at different positions in the reactor, and the concentration of various species such as CO, C_3H_6, NO, NO_2, CO_2, and H_2O. Statistical analysis is important to identify the accuracy and reliability of the measured data based on a few experiments. In addition, statistical analysis can also identify the source of experimental error and test the effect of different variables on the output without wasting time and money to run extra experiments. This section presents the Normal Probability Plot and Hypothesis Testing, used to check if the data follow a normal distribution and if the results are repeatable (reproducibility). In addition the error with each instrument is provided.

Uncertainty

All measurements are subjects to uncertainty. Uncertainty of the devices used is reported in Table (A-2). These values are obtained from the associated manuals [15].

Table A- 2 : Uncertainties associated with Instruments.

Instrument	Uncertainty (+/-)
Mass Flow Controllers	0.5% of the max. value
Heating System	0.8 ℃
Reactor Thermocouples	1° C
FTIR (MKS)	0.9% of the reading
Mass Spectrometry	2-5% of the reading

Reproducibility

The reproducibility of the data was measured to ensure that the experiments can be repeated in the future using the same conditions. Although some of the TPO experiments were only once repeated, the repeats have shown good agreement with the original experiments, as shown in Figure

(A-1). Thus the standard deviations were calculated based on the errors taken from the MKS and thermocouple measurements reported in Table (A-2). CO oxidation TPO at total flow rate of 10 L/min with the inlet gas composed of 1000 ppm CO, 10% O_2, 5% CO_2, 5% H_2O, and N_2 balance was repeated for both the standard and zoned samples. The error bars for these CO oxidation experiments are shown in Figure (A-2). The repeats of both samples fall within the error bar, although admittedly barely, indicating that the experiments are reproducible and the variation between different experiments was small.

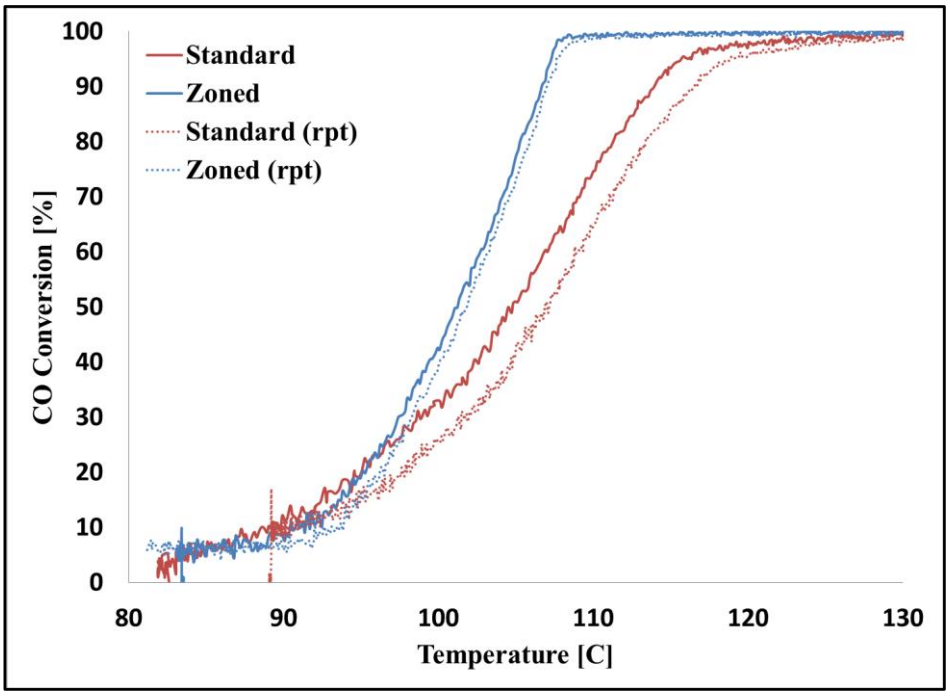

Figure A- 1: CO oxidation as a function of temperature of the standard and zoned sample experiments with the repeats.

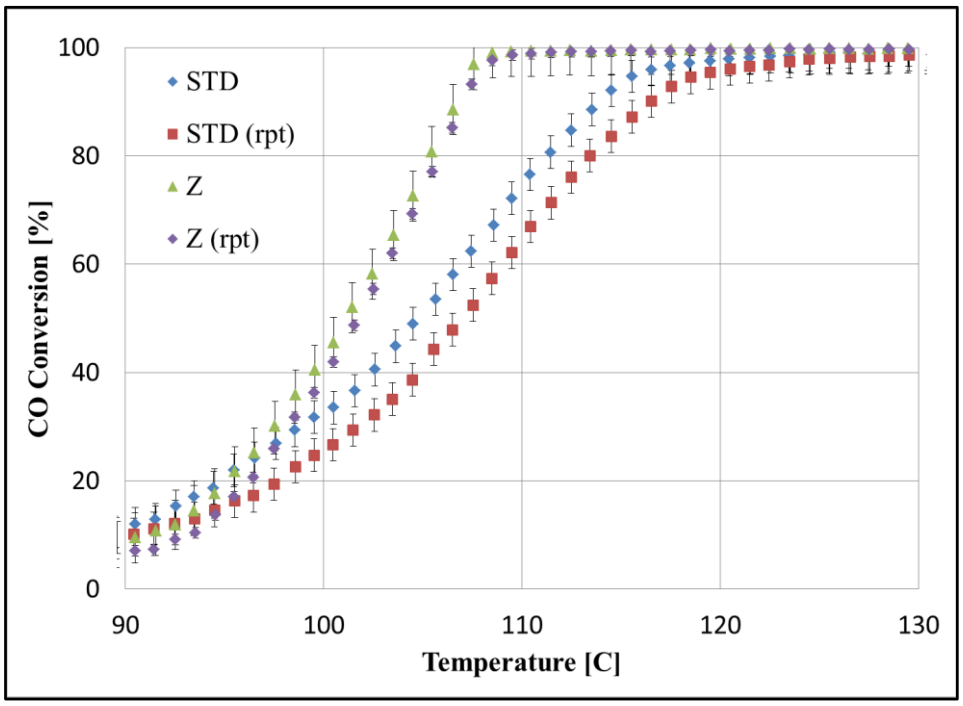

Figure A- 2: CO oxidation as a function of temperature with the error bar corresponding to its standard deviation.

Normal distribution

Normal distribution is widely used in science to describe the trend or behavior of data set or to simplify a complex phenomenon. For example, experimental error due to observation is usually assumed to follow a normal distribution and error propagation is computed using this assumption. The normal probability plot is a technique used in statistics to test whether or not a data set is normally distributed. It is based on a graph where the data are plotted against a theoretical normal distribution values. Normally distributed data will produce a straight line. If there is a deviation from a straight line, then the data are not non-normally distributed. To apply normal probability plot test, first the data are sorted from smallest to highest starting with the smallest value equals to 1. Second the data are ranked using equation (A.3), where i is the rank of the data starting from 1, and N is the total number of data points.

$$\text{Rank (P)} = (i\text{-}0.5)/N \qquad \text{(A.3)}$$

Third the corresponding expected value of each value of (P) is found either in normal probability distribution table (Z-values) or using NORMSIN(P) function in excel. Finally, the expected theoretical value is plotted as a function of observed data. If the data points are normally distributed, it will form a straight line. Normal probability plot tables for standard and zoned samples are shown in tables (A-5) and (A-6) respectively. These temperature-programmed experiments (TPO) were run at 28 L/min, 1000 ppm CO, 5% H_2O, 5% CO_2, and 10% O_2 balanced with N_2. Normal probability plots of the standard and zoned samples are shown in Figures (A-3) and (A-4). As seen in both figures, the data forms approximately a straight line, which indicates that both catalysts data are normally distributed. The value of the coefficient of determination, R2, was close to 1, 0.9719 for standard sample and 0.9715 for zoned sample, which indicates that the model accounts for the data variation with high percentage.

Table A- 3 : Normal probability plot table for CO oxidation (standard sample).

Conversion [%]	Rank [i]	P (rank)	Expected Value
0.043	1	0.024	-1.981
5.043	2	0.071	-1.465
10.064	3	0.119	-1.180
14.507	4	0.167	-0.967
20.204	5	0.214	-0.792
24.949	6	0.262	-0.637
30.203	7	0.310	-0.497
34.499	8	0.357	-0.366
40.463	9	0.405	-0.241
44.910	10	0.452	-0.120
50.621	11	0.500	0.000
54.940	12	0.548	0.120
60.342	13	0.595	0.241
64.646	14	0.643	0.366
69.937	15	0.690	0.497
74.763	16	0.738	0.637

80.507	17	0.786	0.792
84.799	18	0.833	0.967
90.424	19	0.881	1.180
95.024	20	0.929	1.465
99.917	21	0.976	1.981

Table A- 4 : Normal probability plot table for CO oxidation (zoned sample).

Conversion [%]	Rank [i]	P (rank)	Expected Value
0.347	1	0.024	-1.981
5.280	2	0.071	-1.465
10.037	3	0.119	-1.180
14.962	4	0.167	-0.967
20.234	5	0.214	-0.792
25.028	6	0.262	-0.637
30.213	7	0.310	-0.497
35.059	8	0.357	-0.366
39.499	9	0.405	-0.241
45.018	10	0.452	-0.120
49.888	11	0.500	0.000
54.446	12	0.548	0.120
60.474	13	0.595	0.241
65.441	14	0.643	0.366
69.965	15	0.690	0.497
75.536	16	0.738	0.637
80.101	17	0.786	0.792
84.294	18	0.833	0.967
90.354	19	0.881	1.180
95.016	20	0.929	1.465
99.920	21	0.976	1.981

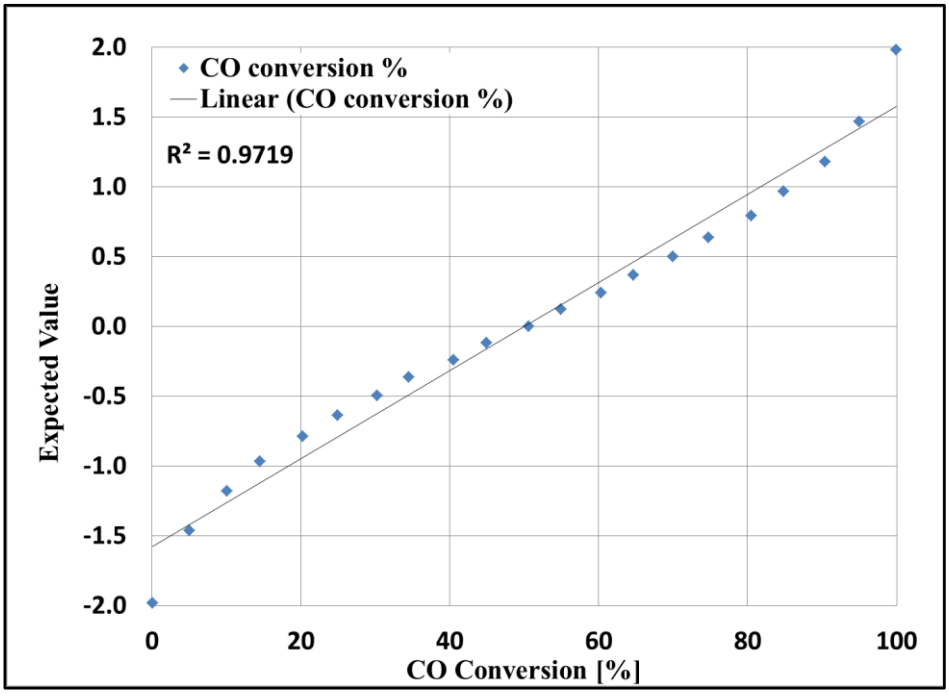

Figure A- 3: Normal probability plot obtained from data taken using the standard sample.

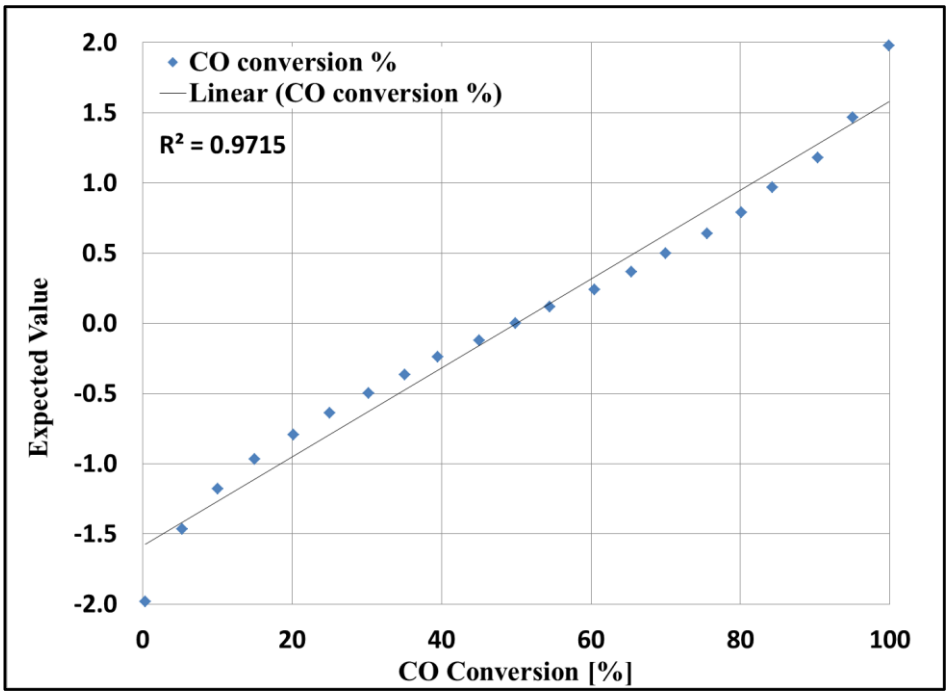

Figure A- 4: Normal probability plot obtained from data taken using the zoned sample.

Appendix B

Auto21 Data

In this section, the rest of the Auto21 data, some of which was discussed in Chapter 6, are presented including: NO oxidation, CO + C_3H_6 + H_2 mixtures, and CO + C_3H_6 + NO + H_2 mixtures. These are simply presented for further reference.

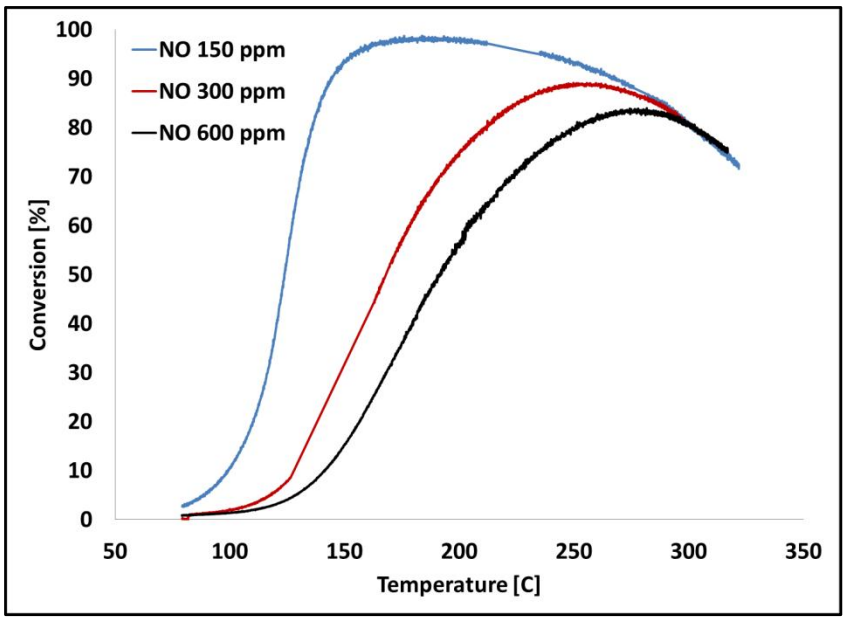

Figure A- 5: NO conversion as a function of temperature with different NO concentrations in the feed.

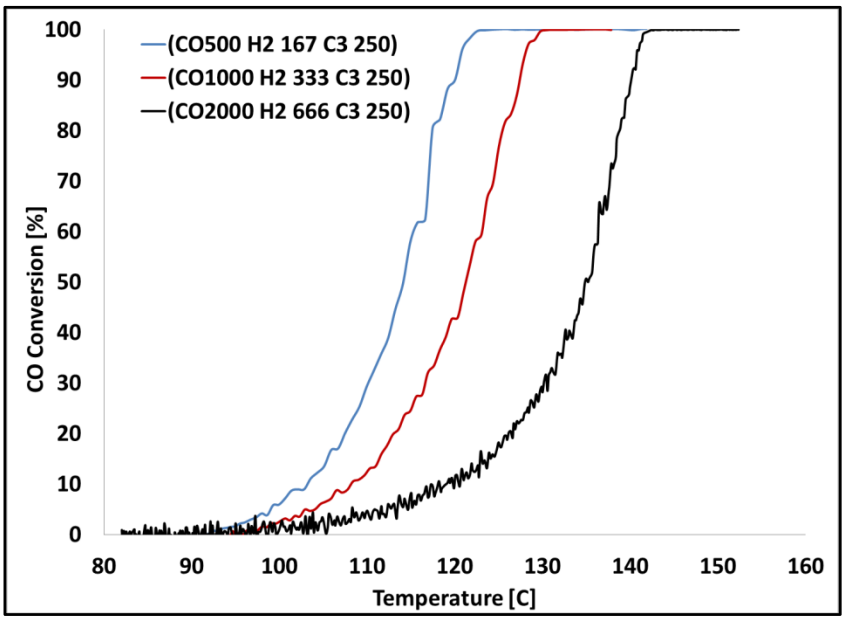

Figure A- 6 : CO conversion as a function of temperature for a CO + C_3H_6 + H_2 mixture with different inlet gas compositions.

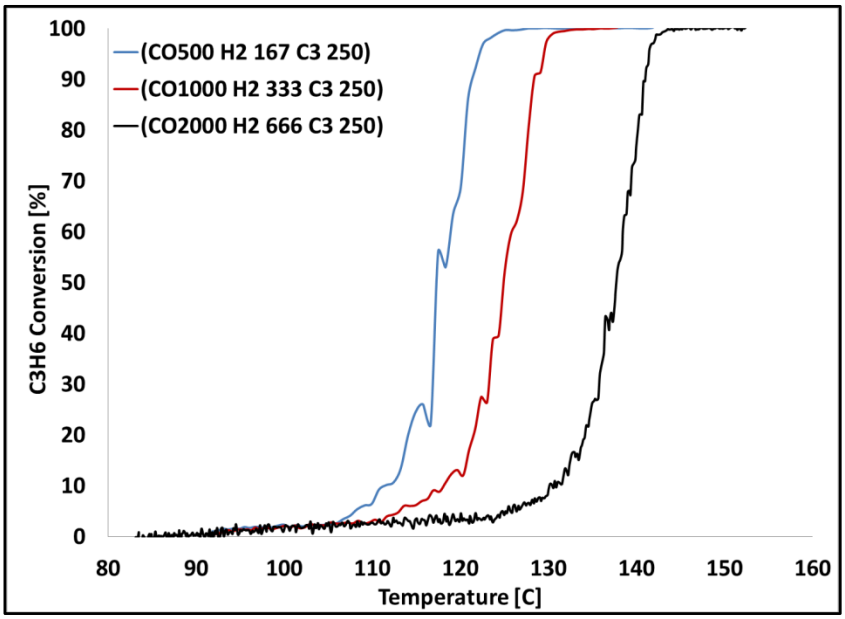

Figure A- 7 : C_3H_6 conversion as a function of temperature for a CO + C_3H_6 + H_2 mixture with different inlet gas compositions.

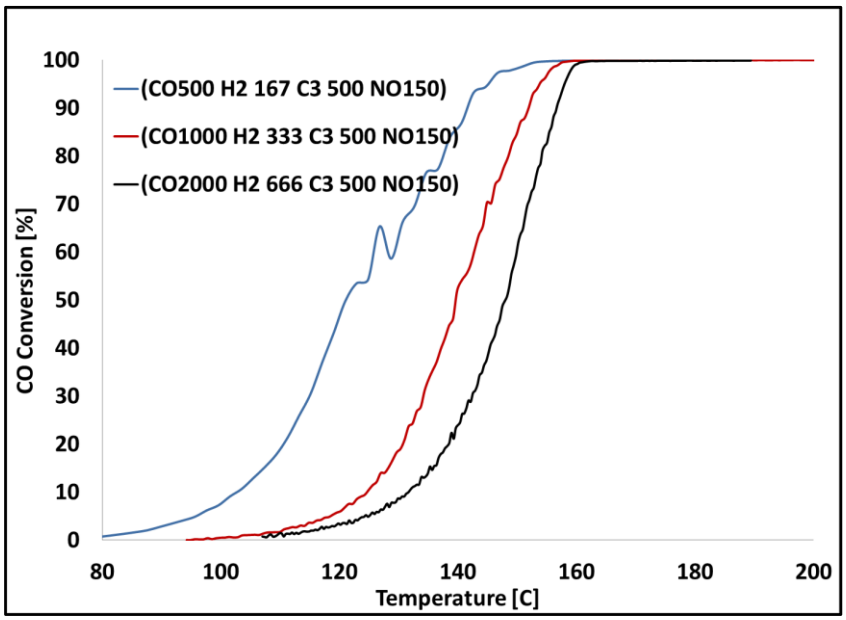

Figure A- 8 : CO conversion as a function of temperature for a CO + C_3H_6 + NO + H_2 mixture with different inlet gas compositions.

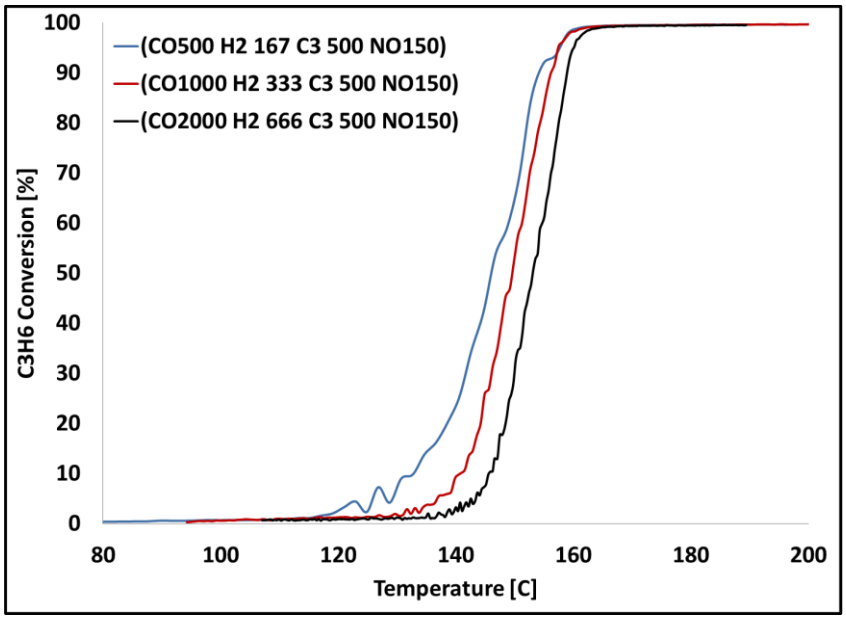

Figure A- 9 : C_3H_6 conversion as a function of temperature for a CO + C_3H_6 + NO + H_2 mixture with different inlet gas compositions.

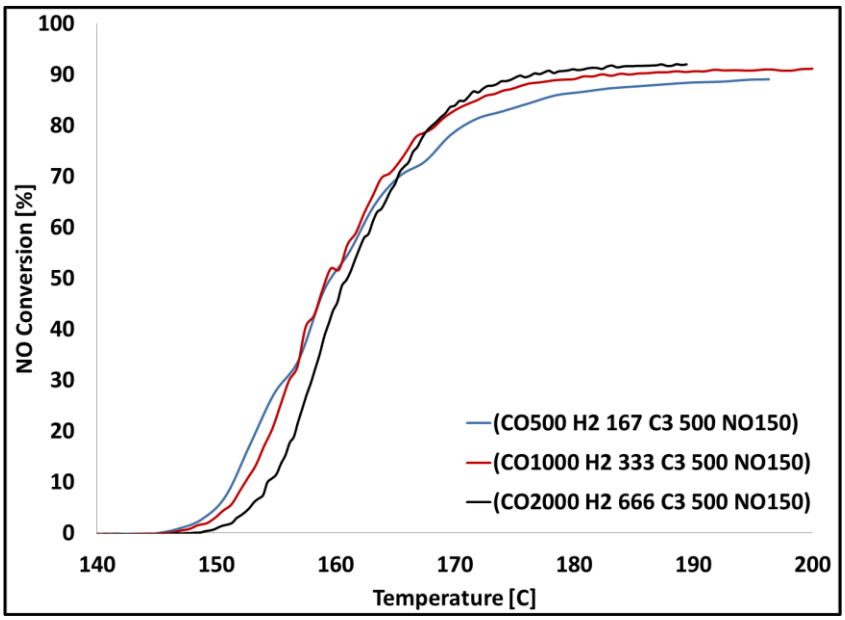

Figure A- 10 : NO conversion as a function of temperature for a CO + C_3H_6 + NO + H_2 mixture with different inlet gas compositions.

The reproducibility of these data was also measured to ensure that the experiments are meaningful. Three repeats of CO oxidation TPO at total flow rate of 9.34 L/min with the inlet gas composed of 500 ppm CO, 10% O_2, 10% CO_2, 10% H_2O, and N_2 balance are shown in Figure (A-11). Based on these repeats the standard deviation was calculated to be 2.4 °C. The repeats with the error are shown in Figure (A-12).

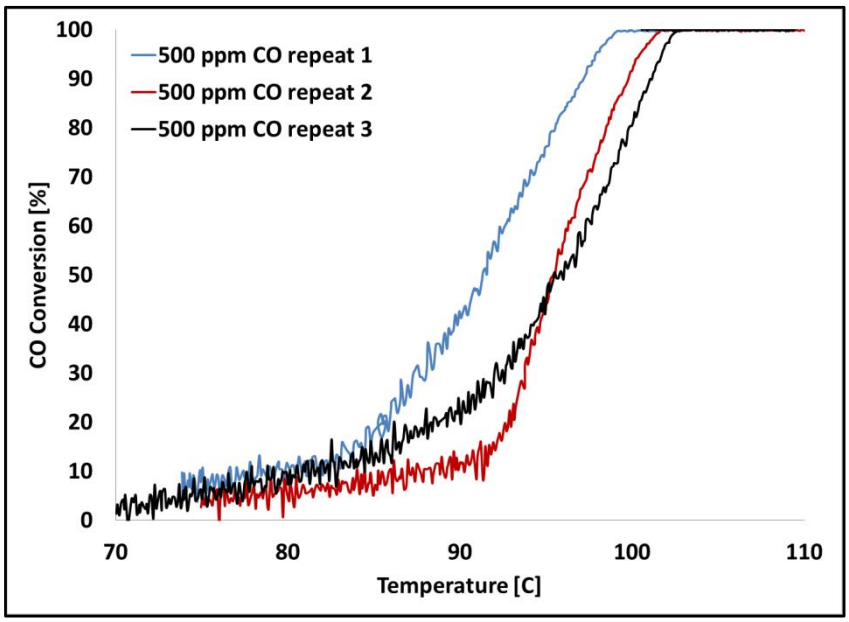

Figure A- 11 : The repeats of CO oxidation as a function of temperature (Auto21).

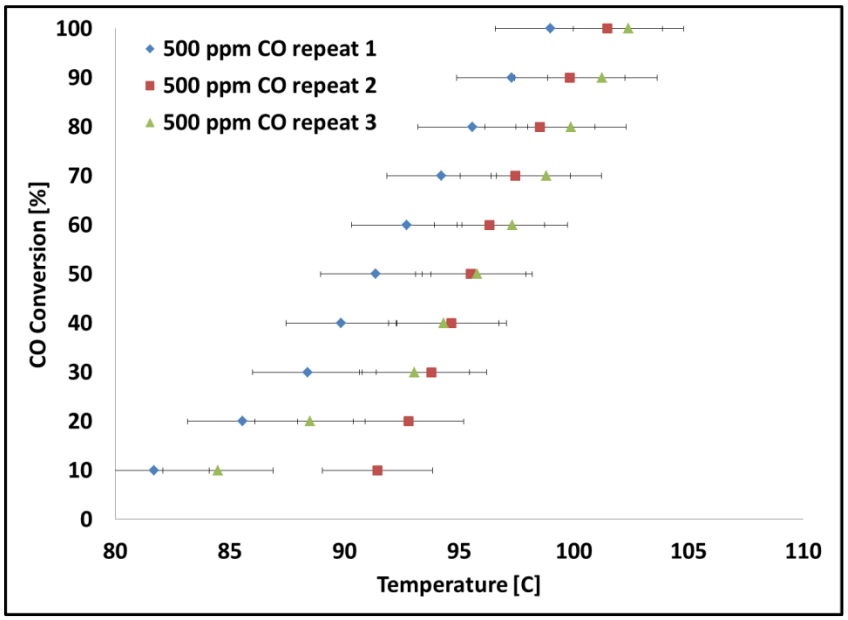

Figure A- 12 : CO oxidation as a function of temperature with the error bar corresponding to its standard deviation (Auto21).

Appendix C

Permissions

This is the permission of Chapter 4 that is published in Catalysis Today Journal.

ELSEVIER ORDER DETAILS

Sep 15, 2012

Order Number	500698493
Order Date	Sep 15, 2012
Licensed content publisher	Elsevier
Licensed content publication	Catalysis Today
Licensed content title	Improved CO, hydrocarbon and NO oxidation performance using zone-coated Pt-based catalysts
Licensed content author	Ali Abedi,Jin-Yong Luo,William S. Epling
Licensed content date	15 May 2012
Number of pages	1
Type of Use	reuse in a thesis/dissertation
Portion	full article
Format	electronic
Are you the author of this Elsevier article?	Yes
Will you be translating?	No
Order reference number	
Title of your thesis/dissertation	The Effect of an Axial Catalyst Distribution on the Performance of a Diesel Oxidation Catalyst and Inverse Hysteresis Phenomena during CO and C3H6 Oxidation
Expected completion date	Sep 2012
Estimated size (number of pages)	130
Elsevier VAT number	GB 494 6272 12

This is the permission of Chapter 7 that is published in Catalysis Letters Journal.

SPRINGER LICENSE
TERMS AND CONDITIONS

Sep 15, 2012

This is a License Agreement between Ali Abedi ("You") and Springer ("Springer") provided by Copyright Clearance Center ("CCC"). The license consists of your order details, the terms and conditions provided by Springer, and the payment terms and conditions.

License Number	2990440459464
License date	Sep 15, 2012
Licensed content publisher	Springer
Licensed content publication	Catalysis Letters
Licensed content title	Inverse Hysteresis Phenomena During CO and C_3H_6 Oxidation over a Pt/Al_2O_3 Catalyst
Licensed content author	Ali Abedi
Licensed content date	Jan 1, 2012
Volume number	142
Issue number	8
Type of Use	Thesis/Dissertation
Portion	Full text
Number of copies	1
Author of this Springer article	Yes and you are the sole author of the new work
Order reference number	
Title of your thesis / dissertation	The Effect of an Axial Catalyst Distribution on the Performance of a Diesel Oxidation Catalyst and Inverse Hysteresis Phenomena during CO and C3H6 Oxidation

Expected completion date Sep 2012
Estimated size(pages) 130

Terms and Conditions

Introduction

The publisher for this copyrighted material is Springer Science + Business Media. By clicking "accept" in connection with completing this licensing transaction, you agree that the following terms and conditions apply to this transaction (along with the Billing and Payment terms and conditions established by Copyright Clearance Center, Inc. ("CCC"), at the time that you opened your Rightslink account and that are available at any time at http://myaccount.copyright.com).

Limited License

With reference to your request to reprint in your thesis material on which Springer Science and Business Media control the copyright, permission is granted, free of charge, for the use indicated in your enquiry.

Licenses are for one-time use only with a maximum distribution equal to the number that you identified in the licensing process.

This License includes use in an electronic form, provided its password protected or on the university's intranet or repository, including UMI (according to the definition at the Sherpa website: http://www.sherpa.ac.uk/romeo/). For any other electronic use, please contact Springer at (permissions.dordrecht@springer.com or permissions.heidelberg@springer.com).

The material can only be used for the purpose of defending your thesis, and with a maximum of 100 extra copies in paper.

Although Springer holds copyright to the material and is entitled to negotiate on rights, this license is only valid, provided permission is also obtained from the (co) author (address is given with the article/chapter) and provided it concerns original material which does not carry references to other sources (if material in question appears with credit to another source, authorization from that source is required as well).

Permission free of charge on this occasion does not prejudice any rights we might have to charge for reproduction of our copyrighted material in the future.

Altering/Modifying Material: Not Permitted

You may not alter or modify the material in any manner. Abbreviations, additions, deletions and/or any other alterations shall be made only with prior written authorization of the author(s) and/or Springer Science + Business Media. (Please contact Springer at (permissions.dordrecht@springer.com or permissions.heidelberg@springer.com)

Reservation of Rights

Springer Science + Business Media reserves all rights not specifically granted in the combination of (i) the license details provided by you and accepted in the course of this licensing transaction, (ii) these terms and conditions and (iii) CCC's Billing and Payment terms and conditions.

Copyright Notice:Disclaimer

You must include the following copyright and permission notice in connection with any reproduction of the licensed material: "Springer and the original publisher /journal title, volume, year of publication, page, chapter/article title, name(s) of author(s), figure number(s), original copyright notice) is given to the publication in which the material was originally published, by adding; with

kind permission from Springer Science and Business Media"

Warranties: None

Example 1: Springer Science + Business Media makes no representations or warranties with respect to the licensed material.

Example 2: Springer Science + Business Media makes no representations or warranties with respect to the licensed material and adopts on its own behalf the limitations and disclaimers established by CCC on its behalf in its Billing and Payment terms and conditions for this licensing transaction.

Indemnity

You hereby indemnify and agree to hold harmless Springer Science + Business Media and CCC, and their respective officers, directors, employees and agents, from and against any and all claims arising out of your use of the licensed material other than as specifically authorized pursuant to this license.

No Transfer of License

This license is personal to you and may not be sublicensed, assigned, or transferred by you to any other person without Springer Science + Business Media's written permission.

No Amendment Except in Writing

This license may not be amended except in a writing signed by both parties (or, in the case of Springer Science + Business Media, by CCC on Springer Science + Business Media's behalf).

Objection to Contrary Terms

Springer Science + Business Media hereby objects to any terms contained in any purchase order,

acknowledgment, check endorsement or other writing prepared by you, which terms are inconsistent with these terms and conditions or CCC's Billing and Payment terms and conditions. These terms and conditions, together with CCC's Billing and Payment terms and conditions (which are incorporated herein), comprise the entire agreement between you and Springer Science + Business Media (and CCC) concerning this licensing transaction. In the event of any conflict between your obligations established by these terms and conditions and those established by CCC's Billing and Payment terms and conditions, these terms and conditions shall control.

Jurisdiction

All disputes that may arise in connection with this present License, or the breach thereof, shall be settled exclusively by arbitration, to be held in The Netherlands, in accordance with Dutch law, and to be conducted under the Rules of the 'Netherlands Arbitrage Instituut' (Netherlands Institute of Arbitration).

References

1. Majewski, W.A. and M.K. Khair, *Diesel emissions and their control*. 2006: SAE International. 561.
2. Lloyd, A.C., *Diesel Engines: Environmental Impact and Control*, in *DEER Conference*. 2002: San Diego, California
3. Service, N.H.D.o.E. *Heavy-Duty Diesel Engines: Trucks and Buses Air Quality Impacts*. 2008; Available from: http://des.nh.gov/organization/commissioner/pip/factsheets/ard/documents/ard-34.pdf.
4. Clerc, J.C., *Catalytic diesel exhaust aftertreatment.* Applied Catalysis B: Environmental, 1996. **10**(1–3): p. 99-115.
5. Kagawa, J., *Health effects of diesel exhaust emissions—a mixture of air pollutants of worldwide concern.* Toxicology, 2002. **181–182**(0): p. 349-353.
6. Rosner, G. *Diesel Fuel and Exhaust Emissions*. 1996; Available from: http://www.inchem.org/documents/ehc/ehc/ehc171.htm.
7. Force, C.A.T. *Problems of Diesel*. Available from: http://www.catf.us/diesel/problems/.
8. Koltsakis, G.C. and A.M. Stamatelos, *Catalytic automotive exhaust aftertreatment.* Progress in Energy and Combustion Science, 1997. **23**(1): p. 1-39.
9. Abrahmowics, A. and W.H. White, *Reanalysis of the Harvard Six Cities and the American Cancer Society of Particulate Matter and Mortality*. 2000, Health Effects Institute: Cambridge, MA. p. 97.
10. Sher, E., *Handbook of Air-Pollution from Internal Combustion Engines - Pollutant Formation and Control* 1998. p. 653.
11. Sullivan, J.L., Baker, R.E., Boyer, B.A., Hammerle, R.H., Kenney T.E., Muniz, L., Wallington, T.J., *CO2 Emission Benefit of Diesel (versus Gasoline) Powered Vehicles.* Environmental Science & Technology, 2004. **38**(12): p. 3217-3223.
12. Jacobsen, M., *Stronge radioactive heating due to the mixing state of black carbon in atmospheric aerosols.* Nature, 2001: p. 695-697.
13. Net, D.; Available from: http://www.dieselnet.com.
14. Chatterjee, S., A.P. Walker, and P.G. Blakeman, *Emission Control Options to Achieve Euro IV and Euro V on Heavy Duty Diesel Engines.* 2008.
15. Al-Harbi, M., *Application of environmental technology management (ETM) to automobile exhaust emission reduction*, in *Chemical Engineering*. 2010, University of Waterloo: Waterloo.
16. Epling, W.S., et al., *Overview of the Fundamental Reactions and Degradation Mechanisms of NOx Storage/Reduction Catalysts.* Catalysis Reviews, 2004. **46**(2): p. 163-245.
17. Salasc, S., M. Skoglundh, and E. Fridell, *A comparison between Pt and Pd in NOx storage catalysts.* Applied Catalysis B: Environmental, 2002. **36**(2): p. 145-160.
18. Held, W., et al., *Catalytic NOx Reduction in Net Oxidizing Exhaust Gas.* SAE Technical Paper, 1990.
19. Havenith, C. and R. Verbeek, *Transient Performance of a Urea deNOx Catalyst for Low Emissions Heavy-Duty Diesel Engines.* SAE Technical Paper, 1997.
20. Jung, J., S. Song, and K.M. Chun, *Characterization of Catalyzed Soot Oxidation with NO2, NO and O2 using a Lab-Scale Flow Reactor System.* 2008.
21. Irani, K., W.S. Epling, and R. Blint, *Effect of hydrocarbon species on no oxidation over diesel oxidation catalysts.* Applied Catalysis B: Environmental, 2009. **92**(3–4): p. 422-428.
22. Tronci, S., R. Baratti, and A. Gavriilidis, *Catalytic converter design for minimisation of cold-start emissions.* Chemical Enginering Community, 1999. **173** p. 53 -77.

23. Farrauto, R.J. and R.M. Heck, *Catalytic converters: state of the art and perspectives.* Catalysis Today, 1999. **51**(3–4): p. 351-360.
24. Katare, S. and P.M. Laing, *A Hybrid Framework for Modeling Aftertreatment Systems: A Diesel Oxidation Catalyst Application.* 2006.
25. Haass, F. and H. Fuess, *Structural Characterization of Automotive Catalysts.* Advanced Engineering Materials, 2005. **7**(10): p. 899–913.
26. Heck, R.M. and R.J. Farrauto, *Automobile exhaust catalysts.* Applied Catalysis A: General, 2001. **221**(1–2): p. 443-457.
27. Ambs, J.L. and B.T. McClure, *The Influence of Oxidation Catalysts on NO2 in Diesel Exhaust.* SAE 1993.
28. Koebel, M., G. Madia, and M. Elsener, *Selective catalytic reduction of NO and NO2 at low temperatures.* Catalysis Today, 2002. **73**(3–4): p. 239-247.
29. Devadas, M., et al., *Influence of NO2 on the selective catalytic reduction of NO with ammonia over Fe-ZSM5.* Applied Catalysis B: Environmental, 2006. **67**(3–4): p. 187-196.
30. Grossale, A., et al., *The chemistry of the NO/NO2–NH3 "fast" SCR reaction over Fe-ZSM5 investigated by transient reaction analysis.* Journal of Catalysis, 2008. **256**(2): p. 312-322.
31. Nova, I., et al., *NH3–NO/NO2 chemistry over V-based catalysts and its role in the mechanism of the Fast SCR reaction.* Catalysis Today, 2006. **114**(1): p. 3-12.
32. Fridell, E., et al., *The mechanism for NOx storage.* Catalysis Letters, 2000. **66**(1): p. 71-74.
33. Allansson, R., et al., *European Experience of High Mileage Durability of Continuously Regenerating Diesel Particulate Filter Technology.* SAE, 2000.
34. Mathieu, O., J. Lavy, and E. Jeudy, *Investigation of Hydrocarbons Conversion Over a Pt-Based Automotive Diesel Oxidation Catalyst: Application to Exhaust Port Fuel Injection.* Topics in Catalysis, 2009. **52**(13): p. 1893-1897.
35. Voltz, S.E., et al., *Kinetic Study of Carbon Monoxide and Propylene Oxidation on Platinum Catalysts.* Product R&D, 1973. **12**(4): p. 294-301.
36. Patterson, W.R. and C. Kemball, *The catalytic oxidation of olefins on metal films.* Journal of Catalysis, 1963. **2**(6): p. 465-478.
37. Harned, J.L., *Analytical Evaluation of a Catalytic Converter System.* SAE, 1972.
38. Abedi, A., J.-Y. Luo, and W.S. Epling, *Improved CO, hydrocarbon and NO oxidation performance using zone-coated Pt-based catalysts.* Catalysis Today, 2012(0).
39. Lambert, C.K., et al., *Post Mortem of an Aged Tier 2 Light-Duty Diesel Truck Aftertreatment System.* SAE Int. J. Fuels Lubr., 2009. **2**(2): p. 167-175.
40. Katare, S.R., J.E. Patterson, and P.M. Laing, *Diesel Aftertreatment Modeling: A Systems Approach to NOx Control.* Industrial & Engineering Chemistry Research, 2007. **46**(8): p. 2445-2454.
41. Erkfeldt, S., E. Jobson, and M. Larsson, *The Effect of Carbon Monoxide and Hydrocarbons on NOx Storage at Low Temperature.* Topics in Catalysis, 2001. **16-17**(1): p. 127-131.
42. Parker, D.H. and B.E. Koel, *Chemisorption of high coverages of atomic oxygen on the Pt(111), Pd(111), and Au(111) surfaces.* Journal of Vacuum Science & Technology A: Vacuum, Surfaces, and Films, 1990. **8**(3): p. 2585-2590.
43. Mulla, S.S., et al., *NO2 inhibits the catalytic reaction of NO and O2 over Pt.* Catalysis Letters, 2005. **100**(3): p. 267-270.
44. Deutschmann, O., et al., *Hydrogen assisted catalytic combustion of methane on platinum.* Catalysis Today, 2000. **59**(1–2): p. 141-150.
45. Katare, S.R. and P.M. Laing, *Hydrogen in Diesel Exhaust: Effect on Diesel Oxidation Catalyst Flow Reactor Experiments and Model Predictions.* SAE Int. J. Fuels Lubr., 2009. **2**(1): p. 605-611.

46. Salomons, S., R.E. Hayes, and M. Votsmeier, *The promotion of carbon monoxide oxidation by hydrogen on supported platinum catalyst.* Applied Catalysis A: General, 2009. **352**(1–2): p. 27-34.
47. Salomons, S., et al., *On the use of mechanistic CO oxidation models with a platinum monolith catalyst.* Applied Catalysis B: Environmental, 2007. **70**(1–4): p. 305-313.
48. Salomons, S., et al., *CO and H2 oxidation on a platinum monolith diesel oxidation catalyst.* Catalysis Today, 2006. **117**(4): p. 491-497.
49. Ahluwalia, R.K., et al., *Performance of CO preferential oxidation reactor with noble-metal catalyst coated on ceramic monolith for on-board fuel processing applications.* Catalysis Today, 2005. **99**(3–4): p. 271-283.
50. Bissett, E.J., S.H. Oh, and R.M. Sinkevitch, *Pt surface kinetics for a PrOx reactor for fuel cell feedstream processing.* Chemical Engineering Science, 2005. **60**(17): p. 4709-4721.
51. İnce, T., et al., *Selective low-temperature CO oxidation over Pt-Co-Ce/Al2O3 in hydrogen-rich streams.* Applied Catalysis A: General, 2005. **292**(0): p. 171-176.
52. Jhalani, A. and L.D. Schmidt, *Preferential CO Oxidation in the Presence of H₂, H₂O and CO₂ at Short Contact-times.* Catalysis Letters, 2005. **104**(3): p. 103-110.
53. Qu, Z., et al., *Low-temperature selective oxidation of CO in H2-rich gases over Ag/SiO2 catalysts.* Journal of Molecular Catalysis A: Chemical, 2005. **239**(1–2): p. 22-31.
54. Sun, M., et al., *Steady-State Multiplicity and Superadiabatic Extinction Waves in the Oxidation of CO/H2 Mixtures over a Pt/Al2O3-Coated Monolith.* Industrial & Engineering Chemistry Research, 2002. **42**(1): p. 37-45.
55. Mhadeshwar, A.B. and D.G. Vlachos, *Is the water–gas shift reaction on Pt simple?: Computer-aided microkinetic model reduction, lumped rate expression, and rate-determining step.* Catalysis Today, 2005. **105**(1): p. 162-172.
56. Carlsson, P.-A., et al., *A transient in situ FTIR and XANES study of CO oxidation over Pt/Al2O3 catalysts.* Journal of Catalysis, 2004. **226**(2): p. 422-434.
57. Keren, I. and M. Sheintuch, *Modeling and analysis of spatiotemporal oscillatory patterns during CO oxidation in the catalytic converter.* Chemical Engineering Science, 2000. **55**(8): p. 1461-1475.
58. McClure, S.M. and D.W. Goodman, *New Insights into Catalytic CO Oxidation on Pt-group Metals at Elevated Pressures.* Chemical Physics Letters, 2009. **469**(1-3): p. 1-13.
59. Schwartz, A., L.L. Holbrook, and H. Wise, *Catalytic oxidation studies with platinum and palladium.* Journal of Catalysis, 1971. **21**(2): p. 199-207.
60. Spivey, J.J., *Complete catalytic oxidation of volatile organics.* Industrial & Engineering Chemistry Research, 1987. **26**(11): p. 2165-2180.
61. Sheintuch, M. and D. Luss, *Reaction rate oscillations during propylene oxidation on platinum.* Journal of Catalysis, 1981. **68**(1): p. 245-248.
62. Bar, M., et al., *Theoretical Modeling of Spatiotemporal Self-organization in a Surface Catalyzed Reaction Exhibiting Bistable Kinetics.* Journal of Chemical Physics, 1992. **96**(11): p. 8595-8604.
63. Bourane, A. and D. Bianchi, *Oxidation of CO on a Pt/Al2O3 catalyst: from the surface elementary steps to light-off tests: V. Experimental and kinetic model for light-off tests in excess of O2.* Journal of Catalysis, 2004. **222**(2): p. 499-510.
64. Hartmann, N., R. Imbihl, and W. Vogel, *Experimental evidence for an oxidation/reduction mechanism in rate oscillations of catalytic CO oxidation on Pt/SiO<sub>2</sub&gt.* Catalysis Letters, 1994. **28**(2): p. 373-381.

65. Turner, J.E., B.C. Sales, and M.B. Maple, *Oscillatory oxidation of Co over a Pt catalyst.* Surface Science, 1981. **103**(1): p. 54-74.
66. Sales, B.C., J.E. Turner, and M.B. Maple, *Oscillatory oxidation of CO over Pt, Pd and Ir catalysts: Theory.* Surface Science, 1982. **114**(2–3): p. 381-394.
67. Yao, Y.-F.Y., *The oxidation of CO and hydrocarbons over noble metal catalysts.* Journal of Catalysis, 1984. **87**(1): p. 152-162.
68. Nibbelke, R.H., et al., *Kinetic Study of the CO Oxidation over Pt/γ-Al2O3and Pt/Rh/CeO2/γ-Al2O3in the Presence of H2O and CO2.* Journal of Catalysis, 1997. **171**(2): p. 358-373.
69. Nakane, T., et al., *Investigation of the Aging Behavior of Oxidation Catalysts Developed for Active DPF Regeneration Systems.* 2005.
70. Bartholomew, C.H., *Mechanisms of catalyst deactivation.* Applied Catalysis A: General, 2001. **212**(1–2): p. 17-60.
71. Neyestanaki, A.K., et al., *Deactivation of postcombustion catalysts, a review.* Fuel, 2004. **83**(4–5): p. 395-408.
72. Winkler, A., D. Ferri, and M. Aguirre, *The influence of chemical and thermal aging on the catalytic activity of a monolithic diesel oxidation catalyst.* Applied Catalysis B: Environmental, 2009. **93**(1–2): p. 177-184.
73. Heck, R.M. and R.J. Farrauto, *Catalytic Air Pollution Control Commercial Technology*. 1995, New York: Van Nostrand Reinhold. 461.
74. LANTEC. [cited 2012 June 13]; Available from: http://www.lantecp.com/monolith/.
75. Avila, P., M. Montes, and E.E. Miró, *Monolithic reactors for environmental applications: A review on preparation technologies.* Chemical Engineering Journal, 2005. **109**(1–3): p. 11-36.
76. Bartholomew, C.H. and R.J. Farrauto, *Fundamentals of Industrial Catalytic Processes*, in *Fundamentals of Industrial Catalytic Processes*. 2005, John Wiley & Sons, Inc. p. 939-953.
77. Agrafiotis, C. and A. Tsetsekou, *The effect of processing parameters on the properties of γ-alumina washcoats deposited on ceramic honeycombs.* Journal of Materials Science, 2000. **35**(4): p. 951-960.
78. Wootsch, A., C. Descorme, and D. Duprez, *Preferential oxidation of carbon monoxide in the presence of hydrogen (PROX) over ceria–zirconia and alumina-supported Pt catalysts.* Journal of Catalysis, 2004. **225**(2): p. 259-266.
79. Jiang, P., et al., *Preparation and properties of a γ-Al2O3 washcoat deposited on a ceramic honeycomb.* Surface and Coatings Technology, 2005. **190**(2–3): p. 314-320.
80. Watanabe, T., et al., *New DOC for Light Duty Diesel DPF System.* 2007.
81. Collins, N.R., et al., *Advanced Three-Way Catalysts - Optimisation by Targeted Zoning of Precious Metal.* 2005.
82. Schlatter, J.C. and K.C. Taylor, *Platinum and palladium addition to supported rhodium catalysts for automotive emission control.* Journal of Catalysis, 1977. **49**(1): p. 42-50.
83. Kawanami, M., et al., *Development of Oxidation and de-NOx Catalyst for High Temperature Exhaust Diesel Trucks.* 1998.
84. Perego, C. and P. Villa, *Catalyst preparation methods.* Catalysis Today, 1997. **34**(3–4): p. 281-305.
85. Spieker, W.A. and J.R. Regalbuto, *A fundamental model of platinum impregnation onto alumina.* Chemical Engineering Science, 2001. **56**(11): p. 3491-3504.
86. Nijhuis, T.A., et al., *Preparation of monolithic catalysts.* Catalysis Reviews, 2001. **43**(4): p. 345-380.
87. Maatman, R., *How to Make a More Effective Platinum-Alumina Catalyst.* Industrial & Engineering Chemistry, 1959. **51**(8): p. 913-914.

88. Heise, M.S. and J.A. Schwarz, *Preparation of metal distributions within catalyst supports: III. Single component modeling of pH, ionic strength, and concentration effects.* Journal of Colloid and Interface Science, 1988. **123**(1): p. 51-58.
89. Schwarz, J.A. and M.S. Heise, *Preparation of metal distributions within catalyst supports: IV. Multicomponent effects.* Journal of Colloid and Interface Science, 1990. **135**(2): p. 461-467.
90. Heise, M.S. and J.A. Schwarz, *Preparation of metal distributions within catalyst supports: II. Effect of ionic strength on catalytic metal profiles.* Journal of Colloid and Interface Science, 1986. **113**(1): p. 55-61.
91. Miller, J.T., et al., *A fundamental study of platinum tetraammine impregnation of silica: 2. The effect of method of preparation, loading, and calcination temperature on (reduced) particle size.* Journal of Catalysis, 2004. **225**(1): p. 203-212.
92. Schreier, M. and J.R. Regalbuto, *A fundamental study of Pt tetraammine impregnation of silica: 1. The electrostatic nature of platinum adsorption.* Journal of Catalysis, 2004. **225**(1): p. 190-202.
93. Villegas, L., F. Masset, and N. Guilhaume, *Wet impregnation of alumina-washcoated monoliths: Effect of the drying procedure on Ni distribution and on autothermal reforming activity.* Applied Catalysis A: General, 2007. **320**(0): p. 43-55.
94. Lekhal, A., B.J. Glasser, and J.G. Khinast, *Impact of drying on the catalyst profile in supported impregnation catalysts.* Chemical Engineering Science, 2001. **56**(15): p. 4473-4487.
95. Kim, Y.-D., S.-J. Jeong, and W.-S. Kim, *Optimal design of axial noble metal distribution for improving dual monolithic catalytic converter performance.* Chemical Engineering Science, 2009. **64**(7): p. 1373-1383.
96. Cominos, V. and A. Gavriilidis, *Theoretical investigation of axially non-uniform catalytic monoliths for methane combustion.* Chemical Engineering Science, 2001. **56**: p. 3455-3468.
97. Koltsakis, G.C., et al., *Model-based Optimization of Catalyst Zoning in Diesel Particulate Filters.* 2008.
98. Psyllos, A. and C. Philippopoulos, *Performance of a monolithic catalytic converter used in automotive emission control: the effect of a longitudinal parabolic active metal distribution.* Industrial & Engineering Chemistry Research, 1993. **32**(8): p. 1555-1559.
99. Theis, J., et al., *Lean NOx Trap System Design for Cost Reduction and Performance Improvement.* 2006.
100. Ramanathan, K., V. Balakotaiah, and D.H. West, *Bifurcation Analysis of Catalytic Monoliths with Nonuniform Catalyst Loading.* Industrial & Engineering Chemistry Research, 2003. **43**(2): p. 288-303.
101. Ramanathan, K., D.H. West, and V. Balakotaiah, *Light-off and Cumulative Emissions in Catalytic Monoliths with Nonuniform Catalyst Loading.* Industrial & Engineering Chemistry Research, 2004. **43**(16): p. 4668-4690.
102. Ramanathan, K., D.H. West, and V. Balakotaiah, *Optimal design of catalytic converters for minimizing cold-start emissions.* Catalysis Today, 2004. **98**(3): p. 357-373.
103. Kim, Y.-D. and W.-S. Ki, *Optimum design of an automotive catalytic converter for minimization of cold-start emissions using a micro genetic algorithm.* International Journal of Automotive Technology, 2007. **8**: p. 563–573.
104. Oh, S.H. and J.C. Cavendish, *Transients of monolithic catalytic converters. Response to step changes in feedstream temperature as related to controlling automobile emissions.* Industrial & Engineering Chemistry Product Research and Development, 1982. **21**(1): p. 29-37.

105. Khanaev, V.M., E.S. Borisova, and A.S. Noskov, *Optimization of the active component distribution through the catalyst bed for the case of adiabatic reactor.* Chemical Engineering Science, 2005. **60**(21): p. 5792-5802.
106. Engel, T. and G. Ertl, *Elementary Steps in the Catalytic Oxidation of Carbon Monoxide on Platinum Metals*, in *Advances in Catalysis*, H.P. D.D. Eley and B.W. Paul, Editors. 1979, Academic Press. p. 1-78.
107. Langmuir, I., *The mechanism of the catalytic action of platinum in the reactions 2Co + O2= 2Co2 and 2H2+ O2= 2H2O.* Transactions of the Faraday Society, 1922. **17**: p. 621-654.
108. Shishu, R.C. and L.S. Kowalczyk, *The Oxidation of Carbon Monoxide on Supported Platinum.* Platinum Metals Review, 1974. **18**(2): p. 58-64.
109. Wei, J., *Catalysis for Motor Vehicle Emissions*, in *Advances in Catalysis*, H.P. D.D. Eley and B.W. Paul, Editors. 1975, Academic Press. p. 57-129.
110. Beusch, H., P. Fieguth, and E. Wicke, *Thermisch und Kinetisch Verursachte Instabilitaten im Reaktionsverhalten einzelner Katalysatorkomer.* Chemie Ingenieur Technik 1972. **44**: p. 445-451.
111. Carlsson, P.-A. and M. Skoglundh, *Low-temperature oxidation of carbon monoxide and methane over alumina and ceria supported platinum catalysts.* Applied Catalysis B: Environmental, 2011. **101**(3–4): p. 669-675.
112. Chakrabarty, T., P.L. Silveston, and R.R. Hudgins, *Hysteresis phenomena in co oxidation over platinum-alumina catalyst.* The Canadian Journal of Chemical Engineering, 1984. **62**: p. 651–660.
113. Gudkov, B.S., A.N. Subbotin, and V.I. Yakerson, *On the phenomenon of temperature hysteresis in hydrogenation reaction over heterogeneous catalysts.* Reaction Kinetics and Catalysis Letters, 1999. **68**(1): p. 125-132.
114. Hauptmann, W., et al., *Inverse hysteresis during the NO oxidation on Pt under lean conditions.* Applied Catalysis B: Environmental, 2009. **93**(1–2): p. 22-29.
115. Hegedus, L.L., S.H. Oh, and K. Baron, *Multiple steady states in an isothermal, integral reactor: The catalytic oxidation of carbon monoxide over platinum-alumina.* AIChE Journal 1977. **23**: p. 632–642.
116. Oh, S.H., et al., *Effects of catalyst particle size on multiple steady states.* Journal of Catalysis, 1979. **59**(2): p. 272-277.
117. Schmitz Roger, A., *Multiplicity, Stability, and Sensitivity of States in Chemically Reacting Systems?A Review*, in *Chemical Reaction Engineering Reviews*. 1975, AMERICAN CHEMICAL SOCIETY. p. 156-211.
118. Smith, T.G., J. Zahradnik, and J.J. Carberry, *Non-isothermal inter-intraphase effectiveness factors for negative order kinetics—CO oxidation over Pt.* Chemical Engineering Science, 1975. **30**(7): p. 763-767.
119. Subbotin, A.N., et al., *Temperature-Hysteresis Effects in CO Oxidation on Cement Catalysts with Various CuO Content.* Russian Journal of Applied Chemistry, 2001. **74**(9): p. 1506-1508.
120. Subbotin, A.N., et al., *Temperature Hysteresis in CO Oxidation on Copper Oxide Catalyst Applied to a Steel Gauze.* Russian Journal of Applied Chemistry, 2002. **75**(4): p. 582-584.
121. Subbotln, A.N., et al., *Temperature Hysteresis in CO oxidation on catalysts of various nature.* Reaction Kinetics and Catalysis Letters, 1999. **66**(1): p. 97-104.
122. Usachev, N.Y., et al., *Hysteresis phenomenon in CO and hydrogen oxidation on Cu–Ce–Zr–O systems.* Mendeleev Communications 2004. **14**(2): p. 79–80.

123. Wei, J. and R. Becker E, *The Optimum Distribution of Catalytic Material on Support Layers in Automotive Catalysis*, in *Catalysts for the Control of Automotive Pollutants*. 1975, AMERICAN CHEMICAL SOCIETY. p. 116-132.
124. Eigenberger, G., *Kinetic instabilities in heterogeneously catalyzed reactions—II: Oscillatory instabilities with langmuir-type kinetics.* Chemical Engineering Science, 1978. **33**(9): p. 1263-1268.
125. Gudkov, B.S., et al., Russian Chemical Bulletin, 1997: p. 347-353.
126. Subbotin, A., B. Gudkov, and V. Yakerson, *Temperature hysteresis phenomena in heterogeneous catalysis.* Russian Chemical Bulletin, 2000. **49**(8): p. 1373-1379.
127. Twigg, M.V., *Rôles of catalytic oxidation in control of vehicle exhaust emissions.* Catalysis Today, 2006. **117**(4): p. 407-418.
128. Russell, A., et al., *Spatially-Resolved Temperature and Gas Species Changes in a Lean-Burn Engine Emissions Control Catalyst.* Industrial & Engineering Chemistry Research, 2010. **49**(21): p. 10311-10322.
129. Russell, A. and W.S. Epling, *Diesel Oxidation Catalysts.* Catalysis Reviews, 2011. **53**(4): p. 337-423.
130. Xue, E., K. Seshan, and J.R.H. Ross, *Roles of supports, Pt loading and Pt dispersion in the oxidation of NO to NO2 and of SO2 to SO3.* Applied Catalysis B: Environmental, 1996. **11**(1): p. 65-79.
131. Olsson, L., et al., *A Kinetic Study of Oxygen Adsorption/Desorption and NO Oxidation over Pt/Al2O3 Catalysts.* The Journal of Physical Chemistry B, 1999. **103**(47): p. 10433-10439.
132. Khanaev, V.M., E.S. Borisova, and A.S. Noskov, *Optimization of the active component distribution through the catalyst bed.* Chemical Engineering Science, 2004. **59**(6): p. 1213-1220.
133. Khanaev, V.M., et al., *Improvement of the catalytic monoliths efficiency for CO oxidation using non-uniform active component distribution along the monolith length.* Chemical Engineering Journal, 2004. **102**(1): p. 35-44.
134. Choi, J.-S., W.P. Partridge, and C.S. Daw, *Spatially resolved in situ measurements of transient species breakthrough during cyclic, low-temperature regeneration of a monolithic Pt/K/Al2O3 NOx storage-reduction catalyst.* Applied Catalysis A: General, 2005. **293**(0): p. 24-40.
135. Choi, J.-S., et al., *Intra-channel evolution of carbon monoxide and its implication on the regeneration of a monolithic Pt/K/Al2O3 NOx storage-reduction catalyst.* Catalysis Today, 2006. **114**(1): p. 102-111.
136. Partridge, W.P., et al., *Time-Resolved Measurements of Emission Transients By Mass Spectrometry*. 2000, SAE International.
137. Luss, D., *Temperature Fronts and Patterns in Catalytic Systems.* Industrial & Engineering Chemistry Research, 1997. **36**(8): p. 2931-2944.
138. Luss, D. and M. Sheintuch, *Spatiotemporal patterns in catalytic systems.* Catalysis Today, 2005. **105**(2): p. 254-274.
139. Shakir, O., et al., *Spatially resolving concentration and temperature gradients during the oxidation of propylene on Pt/Al2O3.* Applied Catalysis A: General, 2009. **365**(2): p. 301-308.
140. Benard, S., et al., *Supported platinum catalysts for nitrogen oxide sensors.* Applied Catalysis B: Environmental, 2005. **55**(1): p. 11-21.
141. Denton, P., et al., *Role of the Nature of the Support (Alumina or Silica), of the Support Porosity, and of the Pt Dispersion in the Selective Reduction of NO by C3H6 under Lean-Burn Conditions.* Journal of Catalysis, 2000. **189**(2): p. 410-420.

142. Després, J., et al., *Catalytic oxidation of nitrogen monoxide over Pt/SiO2.* Applied Catalysis B: Environmental, 2004. **50**(2): p. 73-82.
143. Lee, J.-H. and H. Kung, *Effect of Pt dispersion on the reduction of NO by propene over alumina-supported Pt catalysts under lean-burn conditions.* Catalysis Letters, 1998. **51**(1): p. 1-4.
144. Olsson, L. and E. Fridell, *The Influence of Pt Oxide Formation and Pt Dispersion on the Reactions NO2⇔NO+1/2 O2 over Pt/Al2O3 and Pt/BaO/Al2O3.* Journal of Catalysis, 2002. **210**(2): p. 340-353.
145. Segner, J., W. Vielhaber, and G. Ertl, Israel Journal of Chemistry, 1982. **22**: p. 375.
146. Cavataio, G., et al., *Impact and Prevention of Ultra-Low Contamination of Platinum Group Metals on SCR Catalysts Due to DOC Design.* V118-4, 2009. **2**(1): p. 204-216.
147. Zotin, F.M.Z., et al., *Automotive catalyst deactivation: Case studies.* Catalysis Today, 2005. **107–108**(0): p. 157-167.
148. Seokhwan, L. and B. Choongsik, *The application of an exhaust heat exchanger to protect the catalyst and improve the fuel economy in a spark-ignition engine.* Journal of Automobile Engineering, 2007. **part D**(221): p. 621–628.
149. Shayler, P.J. and C. Belton, *In-cylinder fuel behaviour and exhaust emissions during the cold operation of a spark ignition engine* Journal of Automobile Engineering, 1999(213): p. 161-174.
150. Karkanis, A.N., P.N. Botsaris, and P.D. Sparis, *Emission reduction during cold start via catalyst surface control.* Journal of Automobile Engineering, 2003. **D**(218): p. 1333–1340.
151. Al-Adwani, S.M., J. Soares, and W.S. Epling, *Evaluating the Effects of Precious Metal Distribution along a Monolith-Supported Catalyst for CO oxidation.* Industrial & Engineering Chemistry Research, 2012. **51**(19): p. 6672-6679.
152. Chen, K., K.S. Martirosyan, and D. Luss, *Wrong-Way Behavior of Soot Combustion in a Planar Diesel Particulate Filter.* Industrial & Engineering Chemistry Research, 2009. **48**(18): p. 8451-8456.
153. Sharma, C.S. and R. Hughes, *The behaviour of an adiabatic fixed bed reactor for the oxidation of carbon monoxide—I: General parametric studies.* Chemical Engineering Science, 1979. **34**(5): p. 613-624.
154. Wu, H.-C., L.-C. Liu, and S.-M. Yang, *Effects of additives on supported noble metal catalysts for oxidation of hydrocarbons and carbon monoxide.* Applied Catalysis A: General, 2001. **211**(2): p. 159-165.
155. Carlsson, P.-A., et al., *Induced low temperature catalytic ignition by transient changes in the gas composition.* Catalysis Today, 2002. **73**(3–4): p. 307-313.
156. Epling, W.S., C.H.F. Peden, and J.n. Szanyi, *Carbonate Formation and Stability on a Pt/BaO/γ-Al2O3 NOX Storage/Reduction Catalyst.* The Journal of Physical Chemistry C, 2008. **112**(29): p. 10952-10959.
157. Lercher, J.A., C. Colombier, and H. Noller, *Acid-base properties of alumina-magnesia mixed oxides. Part 4.-Infrared study of adsorption of carbon dioxide.* Journal of the Chemical Society, Faraday Transactions 1: Physical Chemistry in Condensed Phases, 1984. **80**(4): p. 949-959.
158. Morterra, C., et al., *An infrared spectroscopic investigation of the surface properties of magnesium aluminate spinel.* Journal of Catalysis, 1978. **51**(3): p. 299-313.
159. Toops, T.J., et al., *Quantified NOx adsorption on Pt/K/gamma-Al2O3 and the effects of CO2 and H2O.* Applied Catalysis B: Environmental, 2005. **58**(3–4): p. 255-264.

160. Iordan, A., M.I. Zaki, and C. Kappenstein, *Interfacial chemistry in the preparation of catalytic potassium-modified aluminas.* Journal of the Chemical Society, Faraday Transactions, 1993. **89**(14): p. 2527-2536.
161. Kantschewa, M., et al., *Infrared and x-ray photoelectron spectroscopy study of K2CO3/γ-Al2O3.* Applied Catalysis, 1983. **8**(1): p. 71-84.
162. Krupay, B.W. and Y. Amenomiya, *Alkali-promoted alumina catalysts. I. Chemisorption and oxygen exchange of carbon monoxide and carbon dioxide on potassium-promoted alumina catalysts.* Journal of Catalysis, 1981. **67**(2): p. 362-370.